12-2013

The Advancement of Bacterial Cellulose As A Bone and Vascular Scaffolds

Ryan Lee Hammonds
University of Tennessee - Knoxville, rhammon2@utk.edu

To the Graduate Council:

I am submitting herewith a dissertation written by Ryan Lee Hammonds entitled "The Advancement of Bacterial Cellulose As A Bone and Vascular Scaffolds." I have examined the final electronic copy of this dissertation for form and content and recommend that it be accepted in partial fulfillment of the requirements for the degree of Doctor of Philosophy, with a major in Polymer Engineering.

Roberto S. Benson, Major Professor

We have read this dissertation and recommend its acceptance:

Deidra Mountain, Kevin Kit, Wei He

Accepted for the Council:

Carolyn R. Hodges

Vice Provost and Dean of the Graduate School

(Original signatures are on file with official student records.)

The Advancement of Bacterial Cellulose As A Bone and Vascular Scaffold

A Dissertation Presented for the
Doctor of Philosophy Degree
The University of Tennessee, Knoxville

Ryan Lee Hammonds
December 2013

DEDICATION

I would like to dedicate my work to my wife and my parents. Their continuous support was irreplaceable during my pursuit of this degree.

ACKNOWLEDGEMENTS

I would like to point out some of those that have helped me along the way. I owe a great thanks to my major advisor, Dr. Roberto Benson. I would like to thank my committee members for their great advice and assistance in my work. They include Dr. Wei He, Dr. Deidra Mountain, and Dr. Kevin Kit. I also owe a great thanks to my peers: Jonathan Page, Dr. Russell Hallman, Kaan Serpersu, William Gazzola, Tiffany Flick, Tommy Washington, and Josh Fogle. I hope they learned as much from me as I was fortunate enough to learn from them. I would also like to thank Stacey Kirkpatrick and Greg Jones. They provided a helpful hand every time I asked for help.

ABSTRACT

Bacterial cellulose (BC) is a natural hydrogel made of nanofibers. This material has been used in commercial products, including wound dressings. BC can be modified and optimized for improved performance in multiple applications. This work will focus on producing and characterizing resorbable cellulose, a composite for bone applications, and a composite for a synthetic venous valve leaflet.

BC can be produced and modified to perform as a degradable tissue scaffold. This is achieved by an oxidation procedure after the initial production and purification of native BC. A material characterization of oxidized BC was performed to identify the changes in properties associated with varying the degree of oxidation. BC incubated in 20 millimolar periodate solution performed the best during an evaluation with preosteoblast cells.

Another application is as a bone scaffold using hydroxyapatite precipitated on the surface of cellulose fibers. This composite has fibers similar to collagen and a biomimetic ceramic similar to that found in native bone. Evaluation of native BC, oxidized BC, and BC with hydroxyapatite were shown to be effective materials to support cell growth in an animal model.

A separate evaluation utilized BC/hydroxyapatite composites as a source of biomimetic hydroxyapatite for use as a filler or powder in other systems. The extraction of hydroxyapatite from BC can be achieved by either enzymatically or thermally degrading bacterial cellulose. Each method leaves some residual product from the processing procedure, which varies depending on the method of analysis used to quantify the residual product.

Lastly, an alternative application is its use as a fiber-reinforcing component in polyurethane. This cellulose/polyurethane composite is of interest for applications that require high-strength and blood compatibility, such as arterial and venous substitutes. A composite was produced with micron scale thickness, similar to a venous valve leaflet. The polyurethane/cellulose composite exhibited improved strength, modulus, and ductility over native BC. *In vitro* evaluation showed the scaffolds were non-toxic to endothelial cells and support cell growth.

TABLE OF CONTENTS

LIST OF TABLES

LIST OF FIGURES

Chapter 1
Introduction

1.1. Bacterial Cellulose

Bacterial cellulose (BC) is a unique material that has garnered significant research interest in recent years, as shown in Figure 1. BC exhibits properties suggesting its potential as an ideal material for tissue engineering scaffolding. Commercial applications of BC include its use as a dietary fiber supplement and as an acoustic diaphragm. The versatility of BC as a biomaterial in medical applications is shown by its use as wound dressings[1,2], vascular grafts[3-5], bone scaffolds[6,7], and cartilage implants[8,9]. BC is already utilized commercially as wound dressings under the trade names Biofill® and XCell™.[2]

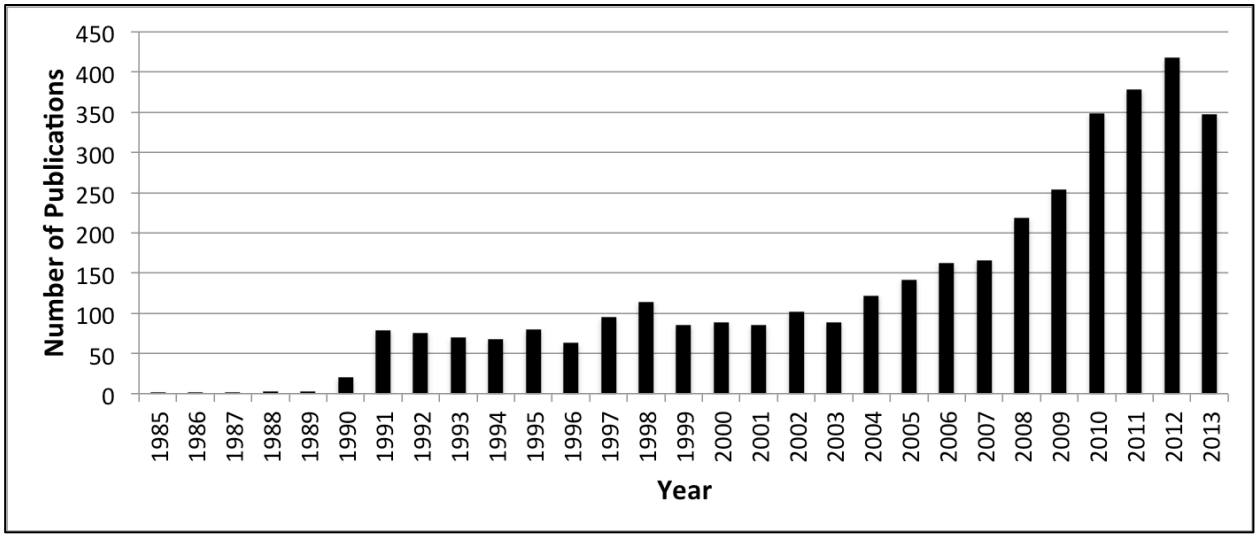

Figure 1: Annual Publications of BC
The number of publications was determined by a Web of Science search in November 2013 using the search term "Bacterial Cellulose".

Gluconoacetobacter is an aerobic organism that is gram-negative and rod-shaped. Rotting fruits and vegetables can house these bacteria. Researchers take advantage of the unique ability of the bacteria to polymerize sugars into cellulose in the laboratory to generate a hydrated biofilm at the air-liquid interface in cell culture media.

Each bacterium polymerizes monosaccharides into individual cellulose chains through a cellulose-synthesizing complex. Individual cellulose chains are excreted through pores of the bacterial cell wall. After excretion out of the cell, these cellulose chains quickly crystallize to form microfibrils that subsequently hydrogen bond together to form ribbons.[10,11] These ribbons are typically observed with morphologies similar to fibers with diameters of 3-4 nm thick, 70-80 nm wide, and 1-9 μm long.[3]

Bacterial cellulose (BC) is chemically identical to cellulose obtained from other sources. The polysaccharide composition consists of repeating pyranose rings linked by β-(1,4) glycosidic bonds to form the polymeric chain. BC has superior mechanical properties in comparison to other cellulose derivatives. The sizeable difference in mechanical properties is largely attributed to the higher crystallinity of BC.[12] The high degree of crystallinity is due to the contributions of hydrogen bonding within the same polymer chain (intramolecular) and hydrogen bonding between different chains (intermolecular) through the three hydroxyl functional groups on each pyranose ring.[3,13] This bonding structure is illustrated in Figure 2.

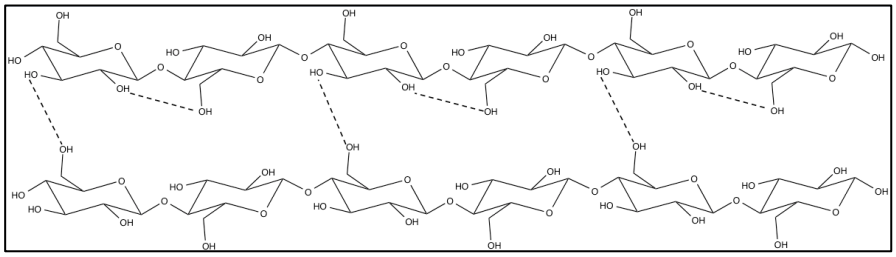

Figure 2: Hydrogen Bonding of Bacterial Cellulose
Intramolecular (within the same chain) and intermolecular (between different chains) hydrogen bonding is illustrated in the figure.

The ability of a material to perform as designed while functioning with appropriate host response is of upmost importance. Wistar rats with 10x10x3 mm^3 BC subcutaneous implants in the back of each rat exhibited host tissue integration into the BC without eliciting any inflammatory reactions in long-term implantation. Additionally,

there was no evidence of *in vivo* degradation taking place during the study.[14] BC has many excellent properties as a biomaterial including its hydrogel nature, nanoporous 3-D fibrous structure, high crystallinity,[3] and excellent biocompatibility.[14]

BC must be imposed on by light, mechanical, chemical, or biological factors in order to be degradable. The human body does not possess the enzyme necessary to hydrolyze the β-(1,4) glycosidic linkages to depolymerize the material into its glucose monomers for resorption by the body for glycolysis and the Kreb's cycle. Previous chemical modifications of BC include 2,2,6,6-Tetramethyl-1-piperidinyloxy (TEMPO), periodic acid, alkaline hypobromite, and chromic acid.[15] Some methods preferentially oxidize cellulose amorphous regions and cause significant side reactions,[15-17] which is undesirable. An ideal method modifies crystalline and amorphous regions so that all cellulose chains can degrade *in vivo*, but does not degrade the cellulose via depolymerization.

Painter demonstrated a method to use sodium periodate to produce oxidized cellulose with minimal side reactions and without depolymerization.[18] Periodate oxidation of BC breaks the ring structure of cellulose between the adjacent hydroxyl groups on the C2 and C3 carbons to form a dialdehyde structure, shown in Figure 3.[15] This converts the native bacterial cellulose from a non-degradable material into one that is degradable *in vivo*[19,20] through oxidation of crystalline and amorphous fractions.[15,22] The degradation products of oxidized dialdehyde cellulose are glycolic acid and 2,4-dihydroxybutyric acid[19-21], which can be excreted through natural metabolic pathways in mammalian hosts.[15,21-23] The periodate method to oxidize bacterial cellulose (OBC) has been investigated and has shown promising use as a resorbable tissue scaffold.[7,24]

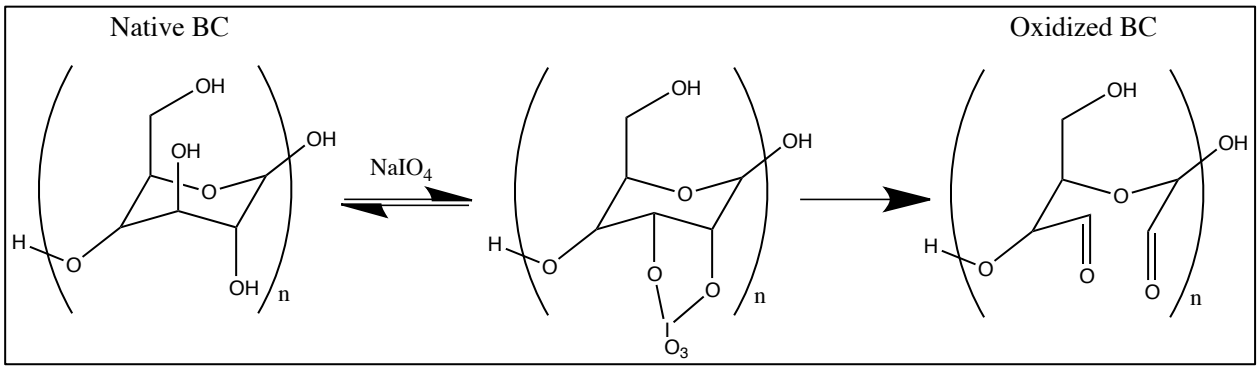

Figure 3: Oxidation of Bacterial Cellulose
This schematic shows the conversion of BC into a degradable form through oxidation by sodium periodate.

1.2. Bone

Bone tissue matrix is extensively vascularized in order to deliver the oxygen and nutrients necessary for bone cells. Highly ordered lacunae contain a central canal possessing blood vessels for the nutrient and oxygen supply. Osteocytes surround the central canal and are connected to it through a network of canaliculi. The osteocytes maintain bone by managing the mineral and protein content of bone.[25]

As part of the continuous remodeling process in bone, bone is continuously broken down and new bone is formed. Osteoblasts are the bone forming cells and produce the organic fraction of bone tissue. To balance the activities of osteoblasts, osteoclasts are responsible for the breakdown of bone, or osteolysis. These cells secrete acids that allow calcium phosphate to be resorbed by the body. The balance between osteoblasts and osteoclasts is critical for normal remodeling processes as well as wound healing.[25]

Bone is essentially a composite made of a fibrous component and a ceramic component. One third of the total weight of bone is from the collagen fibers that provide bone with a tough and flexible characteristic. These fibers are surrounded with calcium phosphates plates. Calcium phosphates comprise the other two thirds of bone weight. Hydroxylated calcium phosphates are recognized as hydroxyapatite (HA).[25]

1.2.1. Hydroxyapatite

Synthetics to replace bone are still in demand for the treatment of disease, traumatic injury, and non-union fractures. Alloplasts, autografts, allografts, and

xenografts can be used as bone substitutes. Each method has its own associated risks. Autografts require additional tissue damage since a tissue-harvesting site in the patient is used. An extra incision means an additional risk of infection and healing errors. Allografts and xenografts differ in the tissue donor species. Both materials have risks of rejection by the host immune system and disease transmission.

Synthetic materials offer an avenue to supply the demand for bone tissue replacements. Ideally, the synthetic material, by acting as a support scaffold, promotes bone formation by up-regulating osteoblast activity and is resorbed at the appropriate time. Preferably, the scaffold should mimic the native tissue extracellular matrix. The anatomy of native bone includes collagen, water, HA, proteoglycans, and non-collagenous proteins. HA is the primary inorganic ceramic and is bioactive through its support of bone growth and osseointegration.[25]

A variety of inorganic ceramics, such as bioglass, β-tricalcium phosphate, and biphasic calcium phosphate (a mixture of β-tricalcium phosphate and HA) have been investigated as bone substitute materials and have shown osteoblast adhesion and proliferation. Since HA is found in native bone, it is desirable to mimic the natural bone structure and use HA in the bone substitute material. The morphology of HA found in native bone is calcium-deficient and it is resorbed as part of bone remodeling.[26] Calcium-deficient HA is resorbable while stoichiometric HA has been shown to be stable *in vitro* for long periods of time and is essentially nonresorbable.[27] Additionally, it has been confirmed that bone colonization is improved by calcium-deficient hydroxyapatite (CdHA) over the stoichiometric form.[28] CdHA can vary in its magnitude of deficiency and is represented as $Ca_{10-x}(HPO_4)_x(PO_4)_{6-x}(OH)_{2-x}$ with $0<x\leq1$ while stoichiometric HA assumes the form of $Ca_{10}(PO_4)_6(OH)_2$.[29] Since CdHA is part of the natural bone matrix, the use of a biomimetic synthetic CdHA for bone regenerating applications is ideal.

The synthesis of HA is typically carried out by wet or solid state reactions. Drawbacks of these methods are the required elevated temperatures, elevated pressures, and final product impurities.[30] Nanoscale rosettes have been produced by precipitation of CdHA on BC fibers.[31] The CdHA product was also shown to be pure.[31] The desirable nanoscale dimensions of CdHA rosettes mimic the nanoscale biological native HA of 20 nm wide, 1.5-5 nm thick, and 40-60 nm long.[32] The smaller dimensions

maximize the surface area to volume ratio and allow for better resorption. The synthetic HA is also calcium-deficient,[31] suggesting that it is resorbable under physiological conditions since biological HA is also calcium-deficient and resorbable.[29] Another unique mimicking property is an elongated c-axis in synthetic HA similar to the elongated c-axis in biological HA.[26] The biomimetic properties of the synthetic hydroxyapatite are expected to perform better as it possesses multiple features similar to biological hydroxyapatite from native bone.

1.3. Vein Anatomy and Physiology

The venous system is composed of superficial and deep veins connected by perforating veins. The veins have bileaflet valves that support one-way flow back to the heart. These one-way regulators break up the column of blood between the heart and the feet.[33] The natural venous valve is comprised of a bileaflet arrangement with attachments at the base of the sinus cavity.[33] The vein valve leaflets are 20 to 50 microns thick and are composed of collagen fibers covered with a layer of confluent endothelial cells. The leaflets are the strongest component of the vein valve. The ultimate tensile strength of the vein wall is 5 MPa, while the leaflet possesses a strength of 9 MPa.[34] Figure 4 shows the venous valve structure and cycle that allows flow towards the heart when it is open, and prevents retrograde flow away from the heart when it is closed. The flow at the leaflet edge produces a vortex in the sinus pockets. The vortex produces pressure equilibrium to keep the valve open during the equilibrium stages.[35-37] Muscle contractions and blood flow variations produce pressure changes that open or close the valve.[35-37]

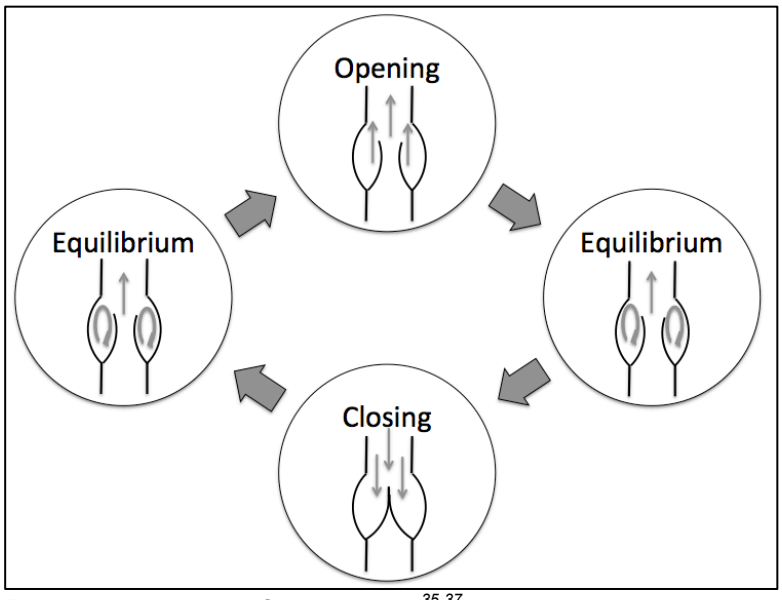

Figure 4: Venous Valve Cycle (Adapted[35-37])
This image illustrates the four major stages in the venous valve cycle.

1.3.1. Polyurethanes

Polyurethanes (PU) are a diverse family of polymers with a wide range of structural forms that may be foamed or solid and flexible or rigid for use in processing, coatings, adhesives, and medical applications.[38] PUs are comprised of urethane bonds formed between a hydroxyl and an isocyanate. Altering the monomer concentrations and the monomer chemical structures can modify polyurethane properties.

1.3.1.1. Chemical Structure

PUs are formed through a polycondensation reaction. This class of reactions frequently has a byproduct, most commonly water. The urethane linkage is formed by a hydroxyl and an isocyanate reaction. This reaction is shown below in Figure 5 without the byproduct. In this schematic, R_1 and R_2 can be any structure of any length. More specifically, this reaction schematic illustrates an end-capping procedure commonly associated with polyurethanes synthesis. A prepolymer is generated as an intermediate product and further polymerized at a later time to form the final polymer. In this scenario, through the control of molar ratios, an end-capped product is produced with isocyanate groups available for further polymerization. A chain extender combined with the prepolymer, shown with the generic schematic in Figure 6, produces the final PU.

This process is a common two-step procedure associated with the preparation of PU materials.

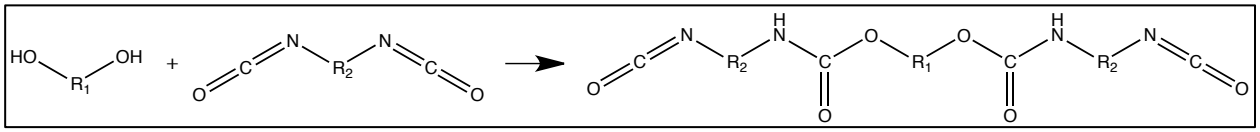

Figure 5: The Urethane Reaction to Form the End-Capped Polyether Prepolymer
The structures shows the reaction between a diol and a diisocyanate to form two urethane linkages and produce a prepolymer with unreacted isocyanate end groups. Controlling the stoichiometric ratio between the diol and diisocyanate in a 1:2 ratio, respectively, produces the drawn structure.

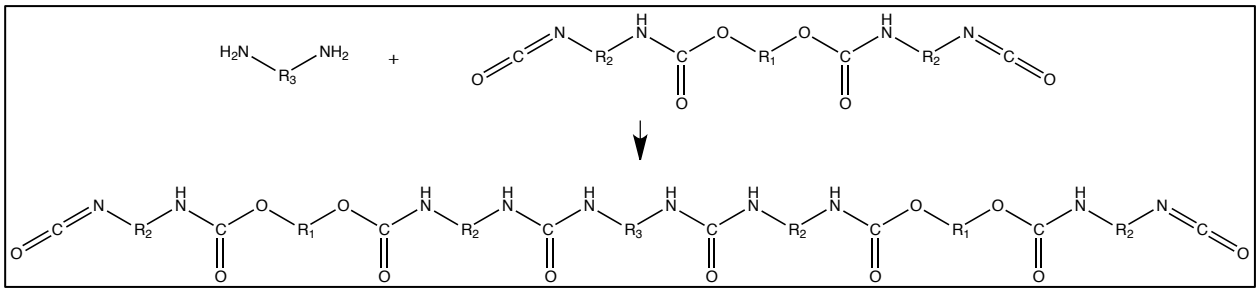

Figure 6: Chain Extender of a Polymer Using a Diamine Molecule
Depicted in the image is the second step of the traditional two-step synthesis of polyurethanes. A chain extender (the diamine in this image) is reacted with the prepolymer to form the final polyurethane.

In order to control the reactions, a rule of thumb is acids retard the reaction while bases accelerate the reaction and are effective at concentrations <1%.[39] Side products include allophanate and biuret linkages between an isocyanate and a urethane or urea group, respectively. The formation of side products disturbs the reactant stoichiometric balance and introduces branches into the main chain, allowing for possible crosslinking. Branching and crosslinking can be avoided by using a system without a catalyst at a temperature in the range of 100-140°C.[40]

PUs contain components designated as soft and hard segments that are important for engineering polyurethanes with the appropriate properties. Polyurethanes separate into microdomains driven by thermodynamic incompatibility. In PUs with elastomeric properties, hard segments form crystalline microdomains and produces a

filler-like discontinuous phase while the soft segment can be crystalline or amorphous and produces a continuous phase.[41] Factors that effect the physical and biological properties of polyurethanes include: the hard segment structure (chemical and molecular weight)[42], the hard segment phase structure[43], soft segment structure (chemical and molecular weight)[44-46], the chain extender effecting the morphology produced,[46-49] the processing conditions[50], the degree of crystallinity[51], and the production of a linear or network structure.[52]

Common polyethers and polyesters with hydroxyl end groups used as soft segments include: poly(ethylene glycol) (PEG), poly(propylene glycol) (PPG), poly(tetramethylene glycol) (PTMG), poly(tetramethylene oxide) (PTMO), polycaprolactone, poly(lactic acid), and poly(dimethylsiloxane). Common diisocyanates used include: 4,4′-methylenebis(phenyl isocyanate) (MDI), toluene-2,4-diisocyanate (TDI), 1,4-butane diisocyanate (BDI), and hexamethylene diisocyanate (HDI). Chain extenders include aliphatic or aromatic molecules that are diols or diamines. For example, ethylene glycol, butane diol, hexane diol, and ethylene diamine are common compounds used as chain extenders.

Common medical grade polyurethanes include Pellethane® and Elasthane™, made from a reaction between PTMO, MDI and butane diol monomers.[53] Biomer®, medical grade Lycra®, is made of PTMG, MDI, and ethylene diamine.[44] ChronoFlex® is a PU comprised of polycarbonate polyol, MDI, ethylene diamine, and 1,3 diaminocyclohexane.[54] This short list begins to reveal that many commercial PUs are produced with varying components, each with its own advantages and disadvantages. Different design requirements for different applications allow for a demand of custom PUs to be designed for the specific applications.

1.3.1.2. Blood Compatibility

PUs can exhibit good non-thrombogenic properties.[55] Still, not all PUs are thromboresistant. The blood contacting properties are dependent on the chemical structure and surface properties.[55] PPG based PUs have been shown to selectively adsorb blood proteins. PUs that preferentially adsorb albumin will exhibit desirable non-thrombogenic behavior while other PUs will instead adsorb other proteins, which initiate fibrin, thrombin, platelet deposition, and clot formation.[56] The selective adsorption of

PPG based PUs was shown in an *in vivo* evaluation.[55] It has also been shown that the tacticity of the soft segment has little to no effect on mechanical properties.[57] Other PUs with PEG, PTMG, and polybutadiene demonstrated the non-thrombogenic behavior depends on the soft segment length.[44] PPG based PUs exhibit a similar trend with non-thrombogenic properties based on soft segment length.[44] PPG based PUs have comparable blood compatibility to Biomer®.[44]

1.4. Composites

The use of composites permits the development of materials with properties that cannot be satisfied by single metals, ceramics, or polymers. By definition, a composite is any multiphase material that exhibits combined properties from each phase while producing a better performing material.[58] The principle of combined action states that better property combinations are formed by the careful material selection of singular materials and subsequent combination.[58] Composite materials are able to satisfy demanding design parameters.

A basic polymeric example of a composite is wood. It is comprised of cellulose fibers and lignin.[58] The cellulose fibers are strong and ductile while the lignin is stiff. The cellulose fibers are surrounded by a matrix of lignin in wood.[58] Additionally, another example of naturally occurring composites is bone.[58] It is a composite of collagen and apatite.[58] The collagen is soft and fibrous while the apatite is hard and performs well in compression. However, these naturally occurring composites do not fit the traditional definition of a composite. A composite traditionally refers to an artificially made multiphase material with dissimilar and separated phases with a distinct interface.[58] The approaches used in this work will utilize synthetic composites to meet the design requirements of the targeted applications.

Fiber-reinforced composite properties are effected by the fiber size, material composition, volume composition of fibers in the matrix, interfacial adhesion between the fiber and matrix, and fiber orientation.[59] The modulus (E) and strength (σ) are traditionally represented by the simple relationships shown in equation 1 and 2, respectively. The matrix property (m) and the fiber property (f) essentially bracket upper

and lower limits for the composite property (L) that is tailored by the fiber volume fraction in the composite (ϕ_f).[59]

$$E_L = (1-\phi_f)E_m + \phi_f E_f \quad \text{Eq. 1}$$

$$\sigma_L = (1-\phi_f)\sigma_m + \phi_f \sigma_f \quad \text{Eq. 2}$$

1.5. Solubility Parameters

The Gibb's free energy (ΔG) (equation 3) governs the criteria required for solubility.[60] The equation accounts for the enthalpy of mixing (ΔH), the entropy of mixing (ΔS), and the temperature (T). The Gibb's free energy describes a solute-solvent system and favors mixing when the value is negative. Therefore, mixing is promoted by decreasing enthalpy or increasing temperature or entropy.

$$\Delta G = \Delta H - T\Delta S \quad \text{Eq. 3}$$

The enthalpy of mixing is defined as shown in equation 4.[60] The enthalpy of mixing (ΔH), the volume fractions of components (ϕ_1, ϕ_2), and the solubility parameters of components (δ_1, δ_2) are included in the calculation. This equation illustrates when the solubility parameters of each component are nearly equal, the enthalpy of mixing is minimized and approaches zero. As the enthalpy of mixing nears zero and the temperature and entropy term contributes a negative value, the Gibb's free energy becomes negative and favors mixing of the components.[60] The equation supports the common principle of "like dissolves like" through similar components having similar solubility parameters.

$$\Delta H = \phi_1 \phi_2 \left(\delta_1 - \delta_2\right)^2 \quad \text{Eq. 4}$$

Each solubility parameter (δ) contains contributions from dispersion forces (δ_d), polar forces (δ_p), and hydrogen bonding (δ_h), as described by equation 5.[60] The solubility parameters for many common solvents and polymers are known. However, in scenarios where the solubility parameter is not known, it can be calculated by the group contribution method using dispersion components (F_{di}), polar components (F_{pi}), and molar volume (V) as described by equations 6-8.[60]

$$\delta^2 = \delta_d^2 + \delta_p^2 + \delta_h^2 \quad \text{Eq. 5}$$

$$\delta_d = \frac{\sum F_{di}}{V} \quad \text{Eq. 6}$$

$$\delta_p = \frac{\sqrt{\sum F_{pi}^2}}{V} \quad \text{Eq. 7}$$

$$\delta_h = \sqrt{\frac{\sum E_{hi}}{V}} \quad \text{Eq. 8}$$

Solubility parameters perform well in describing affinities between solvents and solutes.[61] However, the numerical model does have some limitations when applied to polymer-solvent systems. The approach does not account for the solubility effects of polymer molecular weight.[61-63] As polymers increase in molecular weight, their solubility decreases and the polymer can eventually precipitate out of solution.[60,63] This trend is described numerically with monomers exhibiting smaller solubility parameters than the corresponding polymer.[58,61] Still, solubility parameters are especially helpful for selecting an appropriate solvent for use with a polymer.[61]

Selected solubility parameters are listed in Table 1 for materials that will be used in this work. Comparisons between components will be discussed in greater detail later. At this time, it is important to note the similarity in solubility parameters of water and cellulose. The hydrophilic chemical structure of cellulose has a high affinity for water and helps explain how bacterial cellulose adsorbs water readily.

Table 1: Solubility Parameters ($cal^{1/2}/cm^{3/2}$)
The values listed in the table identify the solubility parameters of materials used in this work including: cellulose, dimethylformamide (DMF), water, hexane, p-xylene, and stannous octoate. Values listed here are commonly reported with the exception of stannous octoate and cellulose. The solubility parameters for these materials were determined by the group contribution method. Details on the calculation are provided in Appendix B.

Parameter	Cellulose	Water	DMF	Hexane	p-Xylene	Stannous Octoate
δ_d	12.8	7.6	8.5	7.3	8.8	7.8
δ_p	7.8	7.8	6.7	0	0	0.9
δ_h	15.6	20.6	5.5	0	0	3.9
δ	21.6	23.3	12.1	7.3	8.8	8.7

1.6. Characterization Techniques

1.6.1. Mechanical Testing

The mechanical properties of materials are crucial as they typically determine if a material can meet the mechanical demands for a given application. The most common test is a tensile test where a moving crosshead places a load on a sample. A strain rate controlled test has the crosshead move at a constant rate while the load exerted by the sample is recorded. The load and elongation data is normalized into stress (σ) and strain (ε) data for comparison between samples. The amount of strain the sample undergoes prior to failure is a measure of its ductility. The modulus of elasticity is a quantified measurement of the rigidity or softness of a material. The modulus is determined in the elastic region, noted by the linear section of the stress versus strain plot. Once the curve deviates from linearity, plastic deformation and yielding occurs. The elastic deformation is recoverable if the load is removed and the plastic deformation is permanent.

1.6.2. Fourier-Transform Infrared Spectroscopy

Infrared spectroscopy (FTIR) is a molecular characterization technique where electromagnetic radiation in the infrared range is exposed to the material. Absorption of the infrared radiation by the material is dependent upon three possible conditions. The first is when the radiation frequency matches the resonance vibrational frequency of the chemical bond. Another possible condition is with a change in the molecule dipole. Lastly, the dipole must change in a direction matching the electric field vector.

Upon passing the infrared beam through a sample, the sample either absorbs certain wavelengths of the radiation or allows those particular wavelengths to pass through. Certain bonds carry out this absorption as they absorb specific frequencies depending on the bond type. This results in a spectrum illustrating molecular absorptions for each wavelength. Each molecule has its own unique spectrum. This is analogous to human fingerprints as no two molecules produce identical infrared spectrums. The common IR regions are identified below in Table 2.

Table 2: FTIR Spectral Regions of Chemical Bonding Information

Wavenumbers (cm^{-1})	**Type of Absorptions**	**Region**
1000-700	C-H Bending	C-H Bending
1600-1000	C-C, C-O, C-N Stretching	Fingerprint
1850-1600	C=O, C=N, C=C Stretching	Fingerprint
2250-2100	Nitrile & Alkyne Stretching	Fingerprint
3400-2800	O-H, N-H, C-H Stretching	

Chapter 2
Bone Regeneration Scaffolds: Resorbable Oxidized Bacterial Cellulose

2.1. Introduction

Bacterial cellulose (BC) has been of interest to researchers for many applications, but especially as a biomaterial.[64] BC has been studied in applications as a vessel substitute,[4,5] a bone scaffold,[6,7] a cartilage scaffold,[9] and as a wound dressing.[2] The biosynthetic material has unique features, as it is a highly hydrated hydrogel with micropores formed by its nano-scale fibers. These fibers are produced by *Gluconacetobacter* species as a pellicle at the air-liquid interface in static cultures.

In order to build a scaffold appropriate for use in bone healing applications, a number of items must be completed to improve our understanding and improve the performance of the scaffold. A characterization study must be performed in a controlled manner to evaluate the effects of oxidation on the resulting mechanical properties and degradation profiles. In order to achieve cell migration into the bulk, porogens will be used. The porogens are particles that generate pores in the scaffolds once the particles are dissolved away. A porogen leaching system will be used to make macroporous scaffolds that will then have CdHA deposited onto them.

Understanding the materials science triangle of the relationship between structure, processing, and properties is the basis for materials engineering research. Using that connection, changes in the properties of oxidized bacterial cellulose with varying degrees of oxidation can be easily predicted. Literature shows a good understanding of the oxidation process. For example, periodate oxidation has been shown to linearly decrease cellulose crystallinity with increasing degree of oxidation, indicating that periodate can oxidize crystalline and amorphous regions of BC.[65,66] However, the oxidation of highly crystalline cellulose from *Cladophora* showed random oxidation points along cellulose fibers, determined through the use of gold labeling.[22] The understanding of BC sodium periodate oxidation is still incomplete and convoluted by reported work commonly using different oxidant concentrations. Studies also typically

use a singular oxidant concentration to compare degradable cellulose to native cellulose. Studies that vary the degree of oxidation normally investigate the oxidation of the material and the degradation, but do not evaluate mechanical properties. Currently, there is not a study available that systematically correlates the degree of oxidation of BC to the resulting mechanical and degradation properties.

Tissue engineering has utilized growth factors with biomaterials to improve tissue regeneration *in vivo*. Bone morphogenetic proteins (BMP) and transforming growth factor-β (TGF-β) have been shown to facilitate new bone growth individually[67,68] and concurrently.[69] BMP has been shown to upregulate vascular endothelial growth factor (VEGF),[70] a protein that stimulates angiogenesis. Combined delivery of BMP and VEGF by poly(lactic-glycolic acid)[71] and alginate and poly(lactic acid)[72] have been shown to be effective in regenerating bone *in vivo*.

BC has been functionalized with an osteogenic growth peptide that regulates TGF, fibroblastic growth factor (FGF), and insulin-like growth factor and showed improved mineralization *in vitro*.[73] Another study demonstrated the ability to load and release albumin using BC.[74] BC was grown in media containing heparin and exhibited a sulfated surface, which is promising since heparin can bind VEGF and FGF.[75] BMP has shown the ability to bind to extracellular matrix components including HA, collagen, proteoglycans, fibronectin, and laminin.[76] The ability to deliver growth factors using BC and HA make the materials ideal for use in bone applications.

HA can be precipitated on BC fibers by an alternating wash in aqueous salt solutions that produces a synthetic material with biomimetic calcium deficiency.[31] The deficiency allows the material to be resorbed under physiological conditions. Coupling the oxidized, resorbable BC with the osteoconductive CdHA produces an ideal composite tissue scaffold.

Still, many articles have reported cell infiltration into the BC scaffold with the infiltration depth as a function of time. It has been reported that the air exposed surface and the liquid exposed surface have different porosities, and therefore different cell infiltration properties. After one week, erythrocytes infiltrated 20 μm on the air side and 100 μm on the liquid side.[14] Similar results have been reported with smooth muscle cells with cell infiltration of 20 μm into the BC scaffolds after one week and an increase

to 40 μm after an additional week.[77] While previous publications show that BC supports cell growth, cell penetration into the scaffold is limited to only the micron range. Previous studies have utilized sieved (90-500 μm) paraffin microspheres with BC to produce a macroporous scaffold.[6,78] The ability to produce a macroporous BC scaffold with CdHA will be advantageous for bone applications to allow for cell penetration into the bulk for improved bone tissue regeneration.

One aim of this study is to oxidize BC to various levels, appropriately identify the actual oxidation level, and measure the corresponding mechanical and degradation properties. The production of OBC will be done systematically by holding liquid volumes and substrate concentrations constant while varying only the oxidant. The second aim is to evaluate native BC, oxidized BC, and BC with CdHA in an animal model by implanting the materials in a bone defect. Lastly, the ability to form macroporous BC deposited with CdHA will be demonstrated.

2.2. Experimental

2.2.1. Material Preparation

2.2.1.1. Bacterial Cellulose Synthesis

Gluconacetobacter sucrofermentans from the American Type Culture Collection (Manassas, VA, USA) (ATCC 700178) was obtained for use in this work. 24-well cell culture plates are used to culture pellicles of BC of 1.6 cm in diameter and grown to a thickness of 0.5 cm at the air-liquid interface after 14 days of growth in Schramm-Hestrin media with mannitol as the sugar source.[79] Cellulose purification is achieved by a four hour wash in 4% sodium dodecyl sulfate solution at 70^{o}C followed by a 4 hour wash in 4% sodium hydroxide solution at 70^{o}C. Sequential Millipore water washes were performed until the solution pH was neutralized.[80]

2.2.1.2. Calcium-Deficient Hydroxyapatite Deposition

CdHA deposition was performed by sequential immersion in 100mM $CaCl_2$ and 60mM Na_2HPO_4 aqueous solutions.[31] BC was incubated in each salt solution for a period of 12 hours at 23°C and switched to the other solution. One CdHA deposition cycle is defined as the treatment of BC undergoing one incubation in $CaCl_2$ solution followed by one incubation in Na_2HPO_4 solution. Higher cycle depositions are achieved

by repetition of the salt solution incubations. BC/CdHA samples subjected to 1, 3, and 5 cycle depositions were prepared for this study.

2.2.1.3. Bacterial Cellulose Oxidation

Periodate oxidation was carried out using a modified protocol developed by Painter[18] and first reported using BC by Hutchens.[7] BC was combined with varying concentrations of 0, 10, 20, and 100 mmol $NaIO_4$ in 5% n-propanol. Each concentration was selected as a ratio to BC concentration to study ratios of 0:1, 1:2, 1:1, and 2:1 with the BC concentration held constant at 20 mmol. Each container was placed on an orbital shaker for 24 h at 23°C and shielded from light. An ice bath was used to slow the reaction with the addition of 0.5 mL of glycerol to consume excess periodate. The cellulose was then purified with several changes of DI water.

2.2.2. Oxidized Bacterial Cellulose Material Characterization

2.2.2.1. Titration

OBC was produced with varying aldehyde content by modifying the periodate concentration used in solution to convert native BC (NBC) to OBC. Titrations were performed to determine the degree of oxidation. Prior to titration, lyophilized pellicles were soaked in a 2x solution of hydroxylamine in DI water. The solution was left for six hours on a shaker to allow for the condensation reaction, shown in Figure 7, to occur. The titrant consisted of 1% NaOH solution and was added to the hydroxylamine and OBC solution with phenol red as a pH indicator. The solution was maintained under constant agitation by a stir bar to evenly distribute the titrant. Titrant was added to the solution until a color change of the pH indicator was maintained for at least 15 seconds. The amount of titrant required was recorded. Titrations were performed on a blank solution with NBC and each OBC sample. The NBC and OBC samples were dried in a vacuum (30 mmHg) overnight, and the masses were then recorded. The degree of oxidation was determined by equation 9 using the experimentally measured OBC mass and titrant required to produce the pH indicator color change.[81]

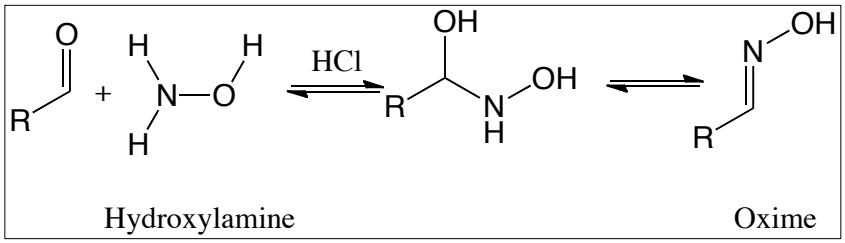

Figure 7: Hydroxylamine Reaction with An Aldehyde

$$\%\text{Oxidation} = \frac{\%\text{Aldehyde}}{2} = \frac{\text{mol OH}}{\text{mass OBC} / 161\ \text{mol/g}} \qquad \text{Eq. 9}$$

2.2.2.2. Degradation Study

BC samples were oxidized using three different concentrations of periodate in solution. Mass loss of each NBC and OBC scaffolds were investigated under static and dynamic conditions in phosphate buffered saline (PBS) solution, pH 7.4 at 37^{o}C. Each pellicle from a 24-well plate was placed into individual 2 mL centrifuge tubes with PBS. The pH was monitored by phenol red, and all solutions were changed weekly. Samples were evaluated at 0, 3, 7, 14, 21, 28, 56, and 84 days. The samples were lyophilized for at least 8 h and massed. An average mass loss of at least three samples for each time point were acquired.[82]

2.2.2.3. Tensile Test

Mechanical properties were evaluated using a dog bone stamp to prepare samples from one continuous sheet of BC. The stamp produced samples with a 6 mm width and 25 mm gauge length. Samples were cut from the same sheet and then oxidized. All non-specifically adsorbed water was removed by placing samples between Kimwipes and light pressure (0.344 Pa, 0.05 psi, 5 pounds over 100 in^2) was applied for two minutes. The samples were then immediately tested. Samples were tested using an ElectroPuls E1000 with Bluehill 2 software (Instron, Norwood, MA) with a 1 kN load cell. All samples were tested at a strain rate of 2 mm/min to allow for comparison between sample groups. All samples fractured along the gauge length. In the rare case that fracture occurred at or near the grips, the sample and its results were discarded.

Data was collected as data points in the form of load (F) and length (l), which were zeroed prior to testing. The length was converted into engineering strain (ε) using equation 10 where l_i is the elongation and l_0 is the initial gauge length. The force was converted into engineering stress (σ) using equation 11 where A is the cross sectional area of the sample calculated simply by thickness times width.[58]

$$\varepsilon = \frac{\Delta l}{l_0} = \frac{l_i - l_0}{l_0} \qquad \text{Eq. 10}$$

$$\sigma = \frac{F}{A} \qquad \text{Eq. 11}$$

After the load versus elongation data was converted to stress and strain values, Hooke's Law, shown as equation 12, was used to determine the elastic modulus (E, also called the Young's modulus) of each sample in the linear (elastic) region of the stress versus strain curve. The ultimate tensile strength (UTS) was calculated by determining the maximum tensile strength on the engineering stress versus strain plot. The percent elongation is a measure of ductility and represents the plastic strain at fracture. This value is calculated by equation 13 where l_0 is the initial gauge length and l_f is the final gauge length.[58]

$$E = \frac{\sigma}{\varepsilon} \qquad \text{Eq. 12}$$

$$\text{Percent Elongation} = \left(\frac{l_f - l_0}{l_0} \right) \times 100 \qquad \text{Eq. 13}$$

2.2.3. In Vitro Evaluation of Osteoblasts on NBC and OBC

2.2.3.1. Cell Culture

MC3T3-E1 preosteoblast cells from American Type Culture Collection (Manassas, VA, USA) (ATCC CRL-2593) were expanded in petri dishes in growth medium. The growth medium was comprised of αMEM (Invitrogen, Gaithersburg, MD), 10% fetal bovine serum (FBS) (Invitrogen), and 1% antibiotic/antimycotic solution (Invitrogen). BC was sterilized in deionized water using steam (1 bar, 121^{o}C) for 20 min. BC was soaked overnight in αMEM so that scaffolds rested in the bottom of each well and water in the void spaces between BC fibers would not dilute αMEM media. Once the cells were confluent, they were rinsed with PBS twice and detached with 0.25% (w/v) Trypsin, 0.53 mM EDTA solution (Invitrogen). Each 24 well sized scaffold (1.9 cm^2 surface area) was seeded at a density of 1x10^4 cells/cm^2. Cells were grown in an incubator at 37^{o}C in 95% air and 5% CO_2, and the growth medium was changed on the third day.

2.2.3.2. Cell Morphology

2.2.3.2.1. Epifluorescence Imaging with Confocal Microscopy

Scaffolds were stained with 2 mL Calcein AM (Invitrogen) at a concentration of 0.5 µL/mL and Ethidium Homodimer-1 (EthD-1) at 2 µL/mL for 30 minutes to perform a traditional live/dead staining. Fluorescence images were obtained using excitation and emission at 494 and 500-550 nm for Calcein AM and 543 and 610-670 nm for EthD-1, respectively. Imaging was performed using a Leica TCS SP2 laser confocal microscope (Leica Microsystems, Buffalo Grove, IL) with Leica Confocal Software.

2.2.3.2.2. Scanning Electron Microscopy (SEM)

After the incubation cycle was completed, the cells for SEM analysis were fixed with 3% glutaraldehyde in PBS. Samples were then washed three times with PBS solution and dehydrated through a series of ethanol solutions from 25 to 100% followed by further dehydration using hexamethyldisilazane (HMDS). Samples were dried in a vacuum desiccator overnight. Dried samples were mounted on carbon tape and sputtered with gold on a Spi Module Sputter Coater (Spi Supplies: Westchester, PA, USA) at 20 mA for 20 s. Samples were then analyzed on a LEO 1525 Scanning Electron Microscope (Zeiss, Oberkochen, Germany). A minimal acceleration voltage, in the range of 1- 5 kV, were used to image each material.

2.2.3.3. Cell Proliferation

Cell proliferation was measured using a water-soluble tetrazolium salt (WST).[83] A formazan product was produced by cellular mitochondrial dehydrogenases by conversion of the WST-1 reagent. The formazan product was measured quantitatively using UV-visible spectroscopy. Samples were measured in triplicates (n=3). After seven days of incubation, 10 μl of cell proliferation reagent WST-1 (Roche Applied Science, USA) was added to each well, incubated at 37°C in a 95% air and 5% CO_2 atmosphere for 4 h, and then mixed thoroughly on a shaker for 1 min. The absorbance of the supernatants was measured against a background control blank using a microplate reader (Synergy 2 Multi-Mode Microplate Reader, BioTek, USA).

2.2.4. In-Vivo Animal Model Using NBC, OBC, and Cellulose/CdHA Composites

The following work was performed according to an approved protocol by the University of Tennessee Institutional Animal Care and Use Committee (UTK IACUC). An animal model was used to evaluate the effectiveness of cellulose and cellulose/hydroxyapatite composites in helping a bone defect heal. Five experimental conditions were analyzed: a control group where an empty defect is used, NBC, OBC, NBC/CdHA, OBC/CdHA. Sprague Dawley Rats (male, 8 weeks old, ~226-250 g) were purchased from Charles River Laboratory (Wilmington, MA). The animals were given a one week acclimation period to recover from stress and environment change.

Surgery was performed by making an incision along the midline of the calvarium with blunt dissection down to the bone and subsequent elevation of the periosteum. One 6 mm defect was made using a bone trephine. The defect was left empty for control subjects and filled with the cellulose scaffold in other subjects. Closure of the periosteum, fascia, and dermal layers using sutures was performed to conclude the procedure.

Scaffolds were recovered 30 days post operatively. A bone saw was used to recover tissue at the implant site and the adjacent area. The harvested tissue was immediately placed into Carson's fixative for 48 hours. The tissue was then dehydrated through an ethanol series of 50, 70, 90, 100% ethanol with a final incubation in 50% ethanol-50% propylene oxide solution. The tissue samples were then embedded in 50% propylene oxide-50% Spur's embedding medium with two changes of medium over a 24

hour period without hardening taking place. Pure Spurr's medium was combined with the hardening component and placed under vacuum. This solution was changed twice over 24 hours. Finally, the sample was placed in fresh Spur's media with hardener overnight in an oven at 65^{o}C. From the embedded sample, 100 micron sections were obtained by cutting then mounting them to a glass slide for subsequent polishing. The samples were then stained using Sanderson's rapid bone stain and counter stained using acid fuchsin to examine bone ingrowth. Each stain was performed on a slider warmer (~45^{o}C) for about one minute each.

2.2.5. Macroporous BC/CdHA Scaffolds

Macroporous scaffolds were produced following a traditional porogen-leaching method, presented in greater detail in Figure 8. Two polyethylene microsphere size distributions of 106-125 μm and 300-355 μm were acquired (Cospheric, Santa Barbara, CA). The polymer microspheres were ethanol sterilized and allowed to dry. Each range of microspheres was combined separately with Shramm-Hestrin media and *Gluconacetobacter sucrofermentans.* BC was cultured for 14 days in the Schramm-Hestrin media with polyethylene spheres. BC was purified with a four hour wash in 4% SDS at 70^{o}C followed by a four hour wash in 4% NaOH at 70^{o}C. Sequential Millipore water washes were performed until the solution pH was neutralized.[80] In order to remove the polyethylene sphere, the BC was placed in boiling xylene for 4 hours. The scaffolds were then placed in isopropanol overnight and then washed with DI water. CdHA deposition was performed by sequential immersion in 100mM $CaCl_2$ and 60mM Na_2HPO_4 aqueous solutions.[31] The BC was incubated in each solution once to complete one cycle of deposition. Scaffolds were frozen at -80^{o}C before lyophilizing overnight. The scaffolds were coated with gold for 20 seconds at 20 milliamperes using a Spi Module Sputter Coater (Spi Supplies, Westchester, PA). Imaging was performed using a LEO 1525 SEM (Zeiss, Oberkochen, Germany).

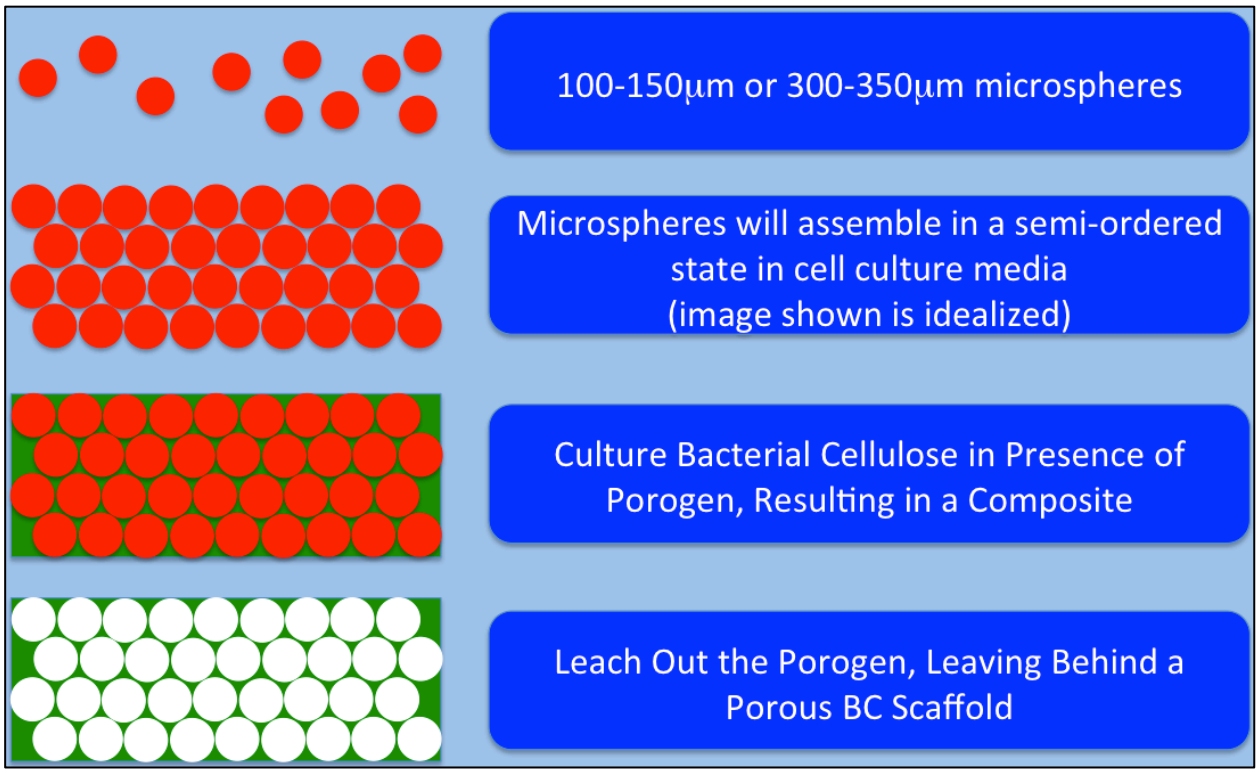

Figure 8: Fabrication of Macroporous Bacterial Cellulose
This image describes the stepwise process to produce macroporous BC by the porogen-leaching method.

2.3. Results

2.3.1. Oxidized BC Characterization

2.3.1.1. Degree of Oxidation

For each oxidation used in this study, the BC concentration in solution was always held constant with only the amount of oxidizing agent varied. The titration of the hydroxylamine showed that, as expected, as the oxidizer concentration increased, so did the degree of oxidation (Table 3). The highest oxidizing concentration was not analyzed for degree of oxidation for reasons that will be discussed later.

Table 3: Degree of Oxidation for Bacterial Cellulose

Sample	Native BC	OBC 1	OBC 2	OBC 3	OBC 4
Periodate Concentration (mmol)	0	10	20	40	100
Degree of Oxidation	0	10.7	14.9	53.5	-

The samples were imaged and are presented in Figure 9 along with the average diameters presented in Figure 10. The diameters were determined by a three-point method in order to minimize error during measurement. The change in pellicle diameters from the oxidation treatments change significantly for OBC 4, produced using 100 mmol sodium periodate concentration.

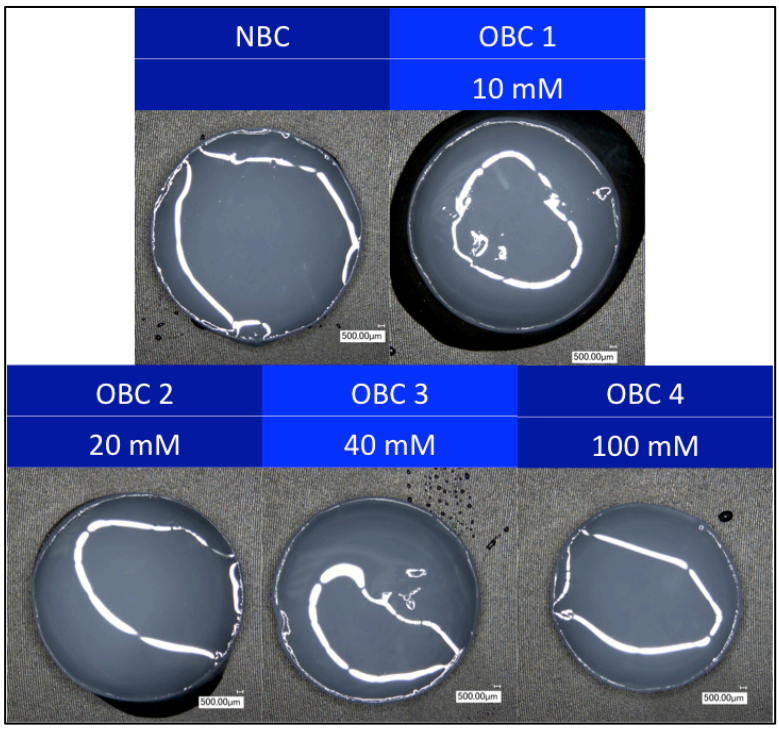

Figure 9: Macroscopic Comparison of Varying OBC Treatment
This figure shows the macroscopic dimensions of samples after incubation with the corresponding sodium periodate concentration.

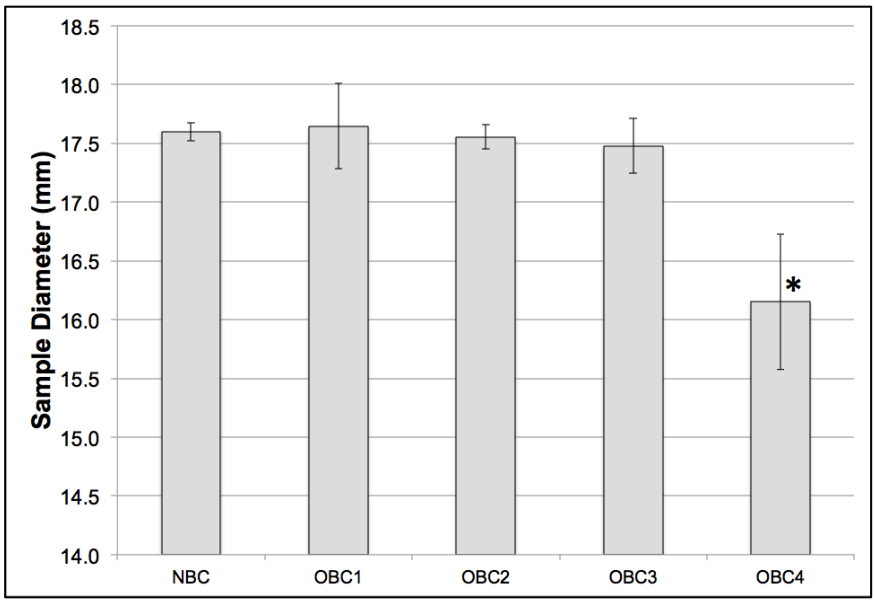

Figure 10: Oxidized Bacterial Cellulose Pellicle Diameters
Illustrated in this figure is the average sample diameter with 95% confidence intervals. The asterisk indicates the experimental group with a statistically significant difference from other experimental sample groups.

2.3.1.2. Degradation Study

The percent mass remaining versus time profiles of static and dynamic incubations of NBC and OBC in PBS are presented in Figure 11. The general trends are as expected with more mass loss in higher degree of oxidation samples. It should be noted that in static evaluation, NBC and OBC 1 initially exhibited increased percent mass with time, but then decreased with longer incubation times. Additionally, the percent mass losses in static incubations were minimal in comparison to the greater percent mass losses measured from dynamic incubations. The mass losses under static conditions at the final time point were statistically significant for same material tested under dynamic conditions (i.e. static NBC showed statistically significant greater mass loss under dynamic conditions).

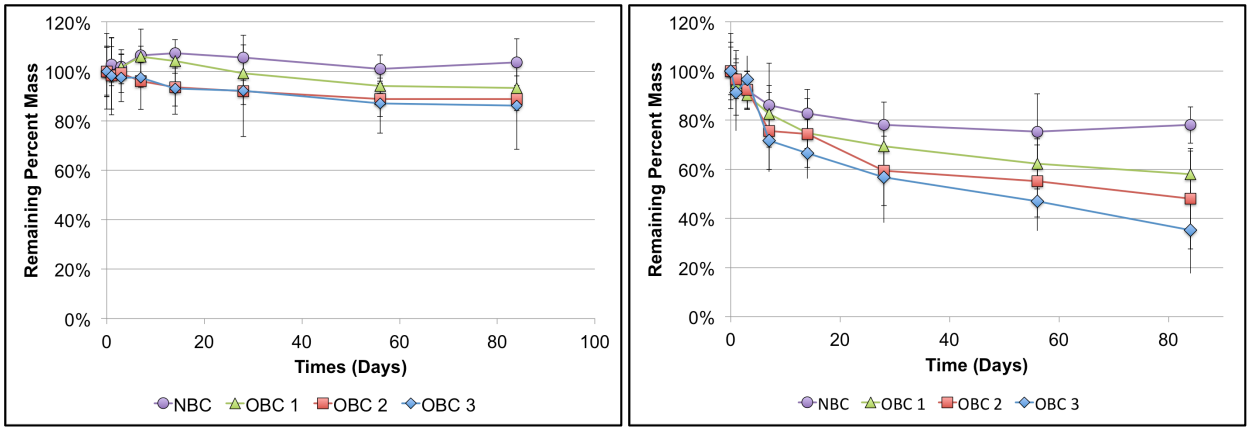

Figure 11: Degradation Profiles of BC and OBC in Static and Dynamic Conditions
In this figure the remaining mass percent versus time is present for BC and varying degree of oxidation of BC for static (Left) and dynamic (Right) incubation.

2.3.1.3. Tensile Testing

The software and computer controlled tensile testing equipment supplied raw data in the form of load and elongation data points. These data points were converted into stress (σ) and strain (ε) data. A representative stress versus strain curve is presented for each experimental group in Appendix C. The elastic modulus (Figure 12), from the slope of the linear region, declines from a maximum with native BC down to the most oxidized BC. The UTS (Figure 13) follows an identical trend as the modulus, with decreasing strength associated with increased oxidation of BC. The elongation at break (Figure 14) increased with a small degree of oxidation but then decreased with further oxidation.

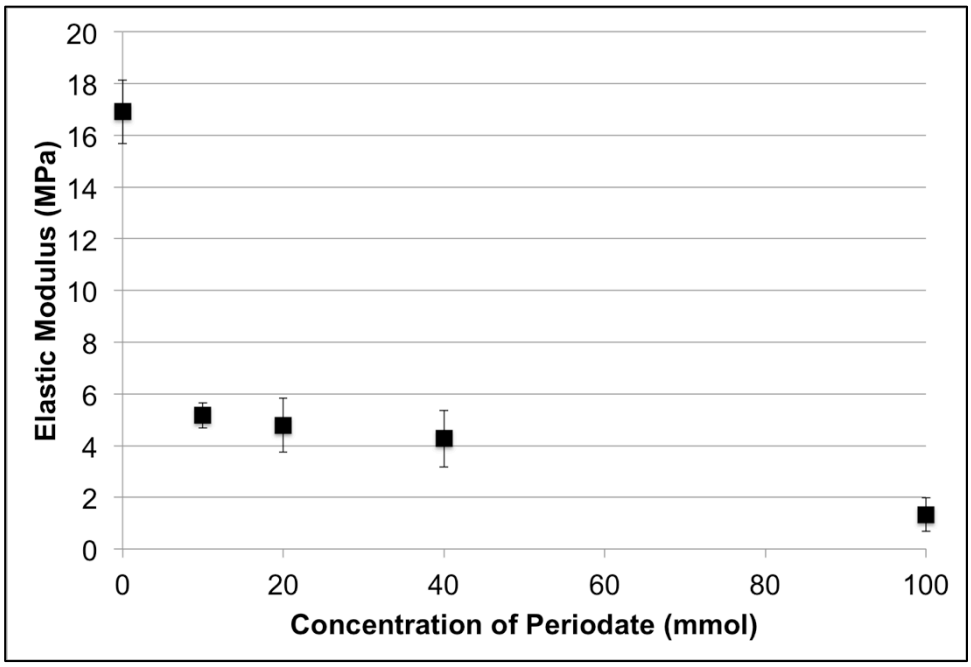

Figure 12: Tensile Elastic Modulus of Oxidized Bacterial Cellulose
Plotted in the figure is the average elastic modulus variations over a range of oxidations varied by the concentration of sodium periodate in solution.

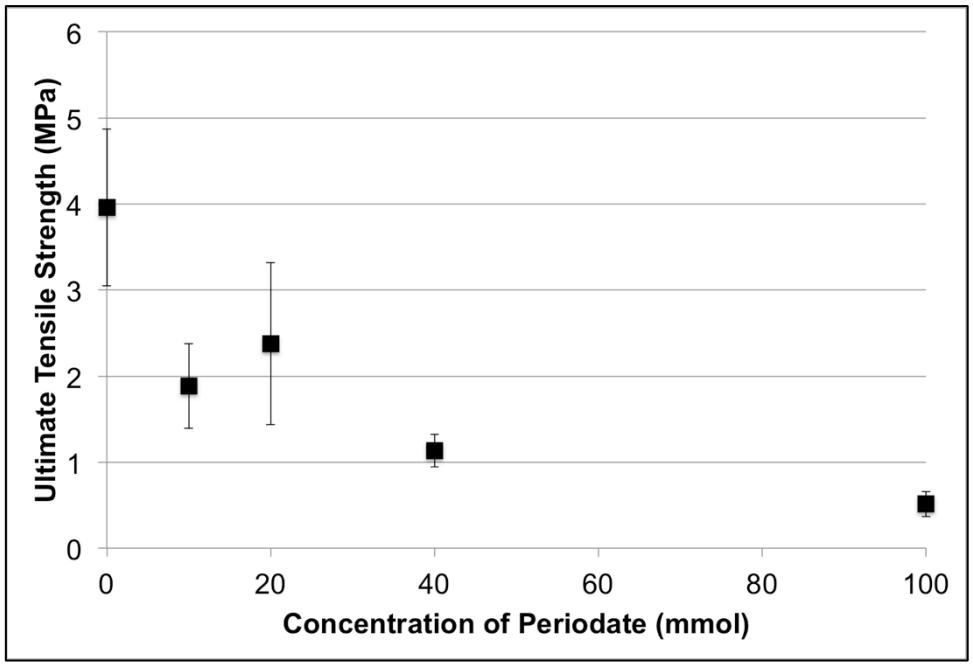

Figure 13: Ultimate Tensile Strength of Oxidized Bacterial Cellulose
Plotted in the figure is the average ultimate strength values over a range of oxidations varied by the concentration of sodium periodate in solution.

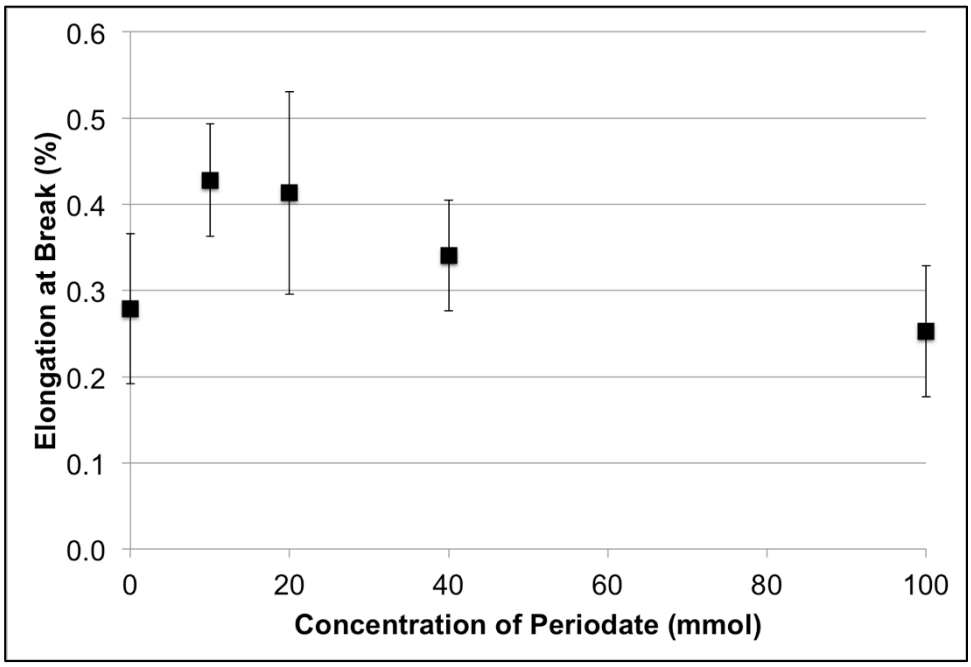

Figure 14: Elongation at Break of Oxidized Bacterial Cellulose
Plotted in the figure is the average percent elongate at break variations over a range of oxidations varied by the concentration of sodium periodate in solution.

2.3.1.4. In Vitro Evaluation of Osteoblasts on BC and OBC

The WST-1 assay (Figure 15) showed that the scaffolds supported cell growth during the 7-day culture. Each value plotted includes error bars showing the 95% confidence interval. All OBC scaffolds on the first day showed statistically similar absorbances. The absorbance for all oxidized scaffolds exhibited statistically significant higher values than native BC on the first day. On the seventh day, OBC 2 showed statistically significant higher absorbance than all other scaffolds.

A set of images is presented in Figure 16 and illustrates the cell viability after seven days. All scaffolds show a high number of viable cells (green) and a low number of dead cells (red). OBC 2 and OBC 3 show higher cell numbers in the spot images than NBC and OBC 1. Additionally, OBC 2 and OBC 3 show improved cell spreading. However, this trend does not come across in the images presented here because the lighter green colors, indicating where cells are spreading, are lost in translating the electronic files to print images.

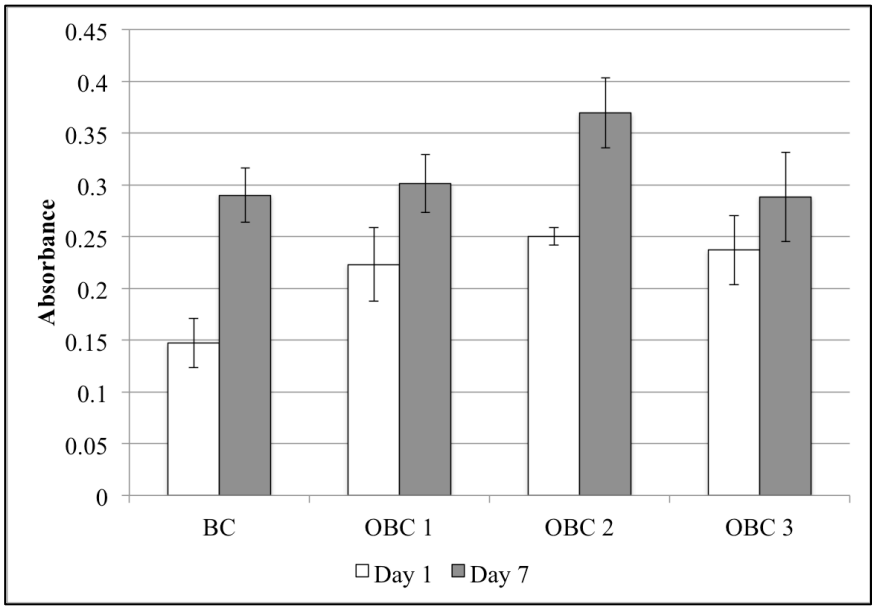

Figure 15: WTS-1 Assay from Cultures on NBC and OBC
This chart evaluates cell growth over the seven day period with evaluation time points at day one and day seven with 95% confidence intervals. The absorbance of NBC at day 1 is less than other scaffolds on day one and statistically significant. The absorbance of OBC 2 on day 7 is greater than other scaffold on day seven and the difference is statistically significant.

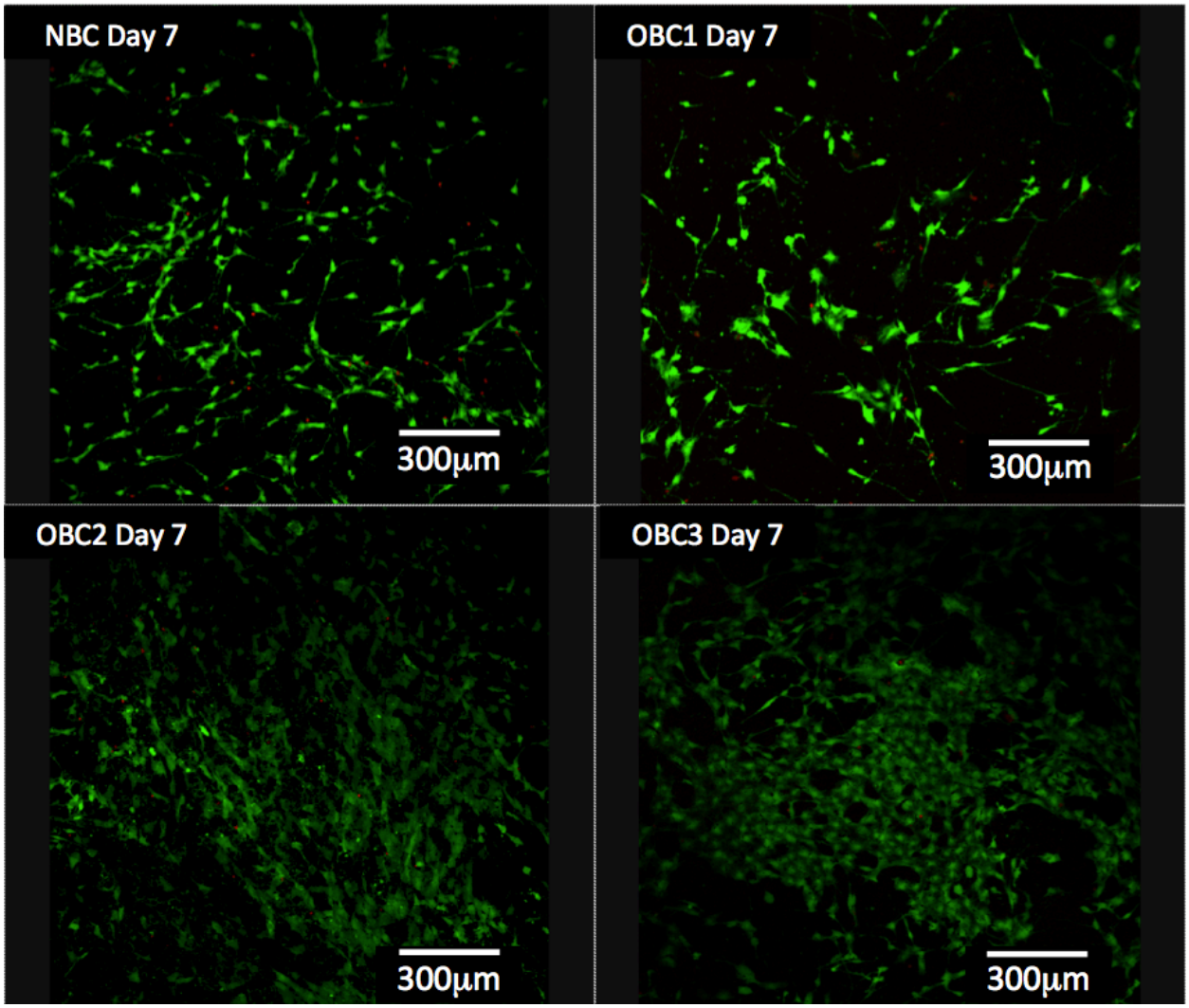

Figure 16: NBC and OBC Confocal Live/Dead Fluorescence Images
The images from day 7 of the study show live cells as green (Calcein AM) and dead cells as red (EthD-1) with only a few cells in each image as red, supporting that these scaffolds are not harmful to the cells.

In order to observe cell morphology, SEM imaging was used and images are presented in Figure 17 through Figure 20. Scaffolds on day one showed cells attached, but oriented along a single axis. Day three images showed a similar trend, but with some improvement towards spreading out multi-directionally. On the seventh day, NBC scaffolds showed improved cell spread in more directions than one axis. OBC 1 still exhibited spreading along a single axis. A significant improvement in cell spreading was observed on the OBC 2 and OBC 3 scaffolds. The spreading has proceeded to such as high degree that there are only small circular regions where cells did not cover the

fibrous scaffold. A higher magnification image is provided for OBC 2 and OBC 3 on the seventh day to illustrate that regions exist that are still the underlying fibrous scaffold and regions are present with cells that cover the fibrous scaffold.

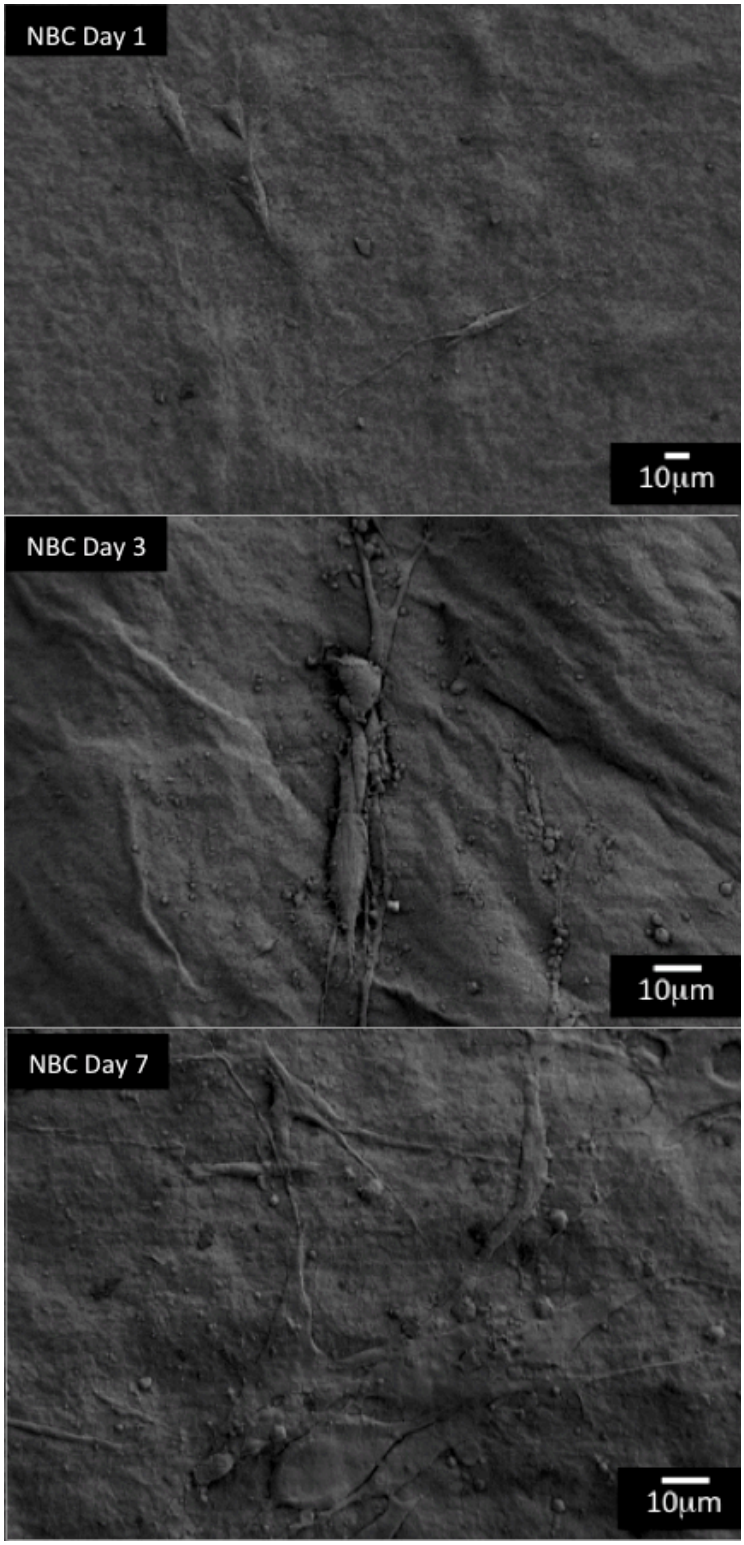

Figure 17: SEM Images of Osteoblasts on NBC
The array of images shows cells on NBC scaffolds from each time point of the study. In each image, individual cells are shown spreading across the scaffold.

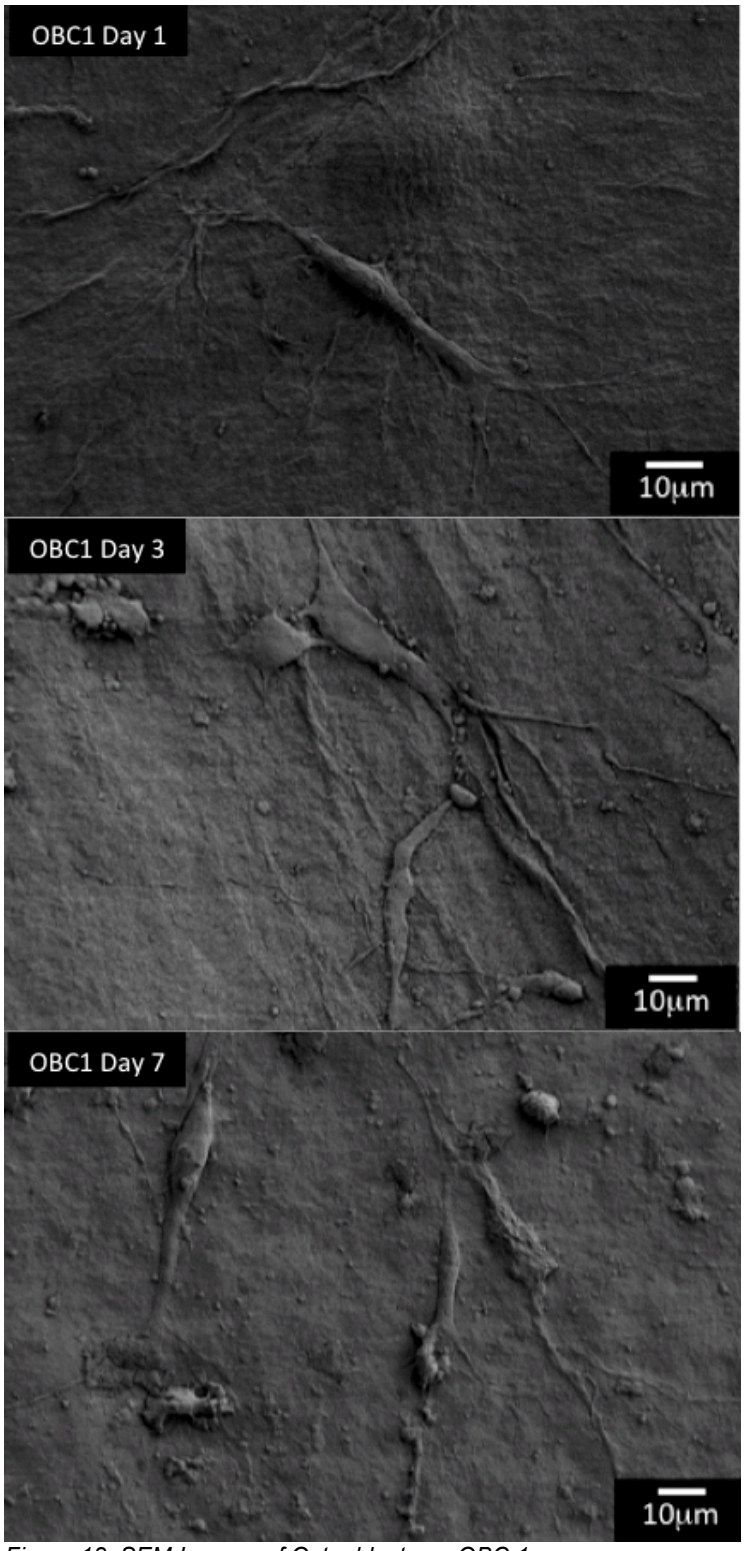

Figure 18: SEM Images of Osteoblasts on OBC 1
The array of images shows cells on OBC 1 scaffolds from each time point of the study. In each image, individual cells are shown spreading across the scaffold.

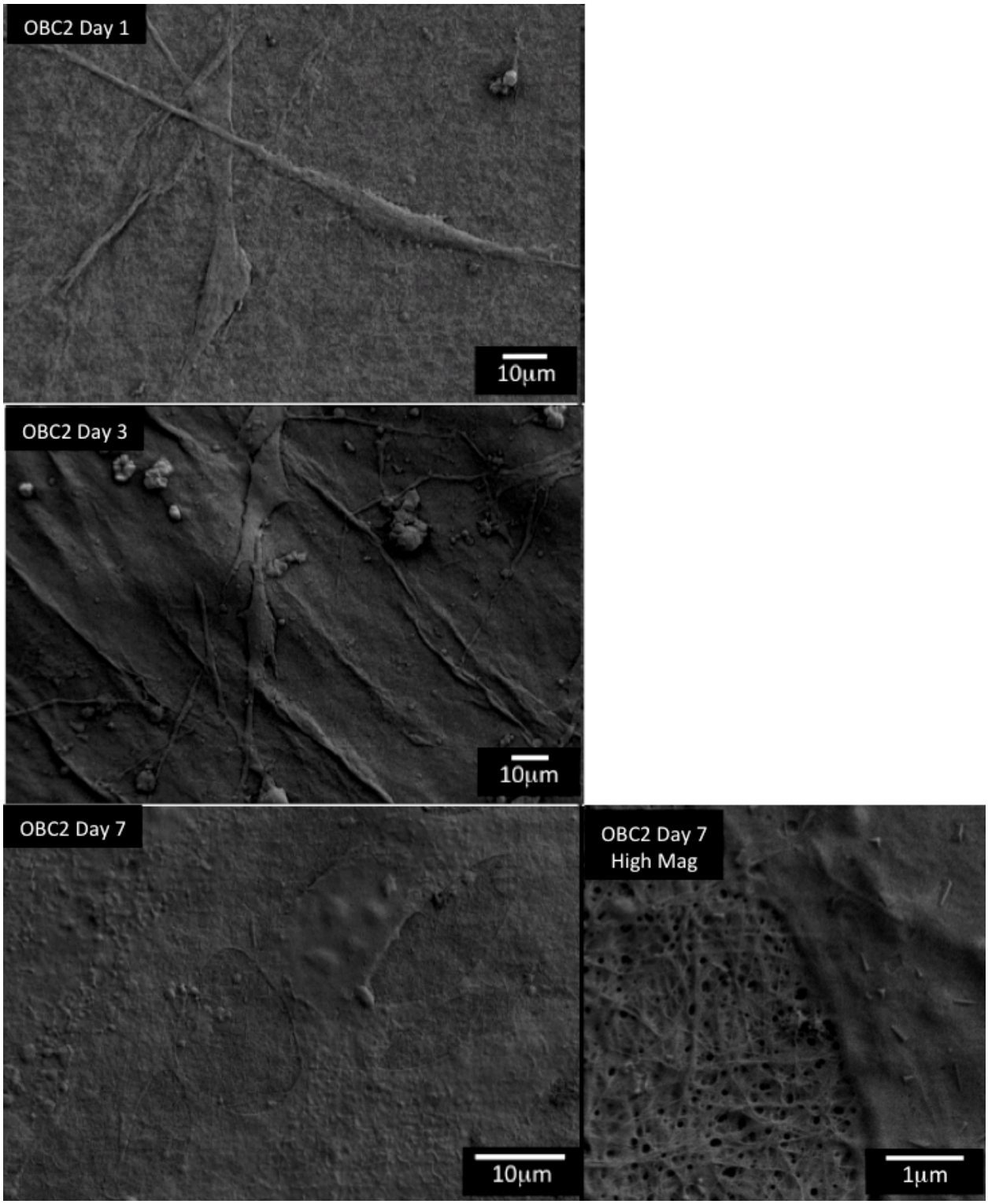

Figure 19: SEM Images of Osteoblasts on OBC 2
The array of images shows cells on OBC 2 scaffolds from each time point of the study. In day 1 and day 3 images, individual cells are shown spreading across the scaffold. Day 7 shows a scaffold that is covered with cells, extracellular matrix product, or both with small, circular regions left showing the fibrous structure of BC. A high magnification image is presented of the day 7 scaffold to show there are regions exhibiting the original fibrous morphology and regions covered with cells.

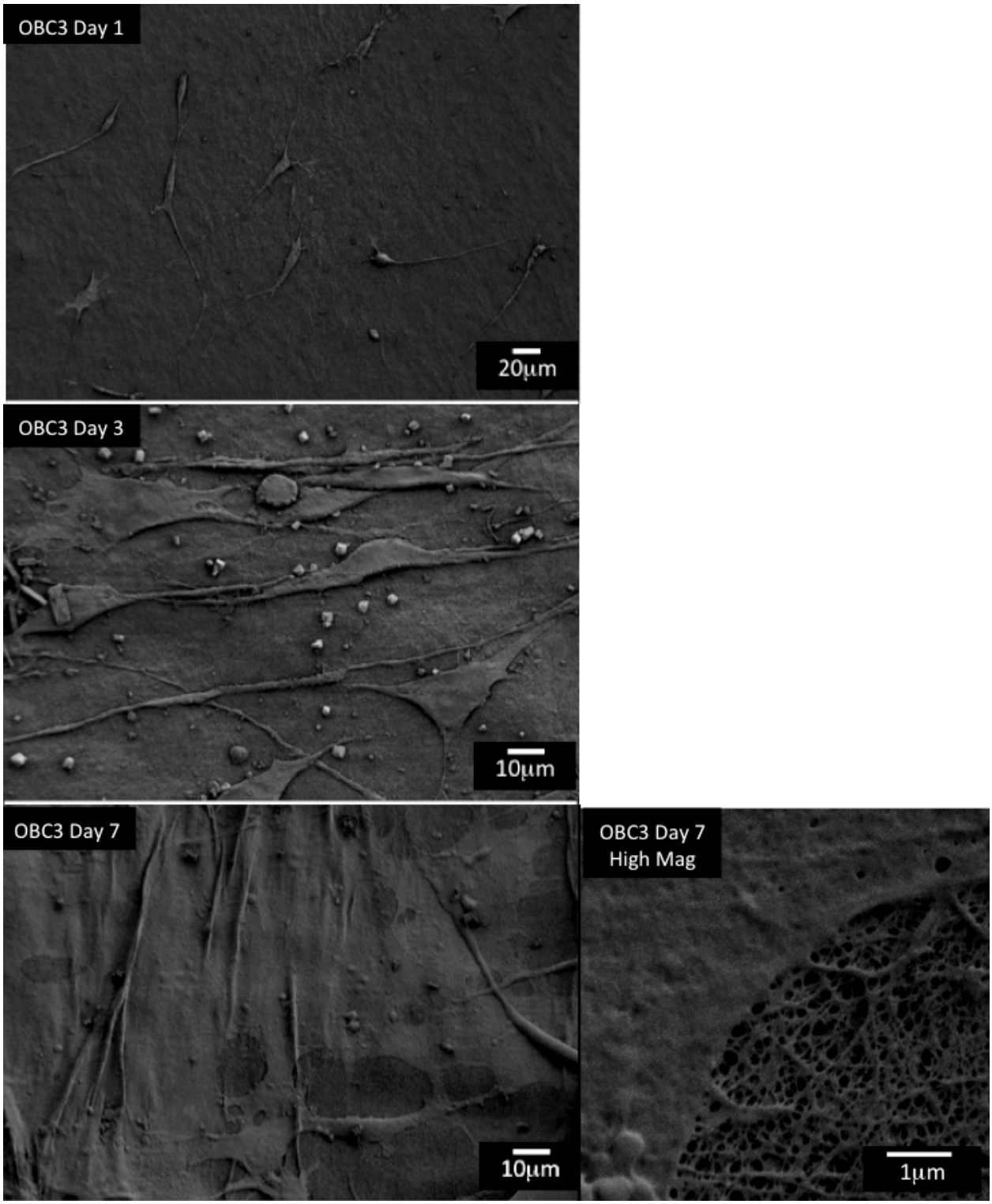

Figure 20: SEM Images of Osteoblasts on OBC 3
The array of images shows cells on OBC 3 scaffolds from each time point of the study. In day 1 and day 3 images, individual cells are shown spreading across the scaffold. Day 7 shows a scaffold that is covered with cells, extracellular matrix product, or both with small, circular regions left showing the fibrous structure of BC. A high magnification image is presented of the day 7 scaffold to show there are regions exhibiting the original fibrous morphology and regions covered with cells.

2.3.1.5. In Vivo Animal Model with BC, OBC, and BC-CdHA

An investigation to access the ability of a non-critical size defect in a rat calvarium to heal with the aid of BC scaffolds was performed. The scaffolds investigated included native BC, oxidized BC, native BC-CdHA, and oxidized BC-CdHA. The OBC in this study used cellulose that was oxidized using a 50 mM periodate solution.[7] The native bone in Figure 21A was stained using a procedure that produces a red color for mineralized bone and a blue or purple color for soft tissue. Native bone is shown in Figure 21A with the periosteum, a membranous soft tissue layer indicated by the thin, dark purple layer, above and below the bone. The majority of the image is bone, shown by the red tint for the mineralized skull tissue. At 30 days post-operation, it was observed that empty defects, which served as controls, exhibited only a thin layer of soft tissue across the defect, which is shown in Figure 21B. The blue stain in the image indicates cells and tissue that is not mineralized.

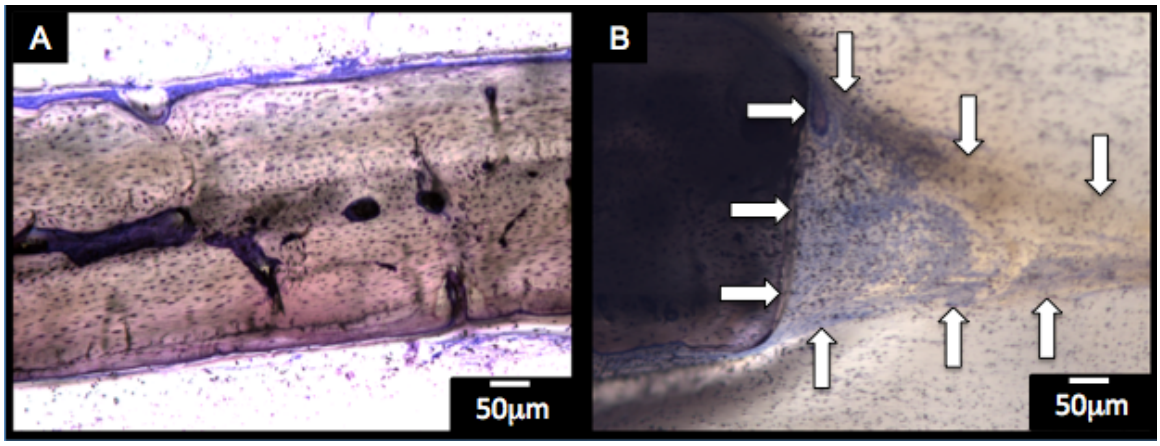

Figure 21: Histology Images of of Rat Calvarium with and an Empty Defect
Native bone tissue (A) and a bone-empty defect interface (B) are presented in the figure. Sandersons rapid bone stain was used with acid fuschin counterstain to show cells and tissue. The native bone tissue, shown in image A, illustrates the structure of undamaged bone tissue. Mineralized bone shows a slight red/pink color and blue/purple regions show soft tissue layers on each side of the bone. The bone-empty defect, shown in image B, shows minimal tissue regeneration after 30 days of healing was allowed. Bone is located at the left of the image. The arrows pointing to the right line the bone defect edge. The area in between the arrows outlines the new tissue that was trying to traverse the defect gap during healing.

BC scaffolds (Figure 22A) and BC-CdHA (Figure 22B) scaffolds exhibited the ability to facilitate cells by providing a structure for cells to span the gap of the defect.

The scaffolds showed small red regions, indicating some mineralization took place. However, this could be attributed to a non-specific staining of CdHA rather than staining osteoblasts or osteocytes. Higher magnification images (not shown here) show that scaffolds did not accommodate cell infiltration into the bulk of the tissue scaffolds. Further, the composites were not producing significant mineralized tissue since the composites mostly stained blue.

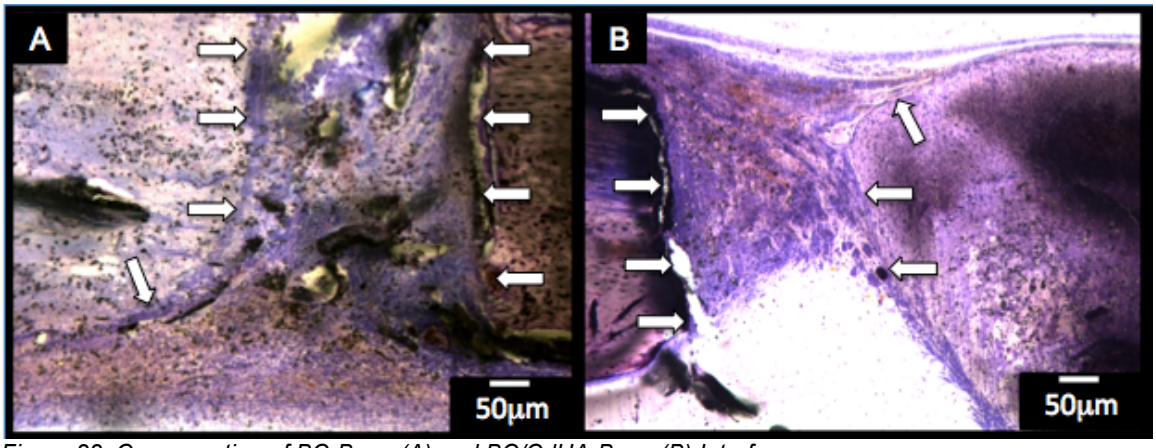

Figure 22: Cross-section of BC-Bone (A) and BC/CdHA-Bone (B) Interfaces
Sandersons rapid bone stain with acid fuchsin counterstain reveals the cell and tissue structures. In the NBC scaffold, shown in image A, the NBC is on the left and the bone is on the right. Arrows on the left line the cellulose edge and arrows on the right line the bone edge. New tissue is located between the arrows. Similarly, the NBC-CdHA scaffold, shown in image B, has bone on the left and the composite on the right. Arrows line the bone edge on the left and the composite edge on the right. New tissue is located between the arrows.

2.3.2. Imaging of Macroporous BC/CdHA Scaffolds

Separate size ranges of polyethylene microspheres were acquired in ranges of 106-125 μm and 300-355 μm diameters. Images of these spheres are shown in Figure 23. The measured diameter averages of the polymer microspheres were 120 and 342 μm with standard deviations of 9.2 and 16.3 μm, respectively.

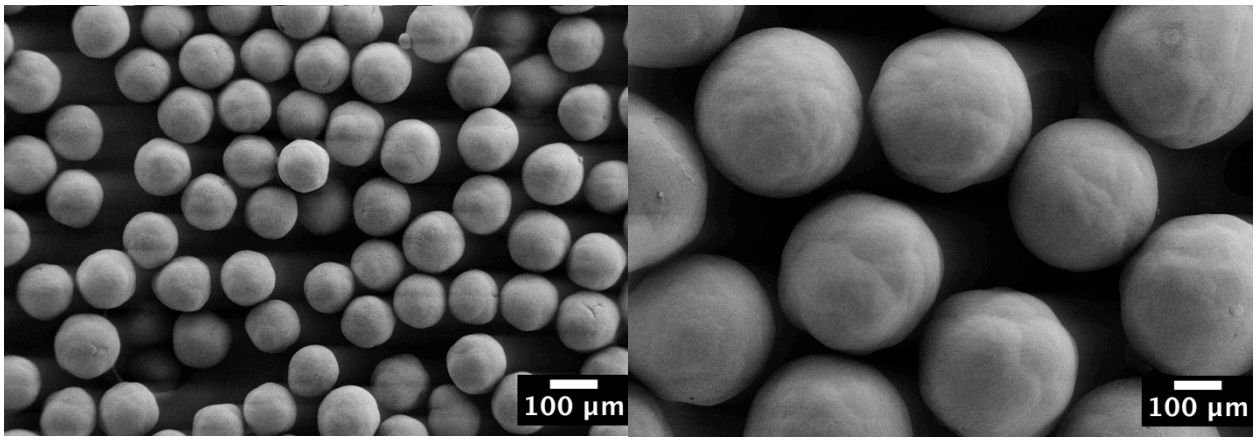

Figure 23: Polyethylene Porogens
Shown by SEM imaging are the polymer microspheres used as porogens in the macroporous cellulose fabrication. In the image on the left are microspheres that averaged 120 μm in diameter and on the right are microspheres that averaged 342 μm in diameter.

Polyethylene porogens of a single size range were used in separate bacteria cultures to generate macroporous structures. The polyethylene microspheres were dissolved using xylene produced the macroporous BC scaffolds. A fracture surface was produced for imaging. Microspheres with an average diameter of 342 μm were used in culture to produce the BC structure imaged and presented in Figure 24. The image shows pores on a similar scale as the 342 μm diameter porogens used in culture with bacteria.

CdHA was deposited on macroporous BC produced from culture with microspheres with an average diameter of 342 μm. The scaffolds were dried and mounted for imaging. The images of the liquid nitrogen fracture surface are presented in Figure 25. Low magnification images in Figure 25A and B show the area imaged in Figure 25C, which shows rosettes of CdHA are present on the BC fibers.

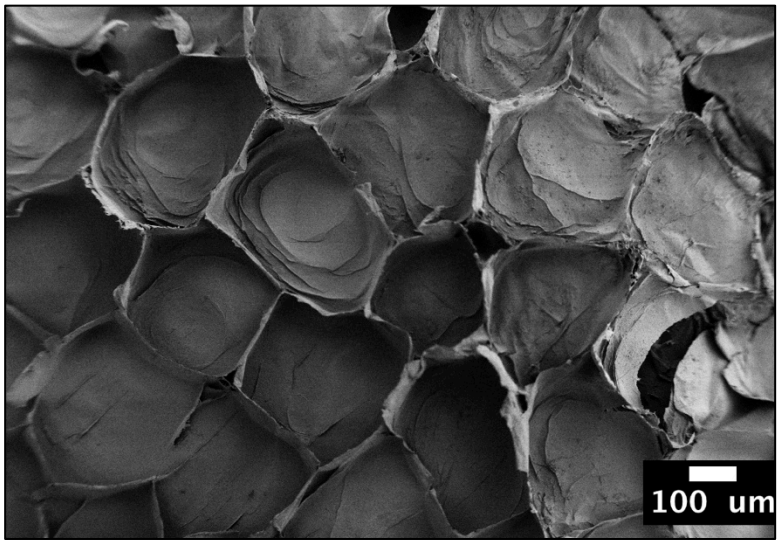

Figure 24: SEM Image of Macroporous BC
An SEM image of BC fracture surface exhibiting a macroporous structure is presented. The voids generated are similar in scale to the 342 μm average diameter of the microspheres used in the BC growth media during culture.

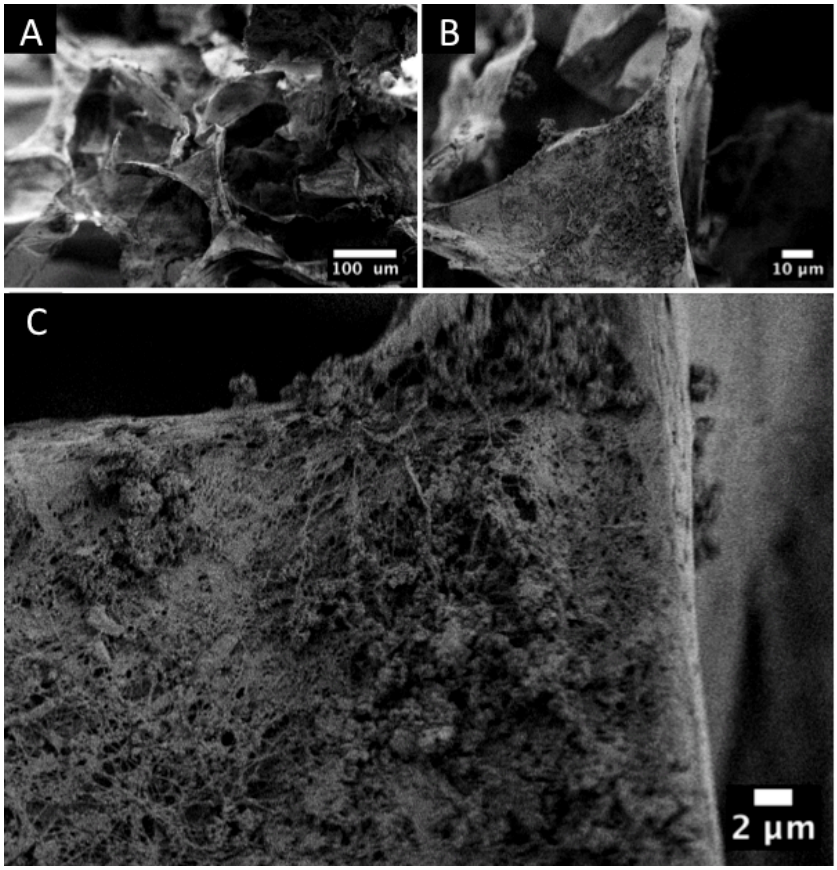

Figure 25: SEM Images of Macroporous BC/CdHA
The images show a low magnification (A), a medium magnification (B), and high magnification (C) of the same spot. Images A and B show a macroporous BC fracture surface. Image C shows BC fibers with CdHA rosettes.

2.4. Discussion

2.4.1. Oxidized BC

The goal of this work was to investigate and determine optimum oxidation conditions to achieve specific properties. At the time of publication, existing reports typically only investigated a single oxidized cellulose sample and compared it to native BC. The studies that reported on multiple levels of oxidation were not interested in the resulting changes in mechanical properties or degradation profiles. This study aims to fill in the knowledge gap.

The images in Figure 9 used for the measurements reported in Figure 10 show a statistically significant change in OBC 4. This change is the result of over oxidation of the sample due to the high concentration of periodate in solution with the cellulose. Therefore, this scaffold was not evaluated in the characterization methods. This experimental group is still valuable as it shows approximately where the upper end of the oxidant concentration is located.

The titration method using hydroxylamine was selected due to its ability to rapidly access the degree of oxidation without significant sample prep or testing time. This method is effective, but has been shown to reveal a slightly lower degree of oxidation in comparison to other test methods.[81] However, the difference between testing methods is only 2-3% percent.[84] Similar precision in evaluation methods was found on polyaldehyde dextrans using the titration method for aldehyde analysis compared to the measurement by combustion.[85] Still, the titration method used in this study is rapid. The speedy assessment will allow for correlation to mechanical properties and degradation rates in order to prepare samples for different tissues with minimal preparation.

During the degradation evaluation (Figure 11), the static NBC briefly gained mass. This can be explained by an adsorption of salts from the PBS buffer left behind in the samples, which added mass to the material. The salts can form complexes with the cellulose hydroxyls, similar to the mechanism that occurs in depositing hydroxyapatite on cellulose using salt solutions,[24] and increase the sample mass. As time passed, the NBC and OBC exhibited mass loss. Increased degree of oxidation was associated with increased mass loss.

The dynamic degradation measurements showed more dramatic mass loss, but incomplete degradation was still present after a three-month evaluation. Previous reports have shown oxidation of crystalline and amorphous regions of cellulose by periodate,[15,22] but Kim *et al* showed the points of oxidation along cellulose fibers are random.[22] This can leave regions of cellulose unaffected by the periodate treatment and, thus, less favorable to completely degrade in a study such as this. Dialdehyde cellulose has been shown to hydrolyze into degradation products of glycolic acid and 2,4 dihydroxybutyric acid.[20] It should also be noted that at the times for PBS solution changes, the OBC 2 and OBC 3 solutions typically were drifting towards a more acidic pH, indicated by the phenol red indicator in the PBS. This observation also supports the plot of dynamic degradation where these two scaffolds lost the most mass and produced the acidic trend through the acid by-products of dialdehyde cellulose degradation.

A previous study from our laboratory used HEPES buffer under static and dynamic conditions to evaluate native BC and OBC after 14 days at 37^{o}C.[24] Each sample was reduced by nearly 37% while the native BC decreased only 8% under static conditions and 20% under dynamic conditions.[24] The results from the previous study are similar to the results measured here with increased mass loss from dynamic conditions. The mass loss under static conditions can be attributed to the salts in solution promoting degradation via hydrolysis since there were no other significant factors to aid the breakdown of the hydrogels. The weight loss in dynamic conditions is due to mechanical agitation accelerating the degradation process. Li *et al* reported that after 7 days of incubation in PBS, the OBC degrades and becomes more porous.[86] That study showed pore diameter increased to 50-100 μm. This finding is desirable and advantageous since the increased pore diameters provide better means for cell infiltration into the polymer bulk.

The mechanical properties of BC and the varying dialdehyde content OBCs are shown in Figure 12 through Figure 14. The tensile strength and modulus compared between native BC and oxidized BC trends similarly with other reported values.[86] The absolute value of moduli in this study is higher likely due to the testing method. All non-specifically adsorbed water was removed in this study prior to testing, thus reducing the

cross sectional area. From Hooke's law, a reduction in cross section area increases the modulus. The strength is due to the number of fibers in the cross-sectional area in the samples. The simple relationship between fiber count and the strength of the mat explains thicker samples will have greater strength due to a higher number of fibers. The similar mechanical properties between OBC 1 and OBC 2 can be explained by the titration measurement (Table 3), which showed similar degree of oxidation.

The periodate reaction produces a linear chain by opening the glucose ring. The change in flexibility has been reviewed as a function of the root-mean-square end-to-end distance, a measurement of polymer conformation of random coiled polymers.[87] This same explanation can be applied to the trends observed in mechanical testing of periodate oxidized BC. Upon oxidation, an increase in ductility is measured (Figure 14). The ductility, after increasing significantly with mild oxidation, decreases with further oxidation. The increase in ductility can be explained by the polymer chain flexibility from the oxidation process. The ring opening oxidation produces a linear chain of five carbons and an oxygen that can rotate to accommodate a loading force. The loading force causes the C-C and C-O bonds to rotate into a conformation that maximizes length prior to fracture. This process is illustrated in Figure 26. The decrease in ductility can be contributed to local over oxidation of regions along the fiber that produces a more brittle behavior.

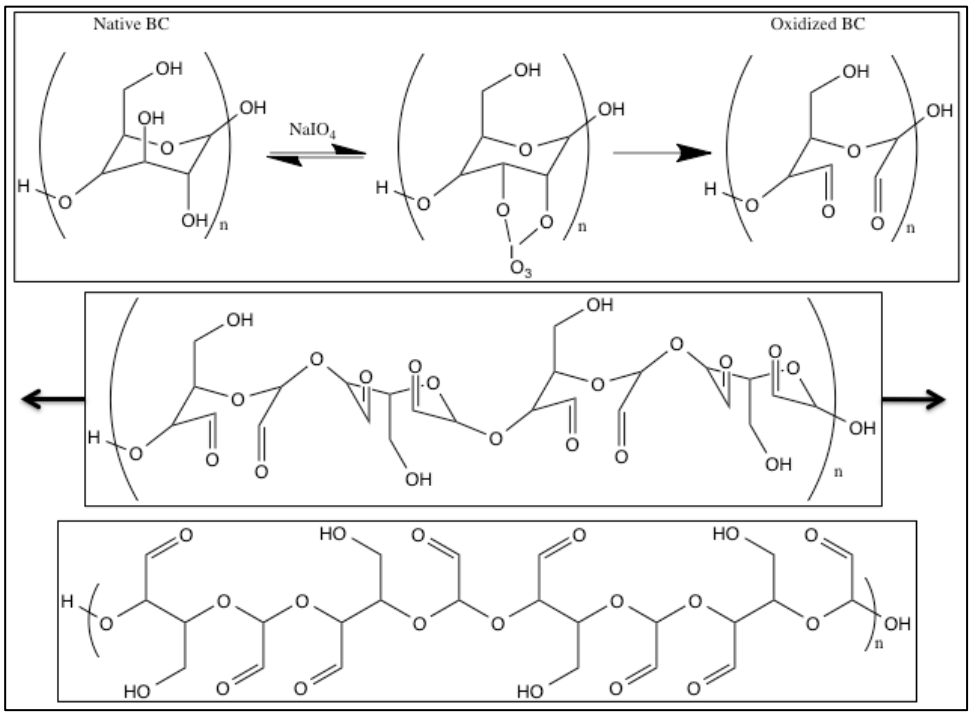

Figure 26: Chain Rearrangement of OBC
This figure summarizes the oxidation process in the top row. The middle row illustrates 4 repeat units of the dialdehyde structure in an arrangement similar to the original ring structure of NBC. Once a load is applied to the structure shown in the middle row, rotations about the C-C and C-O bonds allows for a conformation with an increased length. This diagram helps explain how OBC can exhibit more ductility and undergo greater strain before fracture in comparison to NBC.

2.4.2. In Vitro Model - Cell Culture

The NBC and OBC scaffolds support cell attachment and spreading supported by the following measurements and discussion. The WST-1, Figure 15, measures the number of cells and metabolic activity of cells in culture with the scaffolds. The increased conversion of the reagent on day 7 to the formazan product is a result that can be associated with a larger cell count or more metabolically active cells. On day seven, the absorbance in NBC scaffolds were statistically similar to OBC 1 and OBC 3 scaffolds. OBC 2 is the only scaffold with a statistically significant difference on day seven from other scaffolds. This finding shows that after seven days, cells on OBC 2 were present in higher number or more metabolically active. This analysis, using WST-1, is the best method used in this study to evaluate cell number or metabolic activity of cells on the entire scaffold. The remaining tests used here will evaluate small areas as opposed to the entire scaffold.

All scaffolds demonstrated support of cellular growth with good cell viability, shown by Figure 16. The same images show that OBC 2 and OBC 3 have a greater number of cells present on the spots imaged than NBC and OBC 1. However, this is a cell count in a small area as opposed to the evaluation of the entire scaffold. The OBC 2 and OBC 3 scaffolds show improved spreading of cells on the scaffold, but the light green colors that indicate the spreading do not come through in this report. In order to investigate the cell spreading more accurately, SEM imaging was performed. The SEM images (Figure 19 through Figure 20) show the scaffolds of OBC 2 and OBC 3 are almost completely covered on day seven. The thorough coverage observed by SEM can be explained by improved cell spreading and extracellular matrix production. The production of extracellular matrix has been reported by Wang *et al.*, where MC-3T3 E4 cell lines produced a mineralized extracellular matrix after 10 days of culture.[88] The changes in cell behavior can be attributed to local changes in surface chemistry and fiber modulus where oxidation occurred.

2.4.3. In Vivo Animal Model

A method to repair critical size defects was evaluated. A defect was generated by the removal of bone in the shape of a disk. The defect was generated in the calvaria (skull). The biomaterial composite was then placed into the bone defect site for a period of time to allow bone healing before harvesting the surrounding bone and biomaterial at the defect site for evaluation. The selected animal model for this study was the rat as it has extensive literature for use in similar studies.

This study evaluated four materials through five experimental groups. The experimental groups included 1) a control with an empty defect, 2) NBC, 3) OBC, 4) NBC-CdHA, and 5) OBC-CdHA. These groups were selected as the native BC has previously been shown to be biocompatible, but not bioresorbable. The oxidized BC, produced through periodate oxidation, is believed to be bioresorbable through the resulting chemical modification. The hydroxyapatite was included, as it is believed to promote osseous regeneration. Previous work by Hutchens *et al.* demonstrated the ceramic produced using the synthesis method used here produces HA, shown by XRD diffraction pattern (Figure 27 Left), with a crystal structure similar to that found in native bone with an elongated c-axis (Figure 27 Right).[31]

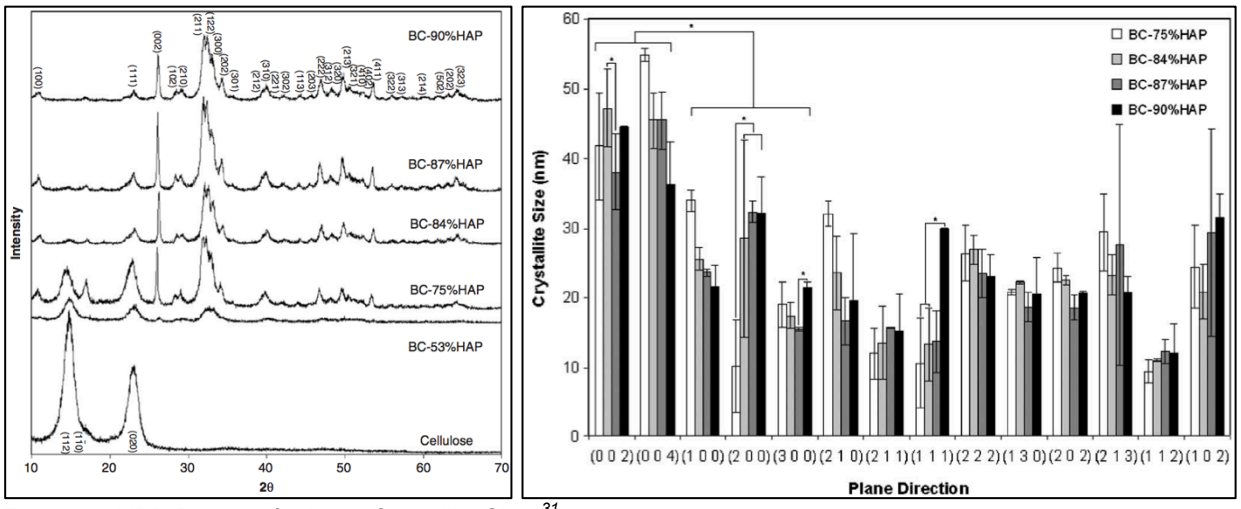

Figure 27: XRD Pattern of HA and Crystallite Sizes[31]
The images are reproduced with permission from Elsevier under license 3258761349499. The x-ray diffraction patterns (Left) are shown with NBC and NBC/HA composites. HA crystallite sizes are shown (Right) with standard deviations shown as error bars. Statistical significance is noted in the image showing elongation on the c-axis ((002) and (004) reflections).

The 6mm defect produced was selected since it is smaller than critical size. Without a bone graft or other bone healing treatment, the defect will heal autonomously. Through comparison between the control group (empty defect) and implant sites where one of the selected biomaterials was placed, no adverse effects were observed. The absence of these adverse effects includes no presence of inflammation or infection.

The staining procedure used in this study was selected since one stain allows for the soft tissue to be visualized and the other stain allows the mineralized tissue to be observed. The lack of bone formation across the defect space in the control animals was expected. The four-week period allowed for healing was sufficient for this study to evaluate the implanted biomaterials, but not long enough for an empty defect to repair itself. As expected, NBC, OBC, and composites of NBC or OBC with CdHA exhibited improved cell growth in the interstitial space between the bone defect edge and the implant over the cell growth and tissue formation observed in the empty defect after 30 days. The implanted scaffolds supported cell growth on the surface without presence of woven bone growth into the bulk of the implanted materials. These observations were confirmed by the surgeon who assisted with the surgeries along with another confirmation from another independent researcher.

A suitable bone substitute must be biocompatible, permit adsorption and proliferation of the bone forming osteoblast cells, be resorbable after performing its function, and promote integration with the surrounding host tissue. The biomaterials (BC, OBC, NBC/CdHA, and OBC/CdHA) tested here have been shown to be biocompatible by the absence of inflammation or infection in the animal model. The material also showed the ability to allow adsorption of bone cells. However, it did not show good host integration. Therefore, a modification in material production must be made to promote better cell infiltration into the material bulk to improve host integration.

2.4.4. Macroporous BC-CdHA Scaffolds

BC scaffolds exhibit a porous structure on the nanoscale; however, for cell migration and proliferation into the scaffold, the porosity must be on the microscale (i.e. 100-350 μm). In order to make the scaffolds more accommodating for cell penetration into the bulk material, a more porous structure must be engineered. The ability to form CdHA rosettes on the material throughout the scaffold is also of interest.

In order to engineer greater porosity into scaffolds, the porogen/particle-leaching technique has been very popular for various applications. The technique was employed to produce macroporous BC, shown in Figure 24. The results are similar to previous reports using sieved (90-500 μm) paraffin microspheres with BC.[6,78] The size of the voids produced in this work are slightly smaller than the 342 μm diameter porogens used. This is due to a lack of control in the production of the fracture surface imaged. The fracture surface is likely going through areas where the maximum diameter of the void is not present. This leads to an image that shows voids slightly less than the diameter of the original porogen.

The porogen used was selected by accounting for the solvent necessary to remove the microspheres from the cellulose matrix. An appropriate solvent will not alter the cellulose or the overall cellulose structure. The solvent was selected using the solubility parameters of cellulose, polyethylene, and solvents. Xylene was selected due to its hydrophobic nature, allowing the solvent to dissolve the polyethylene microspheres and leave cellulose unaffected. This is supported by the solubility parameters listed in Table 1. As listed in the table, xylene does not possess polar forces (δ_p) or hydrogen bonding (δ_h), while cellulose has polar forces and hydrogen bonding.

The overall solubility parameters (δ) of cellulose and xylene are also significantly different, showing unfavorable affinity between xylene and cellulose. Cellulose even resists going into solution with thermodynamically favorable polar solvents due to extensive hydrogen bonding in cellulose.[14,89] *N,N*-dimethyl acetamide (DMAc) with LiCl is one of the few systems that can dissolve cellulose without depolymerizing the cellulose.[90] The DMAc/LiCl system utilizes cations to coordinate with cellulose hydroxyl groups and break the hydrogen bonds. Xylene cannot modify or dissolve cellulose since the components are thermodynamically unfavorable for mixing, and the solvent does not possess the ability to break the cellulose hydrogen bonds.

As an additional step, CdHA was deposited onto the BC fibers of the microporous scaffold, shown in Figure 25, to produce the first reported BC/CdHA macroporous scaffold. The macroporous BC/CdHA scaffold can be further improved by producing an interconnected structure by sintering the microspheres, similar to methods previous reports have used for interconnected structure formation.[91] An interconnected structure will allow for cells to infiltrate the bulk of the scaffold and speed tissue regeneration. A study with stem cells showed varying cell motility dependent on pore diameter.[92] The optimum porogen size and interconnection diameter must be determined for BC and the cell type.

2.5. Conclusions

The OBC characterization study showed that OBC could be tailored to meet various application needs. The mechanical testing showed the ability to tailor mechanical properties by varying the degree of oxidation, thereby altering the modulus, tensile strength, and ductility of the hydrogel. Additionally, the degree of oxidation was shown to be a factor in the degradation profile of the material. Furthermore, the evaluation supported that the materials are bioresorbable due to the measured decrease in mass with time at physiological pH. The use of OBC as a bone scaffold was shown through WST-1 and SEM testing to be possible as preosteoblastic cells performed best on 20mmol periodate oxidized BC. Lastly, an animal model evaluating NBC, OBC, BC/CdHA, and OBC/CdHA demonstrated the materials performed well in a bone healing application through their support of new tissue growth and absence of

infection or inflammation. The performance of the materials can be improved in future evaluations by generating the macroporous structure with deposited CdHA to allow for improved tissue regeneration throughout the material.

Chapter 3
Bone Scaffolds: A Hydroxyapatite Powder from Bacterial Cellulose

*The following chapter was published under "Biomimetic Hydroxyapatite Powder from a Bacterial Cellulose Scaffold". The work is reprinted here with permission from Springer under license 3258391473019. The work remains mainly from the published article with some additions of greater detail.

3.1. Introduction

BC and CdHA have received much attention as biomaterials due to their excellent properties. BC/CdHA composites have been formed and investigated for bone regeneration applications. However, these composites have limitations. Bacteria are cultured and cellulose forms at the air-liquid interface. The BC increases in thickness with time and has the width and length of the container it is cultured in. The BC is unable to attain the complex shapes that are formed at injury and implant sites. Still, the CdHA produced by precipitation on BC is ideal since it possesses a calcium deficiency allowing for it to be resorbed under physiological conditions. Therefore, it is desirable to find other applications for the biomimetic CdHA. One other application for the CdHA is as filler in injectable systems.

The production of CdHA powder from BC/CdHA can be produced using a method that degrades BC. Cellulose can be dissolved using N,N-dimethylacetamide and 1-butyl-3-methylimidazolium chloride[93] or LiCl[90], but residual solvents in biomaterials are always a concern. Two other methods to remove cellulose from a composite include pyrolysis or enzymes. Cellulose is volatilized or turns into a char by-product by pyrolysis. The volatilized products include water, carbon monoxide, carbon dioxide, hydrogen, oils, and hydrocarbons.[94] Factors including the heating rate, temperature, and environment each control the products formed by pyrolysis. Char is minimized by high heating rates and high final temperatures.[94] An oxidizing environment reduces the mass retained. BC can approach zero mass with temperatures above 450°C.[95]

Cellulases are common, heavily studied[96], commercially available enzymes that breakdown cellulose.[97] *Trichoderma reesei* is composed of three enzymes (endocellulase, exocellulase, and cellobiase) that convert cellulose into glucose.[98] Each

enzyme in *Trichoderma reesei* has its own specific role in converting cellulose to glucose, shown in Figure 28. Crystalline, hydrogen-bound cellulose is degraded into linear, amorphous chains of cellulose by the hydrolysis of hydrogen bonding via endocellulase. Cellobiose is produced from cellulose chains through the exocellulase enzyme. Glucose is formed by cellobiase from cellobiose.

This investigation aims to produce biomimetic CdHA powders by using an enzyme or heat to degrade cellulose from BC/HA composites. The powders will be analyzed using SEM, EDX, FTIR, and TGA. SEM will be used to ensure the rosette morphology of the composite is retained. EDX will be used to verify the calcium-deficient morphology is unchanged from the processing. FTIR and TGA will measure the residual material left from each degradation method by chemical and mass composition, respectively.

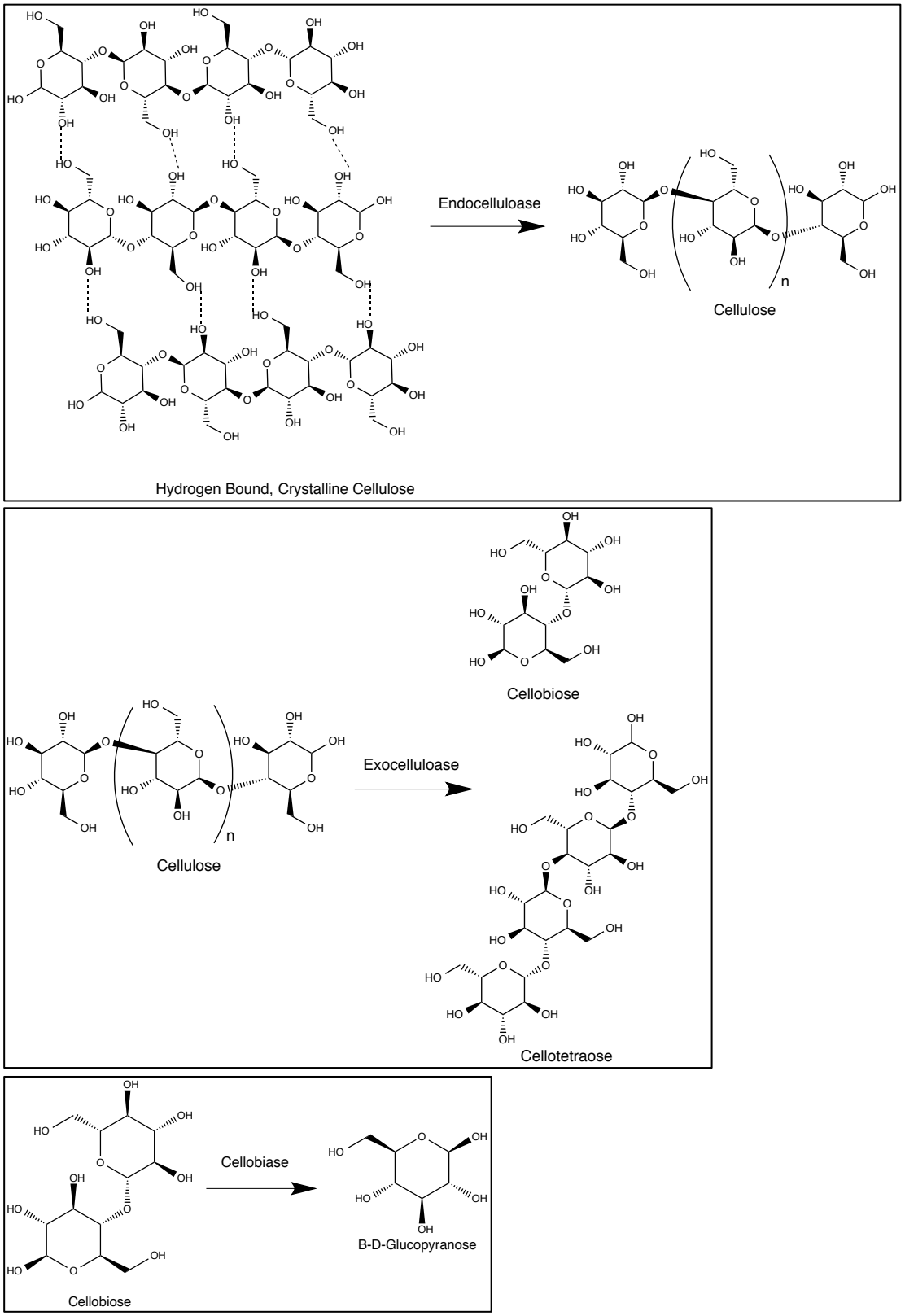

Figure 28: Cellulase Component Roles
This figure illustrates the role of each of the three (endocellulase, exocellulase, and cellobiase) cellulase enzymes. It should be noted that the repeat units for crystalline cellulose were omitted for simplicity of the illustration.

3.2. Experimental

3.2.1. Material Preparation

3.2.1.1. Bacterial Cellulose Synthesis

Gluconacetobacter sucrofermentans from the American Type Culture Collection (Manassas, VA, USA) (ATCC 700178) was obtained for use in this work. 24-well cell culture plates were used to culture pellicles of BC of 1.6 cm in diameter and grown to a thickness of 0.5 cm at the air-liquid interface after 14 days of growth in Schramm-Hestrin media with mannitol as the sugar source.[79] Cellulose purification was achieved by a 4 hour wash in 4% sodium dodecyl sulfate solution at 70°C followed by a 4 hour wash in 4% sodium hydroxide solution at 70°C. Sequential Millipore water washes were performed until the solution pH was neutralized.[80]

3.2.1.2. Calcium-Deficient Hydroxyapatite Deposition

CdHA deposition was performed by sequential immersion in 100mM $CaCl_2$ and 60mM Na_2HPO_4 aqueous solutions.[31] BC was incubated in each salt solution for a period of 12 hours at 23°C and switched to the other solution. One CdHA deposition cycle was defined as the treatment of BC undergoing one incubation in $CaCl_2$ solution followed by one incubation in Na_2HPO_4 solution. Higher cycle depositions were achieved by repetition of the salt solution incubations. BC/CdHA samples subjected to 1, 3, and 5 cycle depositions were prepared for this study.

3.2.1.3. Enzymatic Degradation of BC

Trichoderma reesei (ATCC 26921, Worthington Biochemical Corporation) with 25 units per dry milligram were placed in solution with Millipore water at 0.05 mg/mL and 0.1 mg/mL. Each solution had acetic acid added until a pH of 5.0 was achieved where the enzyme was at optimum conditions for its activity. BC and BC/CdHA samples were placed in respective solutions, separately, for 21 days. The residual materials were harvested after the incubation period by centrifugation at 1,000 rpm and washed three times with fresh Millipore water to remove residual glucose and enzymes. The BC control cultured with the enzyme did not produce a pellet upon centrifugation. Samples were frozen at -80°C, lyophilized, and then characterized.

3.2.1.4. Thermal Degradation of BC

Five-cycle BC/CdHA composites were placed in a covered container to prevent debris from contaminating the samples. The composite was placed in a furnace at 500^{o}C for one hour in air.

3.2.2. CdHA Powder from BC-CdHA Composites Characterization

3.2.2.1. Scanning Electron Microscopy (SEM)

Each material for SEM investigation was frozen using a -80^{o}C freezer and lyophilized for at least 24 hours. Samples were mounted using carbon tape and sputtered with gold using a Spi Module Sputter Coater (Spi Supplies, Westchester, PA) at 20 milliamps for 10 seconds. A LEO 1525 Scanning Electron Microscope (Zeiss, Oberkochen, Germany) was used to image materials using minimal excitation voltage to avoid charging effects during SEM examination.

3.2.2.2. Energy Dispersive X-Ray Spectroscopy (EDX)

Elemental microanalysis of BC, BC/CdHA composites, enzyme treated BC/CdHA composites, and a thermal treated BC/CdHA composite was performed using the LEO 1525 SEM with a Link Pentafet detector and analyzer from Oxford Instruments. Each EDX spectrum was produced using an acceleration voltage of 20kV and collected for 30 seconds or more.

3.2.2.3. Fourier Transform Infrared Spectroscopy (FTIR)

Each starting material and enzyme or thermally treated composite was frozen using a -80^{o}C freezer and lyophilized for at least 24 hours. Moisture was removed from the pellicles using a vacuum oven. The material was ground into KBr and formed for analysis using a screw-type press to produce a pellet. A total of 256 co-added scans were collected using a BioRad FTS6000 Spectrometer (Varian, Palo Alto, CA, USA) at a resolution of 4 cm^{-1}. The CdHA 1032 cm^{-1} phosphate vibration and the BC 1435 cm^{-1} CH_2 bending peak were analyzed to evaluate the removal of cellulose from the original cellulose-hydroxyapatite composites.

3.2.2.4. Thermal Gravimetric Analysis (TGA)

A Mettler TA 4000 TGA was used to evaluate materials under heating conditions. Starting materials of BC, 1 cycle BC/CdHA, and 5 cycle BC/CdHA composites were tested and used as baseline data for comparison to the results from enzyme treated or thermally treated composites. The TGA was purged using nitrogen at 40 mL/min with a sample heating rate of 10°C/min.

3.3. Results

3.3.1. Characterization of CdHA Powder from BC-CdHA Composites

3.3.1.1. Scanning Electron Microscopy (SEM)

Images are presented of native BC and BC/CdHA composites and are as expected from previous publications.[31] The nanofibrous and nanoporous structure of the BC is presented in Figure 29A and shows an average fiber diameter of 34 nm. Figure 29B and C show composites with cellulose fibers covered with ceramic rosettes of hydroxyapatite. As the cycles were repeated, the rosettes grew larger. This is shown in Figure 29C, which shows the 5 cycle BC/CdHA composite. A 5 cycle BC/CdHA that was thermally treated is presented in Figure 30. The image reveals the original rosette structure of nanoscale ceramic plates remains intact with no observable presence of the original underlying cellulose fibers.

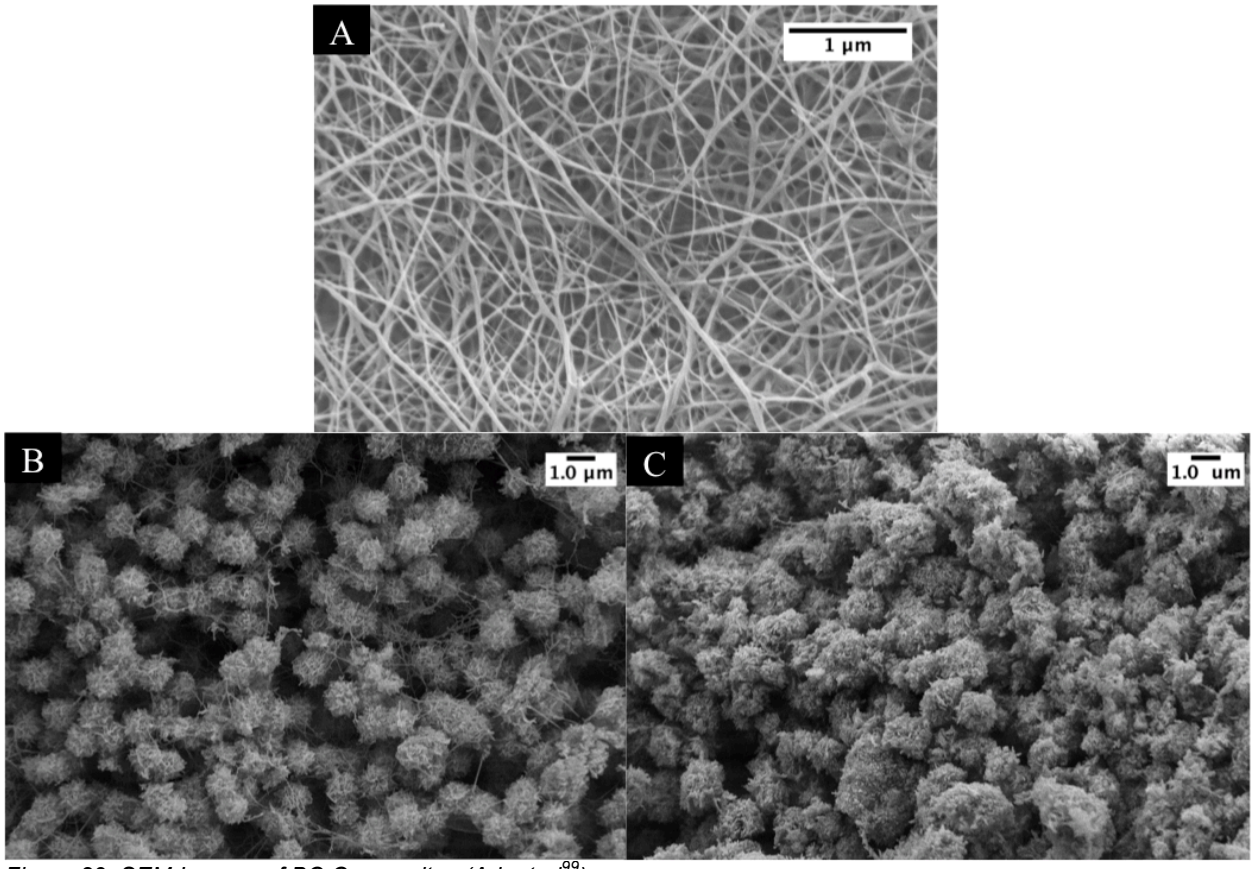

Figure 29: SEM Images of BC Composites (Adapted[99])
Native BC (A), 1 Cycle BC/CdHA (B), and 5 Cycle BC/CdHA (C).

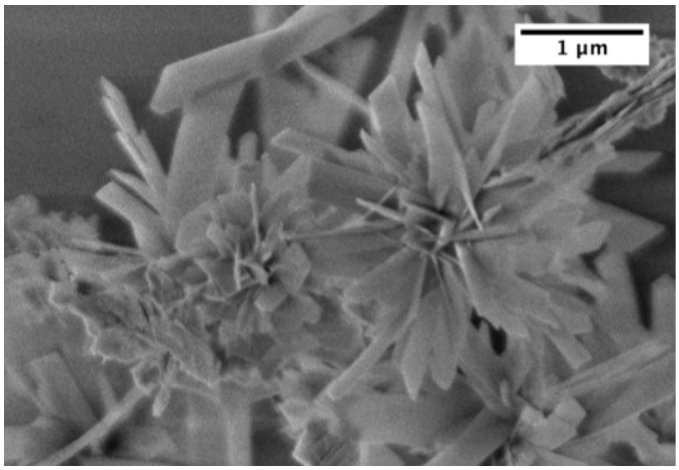

Figure 30: Five BC/CdHA Composite SEM Image After Heat Treatment (Adapted[99])
This high magnification image shows the retained structure of the composite after exposure to a 500^{o}C environment.

Similarly, images are presented in Figure 31 and Figure 32 to qualitatively access the effectiveness of the enzyme treatment. Each image shows small bunches of HA plates. The dimensions of the plates are 600 nm or smaller, and the plates are still intact after the purification step of centrifugation.

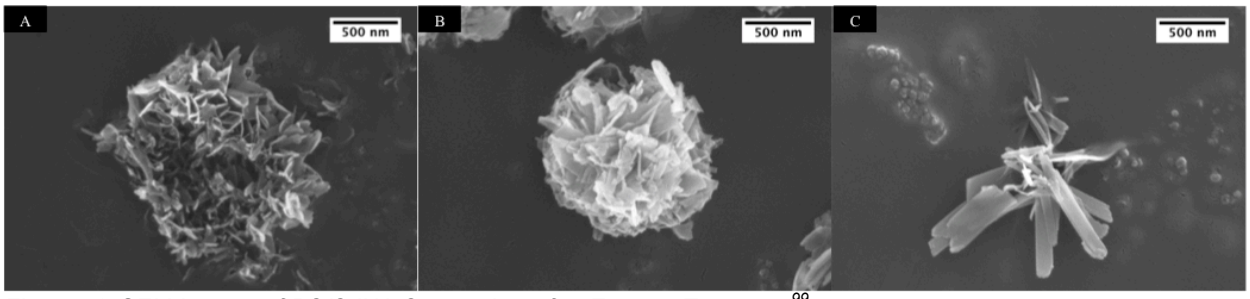

Figure 31: SEM Images of BC/CdHA Composites after Enzyme Treatment[99]
These images are from BC/HA composites of 1 (A), 3 (B), and 5 cycle composites after treatment in an enzyme solution of 0.05 mg/mL.

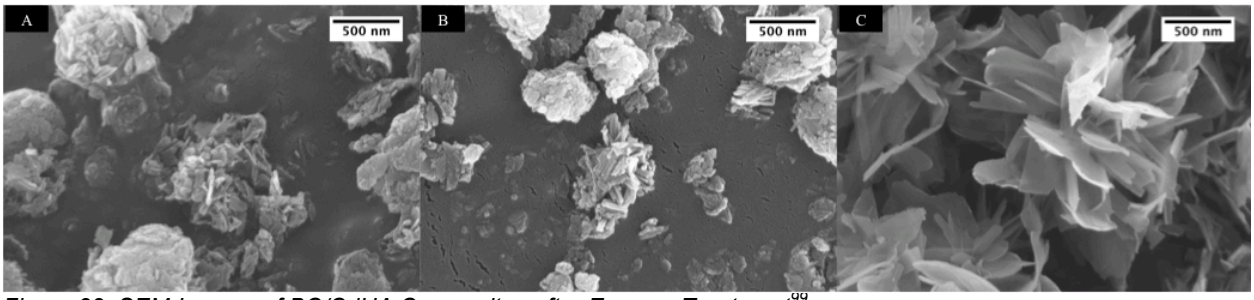

Figure 32: SEM Images of BC/CdHA Composites after Enzyme Treatment[99]
These images are from BC/HA composites of 1 (A), 3 (B), and 5 cycle composites after treatment in an enzyme solution of 0.1 mg/mL.

3.3.1.2. Energy Dispersive X-Ray Spectroscopy (EDX)

EDX was performed on the original BC/CdHA composites and composites after treatment with the enzyme or heat. The method was used to evaluate calcium phosphate ratios by acquiring five measurements on each sample, shown in Figure 33. Each calcium phosphate ratio is presented as an average with 95% confidence intervals shown. All values fall between 1.33 and 1.67, indicating that all hydroxyapatite is calcium-deficient.

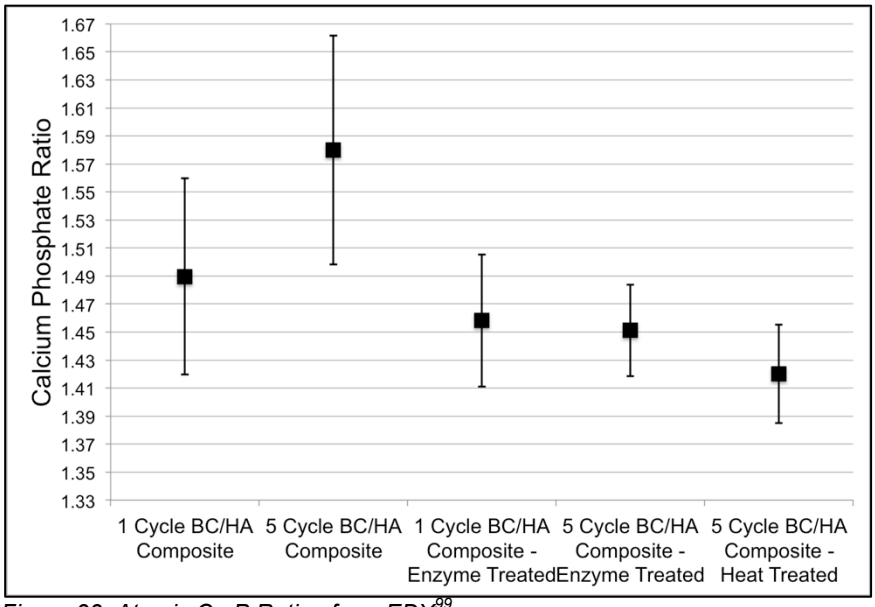

Figure 33: Atomic Ca:P Ratios from EDX[99]
Average Ca:P ratios with 95% confidence interval of the original Composites and enzyme cultured and thermally treated samples.

3.3.1.3. Thermal Gravimetric Analysis (TGA)

TGA was analyzed to determine the composition of BC/HA composites after culture with the enzyme and after heat treatment. As a baseline measurement, NBC and original BC/HA composites were also tested. The results are presented in Figure 34. NBC retained just 7.8% of its original mass from heating to 600^{o}C. Additionally, BC/HA composites of 1 and 5 cycles of deposition retained 53.6% and 88.4%, respectively. Using these results, it was determined that 1 and 5 cycle BC/HA was 53 wt% and 90 wt% HA (Table 4). These values are necessary for analysis to determine residual BC in enzyme cultured and heat treated samples. Figure 35 shows the efficiency of the purification method by reporting the percent of BC material that was not removed from the composites. The enzyme was less effective than the heat treatment in removing cellulose.

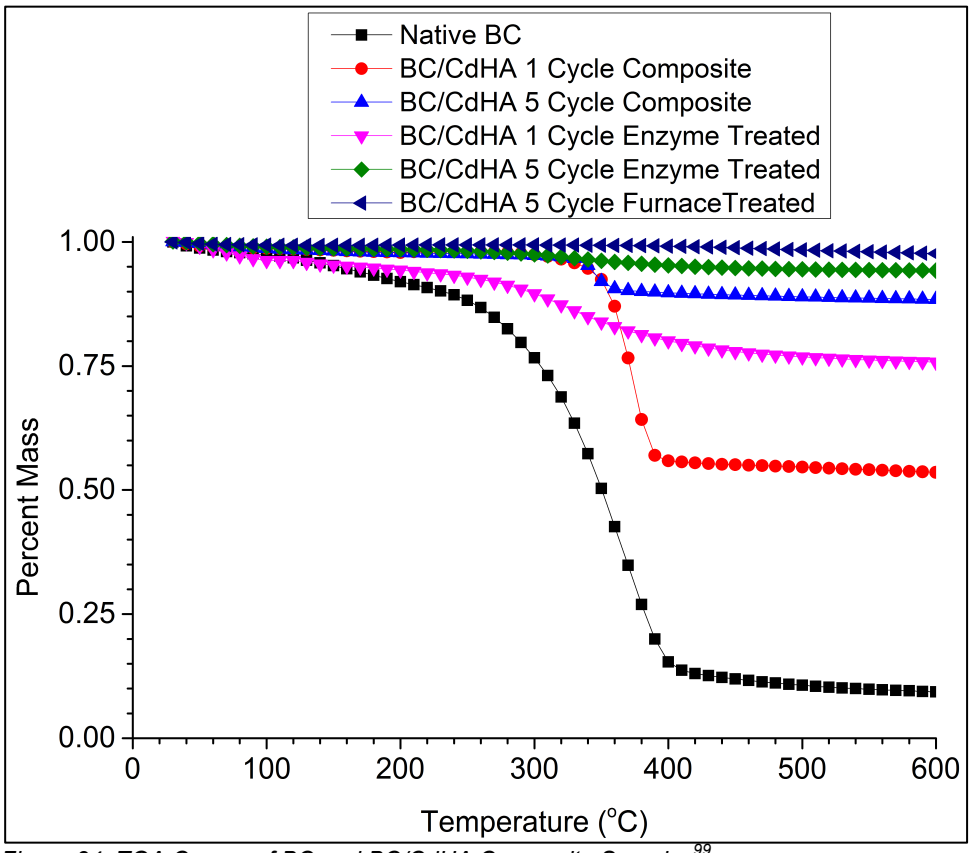

Figure 34: TGA Curves of BC and BC/CdHA Composite Samples[99]
This figure shows the TGA mass loss curves for the starting materials and the composites after incubation with the enzyme or after thermal treatment.

Table 4: Composition of CdHA in BC/CdHA Composites, Determined by TGA

Sample	Weight Percent CdHA
1 Cycle BC/CdHA	53
5 Cycle BC/CdHA	90

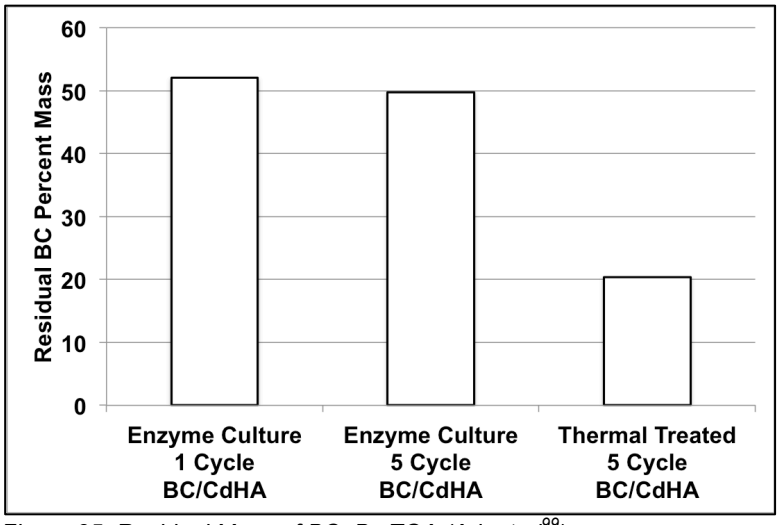

Figure 35: Residual Mass of BC, By TGA (Adapted[99])
This figure shows the residual mass from BC in composites treated with the enzyme or with heat. The values determined by the mass based TGA measurement.

3.3.1.4. FTIR of BC, BC/CdHA Composites, and Enzyme and Thermally Treated Composites

FTIR was used to characterize residual material in composites that were treated with the enzyme or by heat. The analysis produces a similar result as TGA, but this technique provides a measurement based on chemical composition. FTIR spectra, shown in Figure 36, exhibited peaks of NBC that were masked by CdHA absorption bands. As a baseline for anlaysis, NBC and BC/CdHA composites were evaluated. Cellulose removal was determined by the HA phosphate vibrational mode at 1032 cm^{-1} and the BC symmetric CH_2 bending at 1435 cm^{-1}. Figure 37 shows the residual cellulose as a percentage of the cellulose in the original composite. The FTIR reveals less residual cellulose by enzyme and thermal methods than measured by the TGA. Additionally, the FTIR shows a dependence on the original composite composition on the amount of BC that is removed.

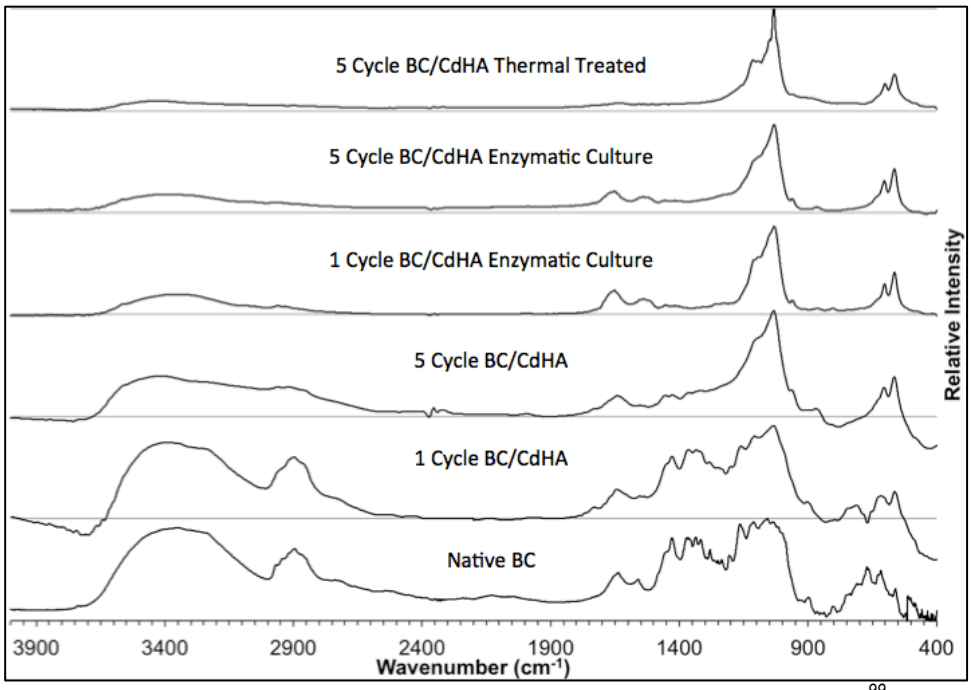

Figure 36: FTIR Spectra of BC, Composites, and Degraded Composites (Adapted[99])
FTIR spectra from native BC, 1 & 5 cycle BC/CdHA composites, 1 & 5 cycle BC/CdHA composites incubated with the enzyme at 0.1 mg/mL, and 5 cycle BC/CdHA composite heat treated are presented here. The trend of absorption masking by CdHA is observed with specific interest in measuring changes the 1032 cm^{-1} phosphate vibration from CdHA and 1435 cm^{-1} CH_2 bending from BC. The same FTIR absorption bands were used to evaluate residual organic material after processing.

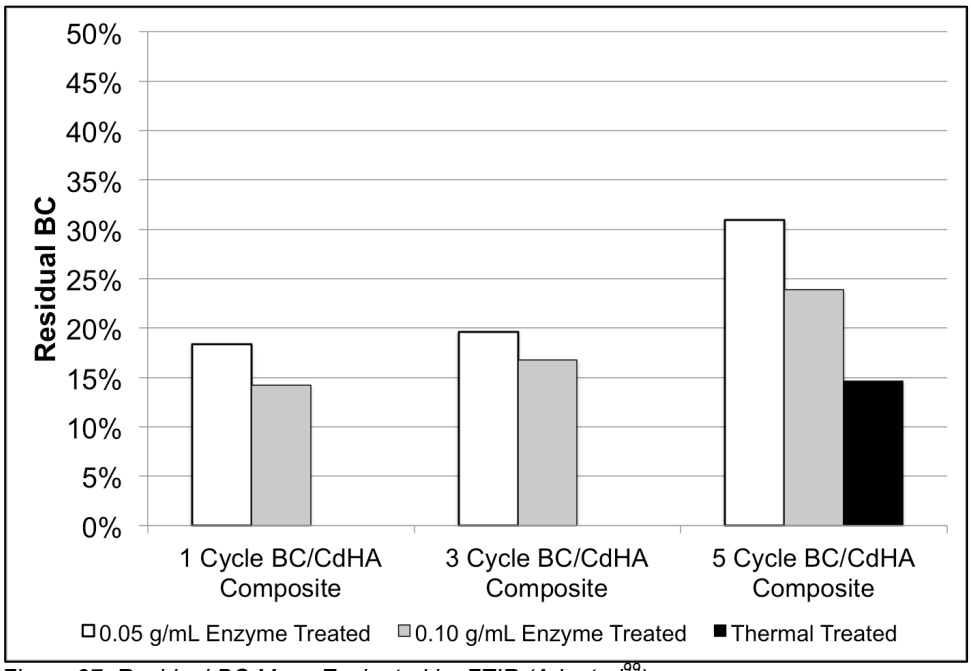

Figure 37: Residual BC Mass Evaluated by FTIR (Adapted[99])
These values represent remaining organic material indicated by the peak at 1435cm^{-1}. Each enzyme culture or thermal treated sample used its original composite FTIR spectra as a baseline for the calculation.

3.4. Discussion

The effectiveness of two different methods to produce the CdHA powder from the original BC/CdHA composite is presented below. SEM was used for qualitative analysis, EDX was used to evaluate Ca:P ratio, FTIR was used to evaluate chemical composition, and TGA was used to evaluate mass composition. The SEM images displayed a ceramic material with rosette structure of CdHA that is retained post treatment. The EDX revealed Ca:P ratios similar to the untreated BC/CdHA composite and similar to the composition in calcium-deficient hydroxyapatite. The TGA and FTIR showed residual BC by varying values depending on the method of analysis.

SEM images in Figure 29 show BC and 1 and 5 cycle BC/HA composites. The BC is shown to be a nanofibrous mat while the composite show rosettes of HA with size dependent on the number of cycles of incubation. One method used to remove cellulose was heat, and its SEM image is presented in Figure 30. It is shown that clusters of HA remain with micro and nano-scale dimensions. Since densification of HA occurs above 900^{o}C [100] and biphasic forms of HA and β-TCP from bulk material transformations occur

above 700°C[100,101], a temperature of 500°C was used in this study. The SEM images show the morphology of HA is unchanged after heat treatment; however, since heat can cause a phase transformation, EDX was used to generate a Ca:P ratio that provides information about the calcium deficiency of the hydroxyapatite. The Ca:P ratios are presented in Figure 33 and show no statistically significant difference between the original composite ratio and the heat treated ratio. Additionally, the ratio produced is within the range of calcium-deficient hydroxyapatite. CdHA can range in Ca:P ratios between 1.33 and 1.67 with stoichiometric hydroxyapatite exhibiting a 1.67 ratio.[102] Additionally, from previous work, the procedure used in the study has been shown to produce CdHA rather than another form of calcium phosphates, such as β-tricalcium phosphates.[31] The data presented here supports and is consistent with calcium-deficient hydroxyapatite.

The lack of pellet production during purification of the BC control enzyme cultured sample is evidence that the BC was degraded sufficiently into its glucose monomers to not leave a significant amount of cellulose after the incubation period. Figure 31 and Figure 32 show BC/CdHA samples after incubation with the enzyme. A notable qualitative trend is the more tightly clustered hydroxyapatite plates in 1 and 3 cycle samples versus the 5 cycle composite samples. The growth of this material must be taken into account as the ceramic is nucleated at a site and grows out radially from the nucleation site. In lower stages of growth, the plates are not separated by considerable distance since the crystals are small. As growth continues, the plates gain greater separation from adjacent plates.

TGA was used to evaluate the remaining material after thermal or enzyme incubations. Figure 34 shows the mass loss curves for each sample. Only small mass losses are observed below 100°C and can be attributed to adsorbed moisture. Depolymerization of cellulose begins around 250°C due to glycosidic bond thermolysis. The most significant mass loss region in native BC is centered at 363°C, shown by the peak in the first derivative mass loss curve in Figure 38. Once the glycosidic bonds begin breakdown above 250°C, they produce charged species. The charged species either volatilize and results in further mass loss or are transformed into a char product that is retained as mass. The charged species can be volatilized into a gas phase

through an intermediate intramolecular cyclization. However, the presence of water alters the reaction path to an alternate route where cellulose is hydrolyzed by the charged species and yields char.[103]

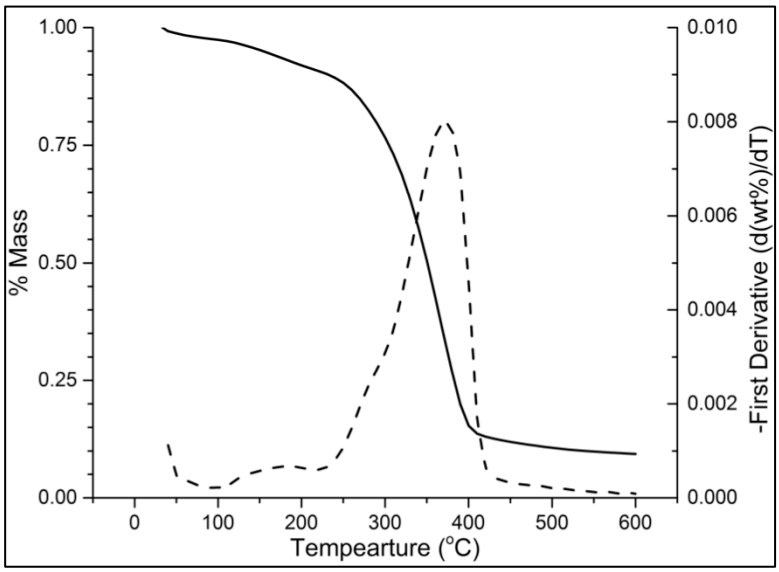

Figure 38: TGA and First Derivative Curves of NBC
This figure shows the TGA mass loss curves for the native BC and the first derivate of the mass los curve for the same native BC sample. The figure indicates peak mass loss takes place at 363°C.

The retention of 8% original mass for BC is expected due to a low heating rate and an inert atmosphere during testing. The retained mass is due to a char product that would be reduced if the heating rate was increased or an oxidative atmosphere was used. Examination of the composite mass loss curves is as expected when taking into account the starting composition of the composite, knowing the polymer will have 8% mass retained, and the ceramic will have no mass change over the testing temperature. To allow for quantitative analysis of the TGA curves of enzyme and thermally treated samples, the original composite TGA curves must be reviewed. The original composition by mass has previously been reported for 1 and 5 cycle BC/CdHA with 47 and 10 weight percent cellulose, respectively.[24] The TGA curves reflect similar values at 600°C once the 8% mass retention is taken into account.

HA is not expected to lose mass upon heating up to 600^{o}C. Therefore, the observed mass loss in TGA measurements can be attributed to the organic components in the material, indicating incomplete removal of BC from the original BC/CdHA composite. Incomplete degradation by the enzyme results in incomplete depolymerization of cellulose chains. Residual organic material by the thermal method leaves behind a char product that is carbonized during TGA testing. In order to maximize cellulose removal by the thermal method, an air environment was used in order for cellulose to oxidize into vapors and minimize the char by-product.

FTIR provides a method to analyze chemical composition, whereas TGA evaluates composition by mass. Similar to the TGA results, the FTIR results show (Figure 36) more efficient removal of cellulose by the thermal method. Also, the concentration of the enzyme is critical as the higher concentration of enzyme was shown to be more productive in removing a greater percentage of cellulose. The composition of the original composite was also a factor in cellulose removal. Higher compositions of CdHA in each starting composite yielded a greater residual percentage of cellulose.

A possible explanation of cellulose removal decreasing with increasing HA composition in the original composite is hinged on the enzyme being inhibited from access to the cellulose. In this scenario, the enzyme is denied access to cellulose by the larger surface area CdHA plates. The ceramic nucleation on BC to form the composites of BC/CdHA can result in an encapsulated polymer fiber by the ceramic. This process would prevent enzyme access to the organic surface.

Enzyme cultures, by data from the manufacturer, were set up to completely degrade in just a few days based upon the reported degradation rate. However, after three weeks of allowing the enzymes to breakdown cellulose, incomplete cellulose removal was found by TGA and FTIR. HA limiting the enzyme access to cellulose is one explanation. Another is the composition of the cellulase enzyme. Shown in Figure 28, the enzyme used here is effective in breaking down cellulose, but BC is different from most other cellulose sources in its high degree of crystallinity. BC's degree of crystallinity can vary between 70 and 89%.[12,104,105] Using a typical enzyme composition, the extensive hydrogen bonded cellulose structure limits the ability of the enzymes

efficacy as a rate-limiting step. This can be corrected in future work by using a larger concentration of endocellulase in the enzyme mixture to speed the breakdown of crystalline cellulose.

The thermal treated sample exhibited the least residual cellulose by FTIR and TGA. Still, the result can be improved by modifying the processing conditions. The air environment is desirable as the oxygen favors vaporization of cellulose into gases. However, the moisture content of the air environment was not a variable that was controlled in this experiment. Water vapor favorably adsorbs onto the hydroxylated cellulose fibers. The presence of water plays a role in converting an intermediate charged species from a path that favors vaporization to a path that converts the charged species into a char product. Future limitation of the humidity of the air environment can further improve the cellulose removal by heat treatment.

3.5. Conclusions

The study demonstrates that cellulase enzymes and heat treatments can be effective methods to produce powdered CdHA from BC/CdHA composites. TGA and FTIR showed different quantities of residual cellulose based upon the principle of the measurement. It is not believed that the residual cellulose from the enzyme purification method is harmful as the enzyme degrades BC into cellulose, cellobiose, and glucose. A lower quantity of residual cellulose was found by using heat as the removal method. Methods to improve the cellulose removal were discussed.

Chapter 4
Polyurethane BC Composite

4.1. Introduction

Venous valves are a critical component for returning blood flow back to the heart. When these valves fail in humans, they are revealed as varicose veins. The undesirable appearance of varicose veins is due to an increased pressure in the vein. Blood exerts a hydrostatic pressure that increases 0.77 mmHg for every centimeter of blood column height.[106] Failing valves cannot reduce the large pressures in the venous system or prevent the backflow of blood away from the heart. A synthetic material to restore the natural venous valve function will have to meet strong mechanical property and hemocompatibility demands.

Chronic venous insufficiency (CVI) is caused by the incompetence of venous valves. CVI is diagnosed as primary valvular incompetence in 20% of cases and as secondary valvular incompetence in the other 80% of cases.[34,106] CVI is estimated to effect seven million people in the U.S. alone.[107] The need for a synthetic material to restore valve function has significant commercial potential since there are no approved materials or valves for the treatment of venous insufficiency.

The incompetence of the valve can lead to a venous valve being unable to relieve elevated static venous pressures. The high pressures lead to deformation of the veins and capillaries.[33] Primary valvular incompetence can be resolved by valve repair, but the procedure is a limited option due to leaflet damage.[108,109] However, the more common secondary valvular incompetence requires a new valve since the leaflet is destroyed in this scenario. Remedies for this approach exist, but are limited as a result of scar tissue formation.[110]

4.1.1. Existing Artificial Venous Valves

The approaches for valve replacements to this point have failed in animal trials or had minimal clinical success. Attempted materials include titanium/platinum[111] and a bioprosthetic[112,113] that failed due to neointimal hyperplasia (abnormal new tissue growth over an implanted material or device) and a xenograft that failed due to thrombosis.[114] Currently two universities are developing artificial prostheses. The first

still needs to be evaluated in an animal model[115], and the second requires a biocompatibility evaluation after it passed the simulated *in vitro* testing.[116] Thus, there is a need for a material to meet the mechanical and blood compatibility demands. This study will evaluate a polymeric composite aimed at taking advantage of the mechanical properties of nanofibrous BC nonwoven mats and the hemocompatibility of poly(propylene glycol) (PPG) based polyurethanes to produce synthetic composites that can serve as venous valve leaflets.

4.1.2. Fiber Reinforced Composites

Cellulose is ideal for use in composites due to the renewable sources and high modulus associated with the crystalline cellulose. The modulus for cellulose crystallites that are parallel with the fiber axis is 167.5 GPa.[117] The cellulose source, impurities, or low crystallinity can greatly decrease the measured moduli of cellulose. Therefore, techniques are used to remove the impurities and amorphous cellulose. The most common method is microfibrillation, which was first reported in 1983.[118,119] Articles vary on the exact dimensions of microfibrillated cellulose (MFC), but these cellulose fibers are approximately 10-50 nm in diameter, at least one micrometer in length, and have an approximate aspect ratio of 100-150. MFC sources are abundant and include tunicate, cotton, ramie, sisal, straw, bacterial cellulose, and sugar beet.[120] The production of MFC can vary depending on the raw material used, but nearly all utilize a mechanical treatment to form the MFC.[121]

Bacterial cellulose is an ideal cellulose source since it has been reported that the modulus of single filaments can be as high as 114 GPa.[122] Sheets of anisotropic BC fibers have been reported to have properties as high as 30 GPa[123] with stress-strain response similar to carotid arteries.[77] The submicron dimension of BC allow for a large surface area for interaction with other materials. The interaction between the BC fibers and a polymer matrix is a key factor in composite design. These promising properties make BC an ideal candidate to combine with another polymer matrix to tailor properties for an application.

MFC in PU matrices have been shown to be effective strengthening components One study showed 500% increase in strength and 3,000% increase in modulus with just 16 wt% MFC in PU.[124] Another report showed the effective use of polyurethane

elastomers with cellulose nanocrystals as a filler.[125] The study showed effective increases in the tensile strength of 62 MPa and modulus of 44 MPa from original values of 8 MPa and 7.5 MPa, respectively, that were able to undergo high strain prior to fracture. However, these studies have used wood and plant cellulose sources while BC can further enhance the properties due to its high crystallinity, superior mechanical properties, and more mild purification process compared to other cellulose sources.

Some work has been performed with BC fiber-fiber composites[126], but only fiber reinforced polymers using BC will be discussed here. BC has been used in optical applications to reinforce acrylics.[127] One study showed improvement of PLA stiffness by compounding the material with ground BC.[128] A study using BC nonwovens and a phenolic resin demonstrated how BC was more effective in enhancing the properties of the composite over MFC.[129] Composites of BC and cellulose acetate butyrate with 32 vol% reinforcement showed nearly 400% increase in strength, 2% increase in strain, and nearly 300% increase in modulus.[130]

The approach in this work will be to use BC in its native form (i.e. nonwoven mat), not as dispersed MFC. Additionally, the native BC nanofiber nonwovens will be coated with polyurethane for hemocompatibility. The polyurethane also serves to improve the ductility of the composite. As previous studies indicate, PPG based PUs perform well in blood contacting applications. PPG will be used as the soft segment in the PU to produce a BC/PU composite.

4.2. Experimental

4.2.1. Material Preparation

4.2.1.1. Bacterial Cellulose Synthesis

Gluconacetobacter sucrofermentans from the American Type Culture Collection (Manassas, VA, USA) (ATCC 700178) was obtained for use in this work. 24-well or 96-well cell culture plates were used to culture pellicles of BC of 1.6 cm in diameter and grown to a thickness of 0.5 cm at the air-liquid interface after 14 days of growth in Schramm-Hestrin media with mannitol as the sugar source.[79] Cellulose purification is achieved by a 4 hour wash in 4% sodium dodecyl sulfate solution at 70^{o}C followed by a 4 hour wash in 4% sodium hydroxide solution at 70°C. Sequential Millipore water washes are performed until the solution pH was neutralized.[80]

4.2.1.2. HDI End Capped PPG Prepolymer Synthesis

The polyether prepolymer is a hexamethylene diisocyanate (HDI) end-capped poly(propylene glycol) (PPG), shown in Figure 39. HDI (Acros, Belgium) was used as received, and PPG M_n 425, 725, 1000 (Sigma-Aldrich, St. Louis, MO) and PPG M_n 2000 (Acros, Belgium) were used as received with a drying step. The synthesis was performed in a three-neck round bottom flask using an oil bath for heating. The HDI was stirred and heated to 80°C before PPG was introduced drop-wise. The reaction was allowed to occur for 24 hours under a nitrogen purge.

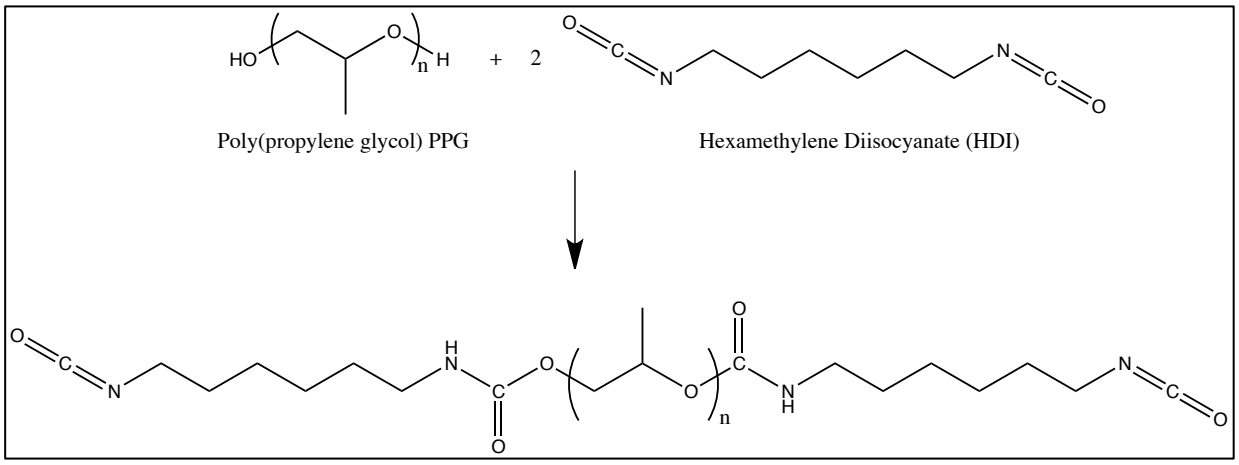

Figure 39: HDI End Capped Polyether Based Prepolymer
The polyether prepolymer is formed through molar ratio control of hexamethylene diisocyanate and poly(propylene glycol).

4.2.1.3. Polyurethane Synthesis

The polyurethane for composite formation was synthesized using hexamethylene diisocyanate (HDI), poly(propylene glycol) (PPG), and 1,4-butane diol. HDI (Acros, Belgium) and 1,4-butane diol (Sigma-Aldrich, St. Louis, MO) was used as received and PPG M_n 425, 725, 1000 (Sigma-Aldrich, St. Louis, MO) and PPG M_n 2000 (Acros, Belgium) were used as received with a drying step. The overall procedure to produce the polyurethane used in this work is summarized in Figure 40. The hard segment, soft segment, and chain extender were maintained at a 2:1:1 ratio, respectively. Stannous octoate (Sigma-Aldrich, St. Louis, MO) was used as a catalyst for the synthesis of the

PU. The catalyst was always used at a 0.4 mol% concentration, and the materials were dissolved in dimethylformamide (DMF) (Sigma-Aldrich, St. Louis, MO) at 80°C under stirring. The synthesis was performed in a three-neck round bottom flask using an oil bath for heating. The initial reaction was performed with a composition of hard segment and soft segment in a 2:1 ratio for one hour, and then the chain extender was added. The polymer was precipitated out of solution using water and dried prior to characterization. An additional hexane wash was performed by again dissolving the PU in DMF in order to extract the catalyst. The polymer was again precipitated out of solution using water and dried in a vacuum oven for storage until use.

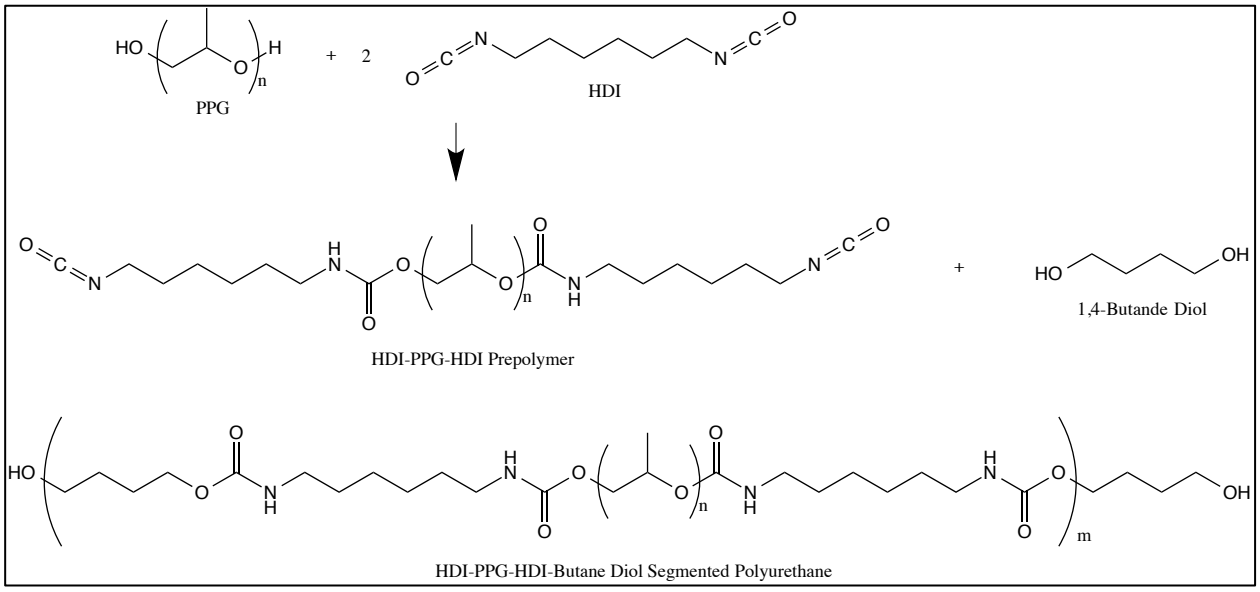

Figure 40: HDI-PPG-HDI-Butane Diol Segment Polyurethane
Presented here is the two-step procedure to produce the polyurethane used for composite formation with BC. The PPG and HDI were prepared to produce an HDI end-capped prepolymer that was reacted with butane diol to produce the final polyurethane.

4.2.1.4. PU-BC Polymerization/Composite Formation

BC was dried in a vacuum oven prior to composite formation, illustrated in Figure 41. Vacuum drying was selected as it produced a thin nonwoven on the micron scale. This method allowed the mat to condense as water was evaporated out of the original

hydrogel matrix, whereas the lyophilization leaves fibers in their original position as they were in the hydrogel structure.

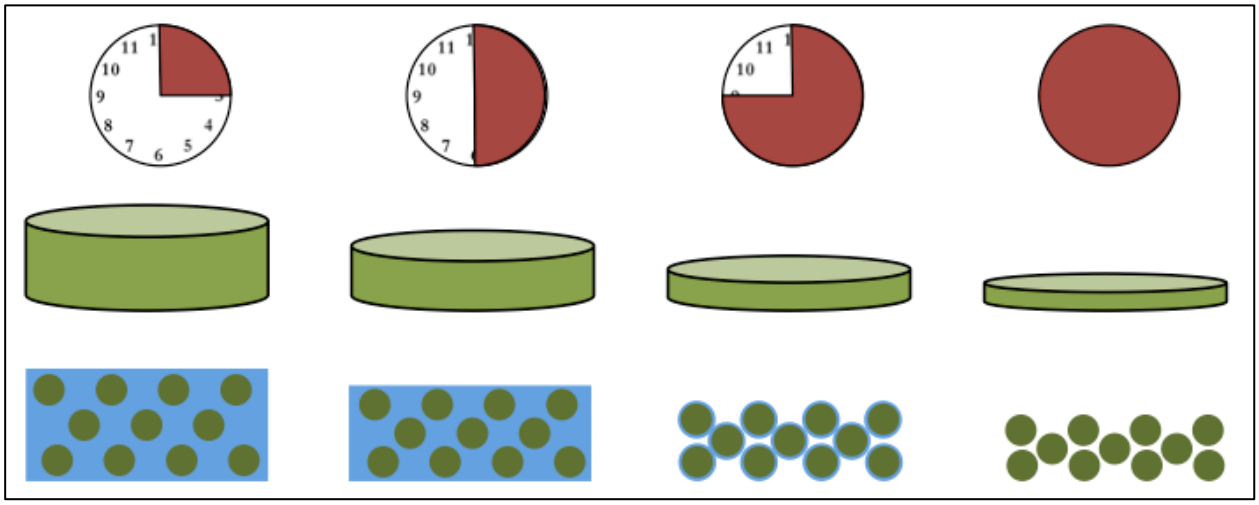

Figure 41: BC Drying to Produce Micron-Scale Samples
The top series of images depicts time in this elapsed depiction of the processing. The second row illustrates the reduction in thickness of the hydrated BC pellicle until it reaches its final thickness. The final row shows the changes between the cellulose fibers (green) and the water (blue) as the drying proceeds with a final layer of adsorbed water prior to complete dehydrated leaving a purely cellulosic mat of thin fibers.

The composite was formed by combining vacuum dried BC pellicles with 10 wt% PU in DMF for 10 minutes with agitation. Samples were placed against Teflon® films (American Durafilm, Holliston, MA) and dried overnight under 30 inHg vacuum at 90°C using an Isotemp Vacuum Oven 285A (Fisher Scientific, Waltham, MA). This process is illustrated in Figure 42.

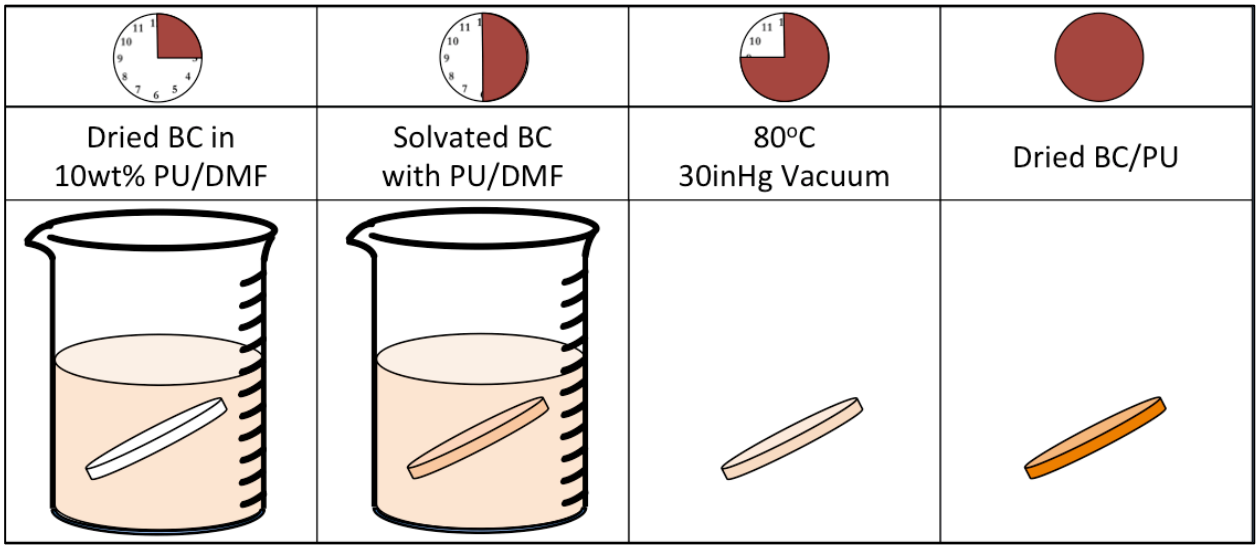

Figure 42: BC/PU Composite Formation by Solution Dip Coating
The top series of images depicts time in this elapsed depiction of the processing. The second row describes the procedure with the respective step while the final row shows the general procedure pictorially. The dried BC mat is placed in a polyurethane solution, removed from solution, and dried in vacuum with heat. During the drying step, the composite is placed against a Teflon® film.

4.2.2. Prepolymer Characterization

4.2.2.1. Fourier-Transform Infrared Spectroscopy (FTIR)

The end-capping reaction was followed using FTIR by a FTS-6000e spectrometer (Varian, Palo Alto, CA, USA). Two sodium chloride salt windows were used to suspend the liquid components for measurement of the solution by transmission. The collection of spectra was a simulated *in situ* measurement using a Watlow SD controller and ¼" thick 3" diameter aluminum plate to heat each sample in a nitrogen filled environment. The reaction was carried out at 80°C, controlled to ±0.1°C, and maintained within ±0.2°C for the duration of the measurements. The sample was removed from the heated inert environment for measurement each half hour. Infrared spectra were collected over a range of 700-4000 cm^{-1} at a resolution of 4 cm^{-1}. Spectra were collected in thirty-minute intervals, each comprised of 64 co-added scans. Each spectrum was baseline corrected using 2250 cm^{-1} as zero and normalized using the CH_2 associated peaks in the range of 2850 to 2950 cm^{-1}. Spectra were fitted using the curve fitting toolbox in MATLAB (MathWorks, Natick, MA) to fit a Gaussian peak to the 1530 cm^{-1}, 1710 cm^{-1}, and 2272 cm^{-1}. These selected absorption bands are associated with N-H bending in the urethane group, free carbonyl in the urethane group, and the

isocyanate peak, respectively. From the fitted equations, the area under each curve was determined and reported.

4.2.3. Characterization of PU-BC Composites

4.2.3.1. Scanning Electron Microscopy (SEM)

SEM was utilized to ascertain the infusion of the BC throughout the bulk of the BC nonwoven. PU-BC composites were dried in vacuum overnight and fracture surfaces were made by freezing the composites in liquid nitrogen. Samples were mounted on carbon tape and sputtered with gold on a Spi Module Sputter Coater (Spi Supplies: Westchester, PA, USA) at 20 mA for 10 s. They were analyzed on a LEO 1525 Scanning Electron Microscope (Zeiss: Oberkochen, Germany).

4.2.3.2. Tensile Test

A continuous sheet of BC was cut into sections for use in mechanical testing. The sections were vacuum dried and then combined with a PU. These BC/PU sections and vacuum dried NBC were cut into 12.5 mm wide strips with a 40 mm gauge length. Samples were tested using an ElectroPuls E1000 with Bluehill 2 software (Instron, Norwood, MA) with a 1 kN load cell. All samples were tested at the same strain rate of 4 mm/min to allow for comparison between sample groups after the load versus elongation data was converted to stress and strain values.

4.2.3.3. Cell Culture

Human aortic endothelial cells (HAECs) (male, passages 3-6) were cultured and grown in VascuLife growth media with SMC-supplement kit (LifeLine Technologies) with gentamicin/amphotericin and passaged at 80% confluency. BC/PU composites were sterilized using a 30 minute incubation in 70% ethanol, washed with two sterile DI water rinses, and washed with CMF buffer. HAECs were seeded on 96-well sized composites at a density of 18,000 cells/cm^2 in 0.2 cm^2 chamber glass slide. The cells were incubated at 37^oC for 72 hours prior to examination. The composites with cells were stained using Diff-Quick to examine cells on composites. The remaining cells in each chamber were stained with a live/dead fluorescent stain to examine if any leaching from the composites took place. A green stain, Calcein AM, was used for live cells and a red stain, propidium iodide (PI), was used for dead cells.

4.2.3.4. Protein Absorption

Protein deposition was evaluated by static adsorption of proteins and then desorbed using a surfactant. The desorbed protein was then quantified using UV-Vis spectroscopy.[131] Prior to incubation with protein, BC/PU composites were pre-wetted with 100% ethanol for one hour and followed by incubation in PBS for 30 min and repeated incubation in fresh PBS for another 30 minutes. During each incubation period, composites and solution were placed in a partial vacuum to remove any air bubbles from the composite surfaces. The wetted composites were then left in PBS and on a shaker overnight. PU-BC composites were incubated in 100 μg/mL bovine serum albumin (BSA) (Sigma-Aldrich, St. Louis, MO) solution in PBS for four h on the shaker (25 rpm). After 4 h of incubation, each composite was removed from the protein solution and placed in a polypropylene tube. Washing of each composite consisted of three five minute incubations with 600 μL of PBS under gentle agitation. This washing procedure removes any nonspecifically adsorbed proteins. The remaining protein is considered to be adsorbed and is harvested by three one hour incubations with 1% sodium dodecyl sulfate (SDS) solution. After each incubation period, the SDS and BSA solution were collected. Absorbance spectra of BSA, SDS, and PBS solutions was performed using an Evolution 600 UV-Vis (Thermo-Scientific) and VisionPro software. The absorbance at 265 nm was used with a calibration curve to determine the concentration of BSA in solution. A Teflon® FEP film (American Durafilm, Holliston, MA) was used as a control as it is expected to be unfavorable for protein adsorption due to its hydrophobic chemical structure.

4.2.3.5. Contact Angle

As a measure of wettability, contact angle measurements were performed and the results presented in Figure 59. Composites were evaluated with a Contact Angle Meter Model CAM-Plus (ChemInstruments, Mentor, OH). Each sample was allowed 30 seconds to equilibrate once the 10 μL of Millipore water was applied to the surface.

4.3. Results

4.3.1. Characterization of Prepolymer

4.3.1.1. Fourier-Transform Infrared Spectroscopy (FTIR)

Tracking of the polycondensation reaction can be performed with FTIR. The spectra from the diisocyanate and polyethers are presented in Figure 43 for baseline measurement. The characteristic peaks of HDI and PPG are identified in Table 5 and Table 6, respectively. Most notably, the HDI spectrum shows the isocyanate peak (2272 cm^{-1}) without any overlap of that region from PPG spectra. Additionally, absorbance at 1530 and 1710 cm^{-1}, which are associated with urethane formation, is not present. This allows for the urethane formation to be followed without interference from other peaks.

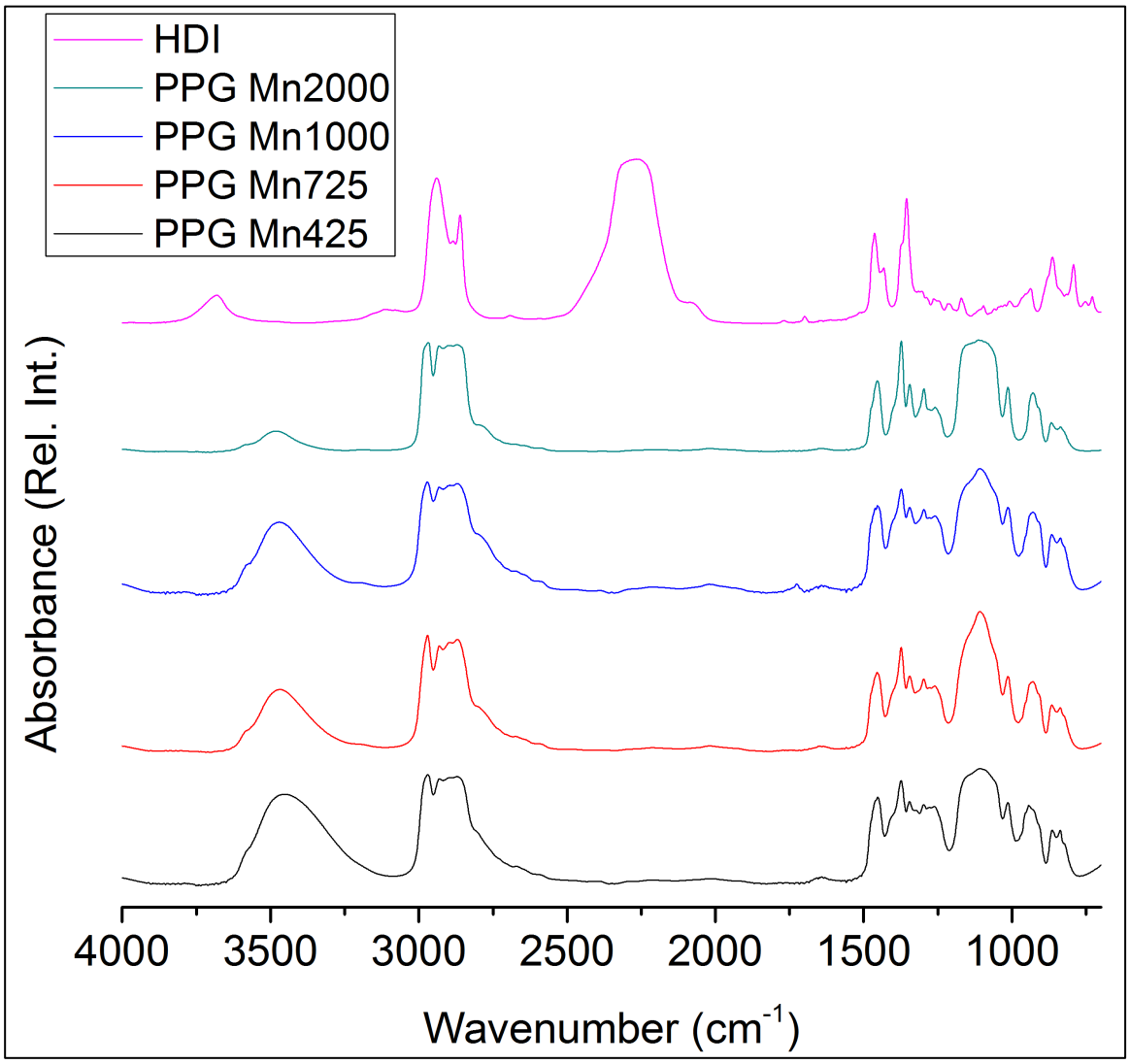

Figure 43: FTIR of Starting Materials
Shown here are spectra of each PPG (Mn of 425, 725, 1,000, and 2,000) and HDI.

Table 5: FTIR Absorption Bands for PPG

Frequency (cm^{-1})	Assignment
1110	Broad ether stretching (CH_2-O-CH_2)[132]
2897	CH_2 Polyether C-H Stretch[133]
2970	CH_3 Polyether C-H Stretch[133]
3450	Terminal –OH From PPG[132]

Table 6: FTIR Absorption Bands for HDI

Frequency (cm^{-1})	Assignment
2272	Isocyanate (R-N=C=O) N=C and C=O contributions[92]
2868	CH_2 C-H Symmetric Stretch[133]
2932	CH_2 Aliphatic C-H Asymmetric Stretch[133]
3650	N-H Stretch

As the reaction proceeds between HDI and PPG, urethane peaks appear at 1530 cm^{-1} and 1710 cm^{-1}. The peak at 1530 cm^{-1} is associated with the N-H bending vibration in the urethane group. The 1710 cm^{-1} absorption band is associated with carbonyl (C=O) stretching of the urethane group. Additionally, a new peak is present in the final prepolymer product (Figure 44) at 3350 cm^{-1} from the urethane group N-H stretching. There is also an elimination of the 3450 cm^{-1} peak from the terminal hydroxyls of PPG since these end groups reacted with the isocyanate. These trends show the reaction between PPG and HDI occurred.

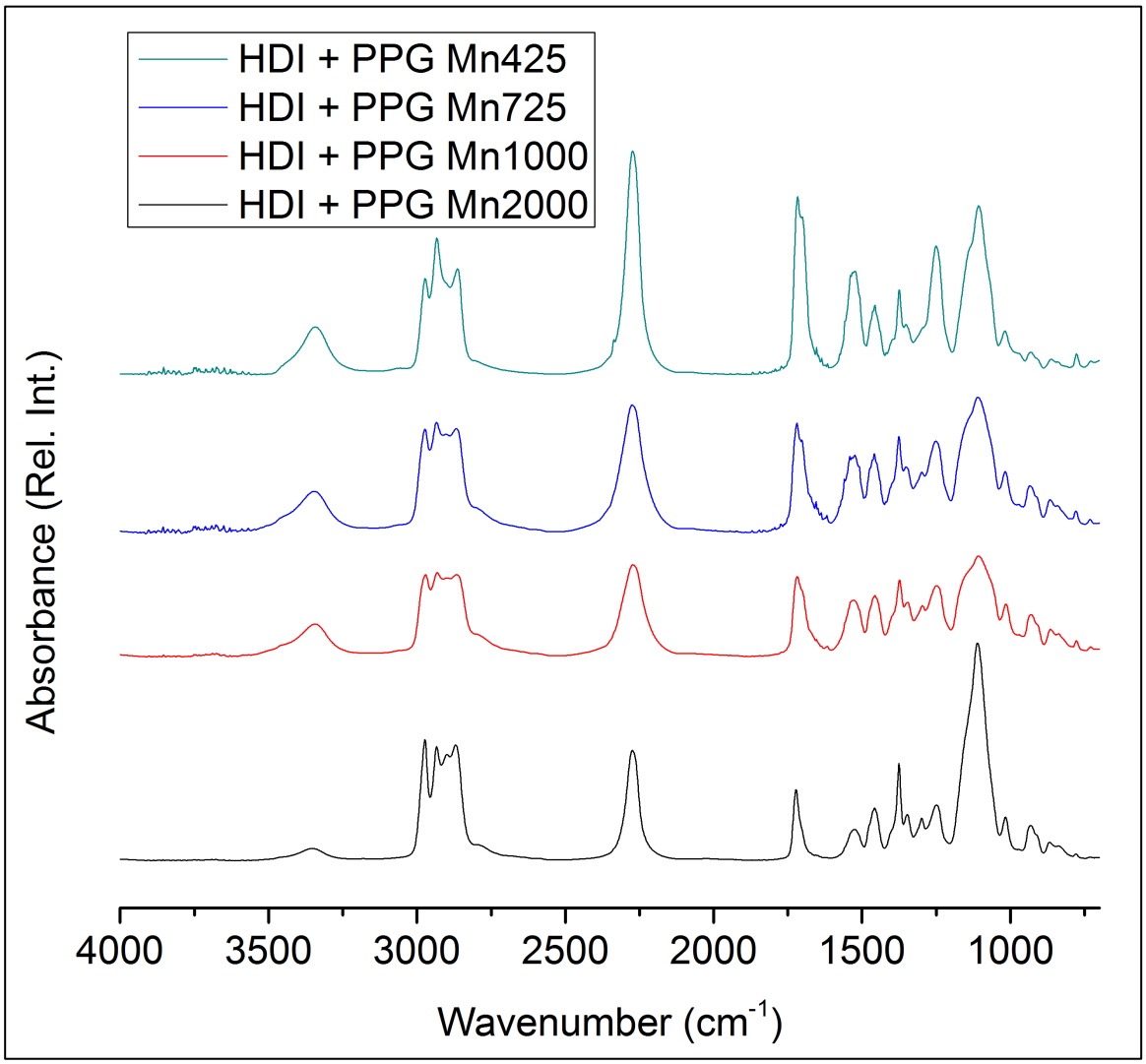

Figure 44: FTIR of Materials after 24hr of Reaction
Shown here are spectra of each PPG (Mn of 425, 725, 1,000, and 2,000) and HDI.

Table 7: FTIR Absorption Bands for Polyether Prepolymer Formation

Frequency (cm^{-1})	**Assignment**
1109	Broad ether stretching band[133]
1530	Amide II, N-H bending[133]
1710	Amide I, C=O stretching[133,134]
2272	Isocyanate (R-N=C=O) N=C and C=O contributions[92]
2868	CH_2 Aliphatic C-H Symmetric Stretch[133]
2897	CH_2 Polyether C-H Stretch[133]
2932	CH_2 Aliphatic C-H Asymmetric Stretch[133]
2970	CH_3 Polyether C-H Stretch[133]
3350	N-H Stretch on the Urethane Group[133]

Spectra collected in 30 minute intervals are shown in Figure 45 for HDI and PPG (Mn=425 Da) in a ratio of 2.01:1. It is shown in the figure that the initial peaks corresponding to urethanes (1530 and 1710 cm^{-1}) are initially not present but do evolve as time elapses. Additionally, the breadth of the isocyanate peak at 2272 cm^{-1} decreases before a decrease in intensity is observed. The decrease in the isocyanate peak and evolution of the urethane peaks occur simultaneously. Similar results and trends are found in Figure 46 for HDI and PPG 725, Figure 47 for HDI and PPG 1000, and Figure 48 for HDI and PPG 2000.

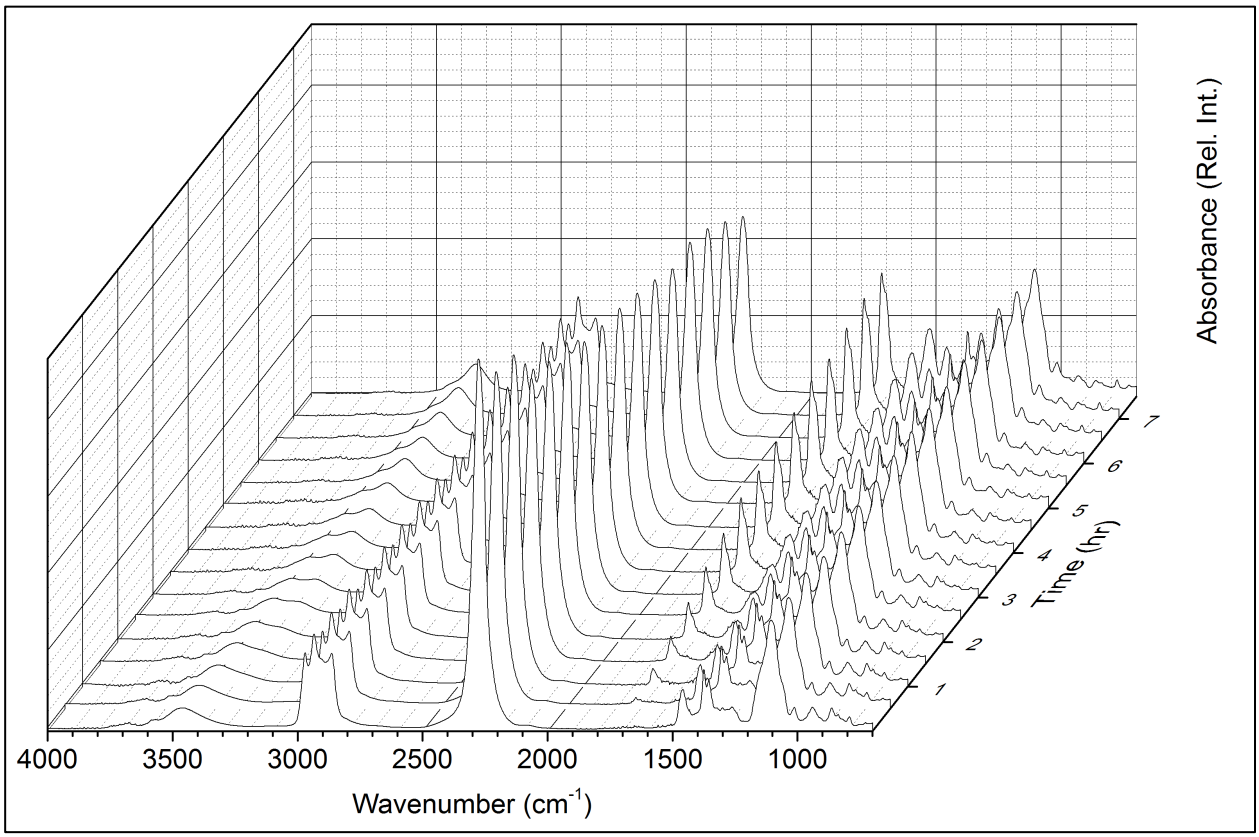

Figure 45: Time Resolved FTIR Spectra of PPG Mn 425 with HDI Reaction
The figure here shows the spectra, in 30 minute intervals, of the prepolymer reaction between HDI and PPG (M_n 425 Da) in a molar ratio of 2.01:1.

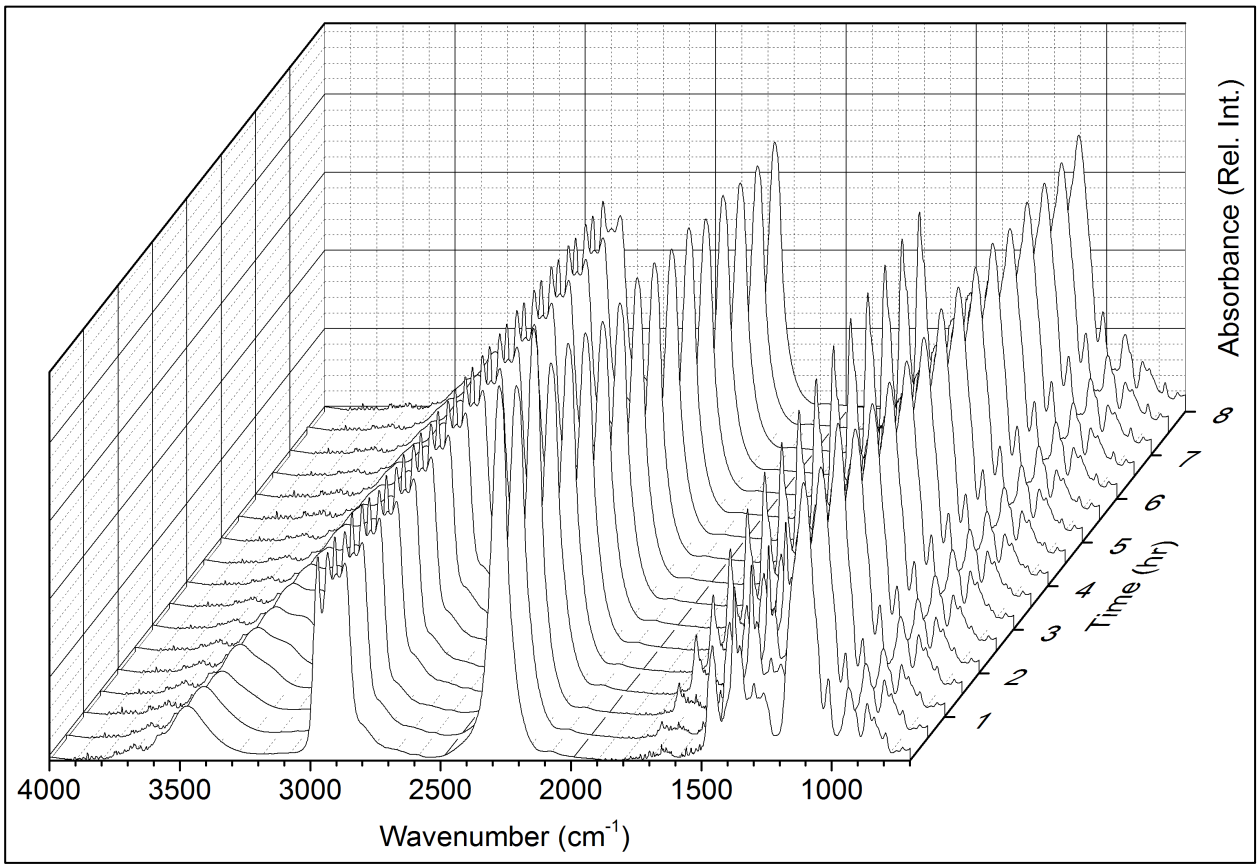

Figure 46: Time Resolved FTIR Spectra of PPG Mn 725 with HDI Reaction
The figure here shows the spectra, in 30 minute intervals, of the prepolymer reaction between HDI and PPG (M_n 725 Da) in a molar ratio of 2.01:1.

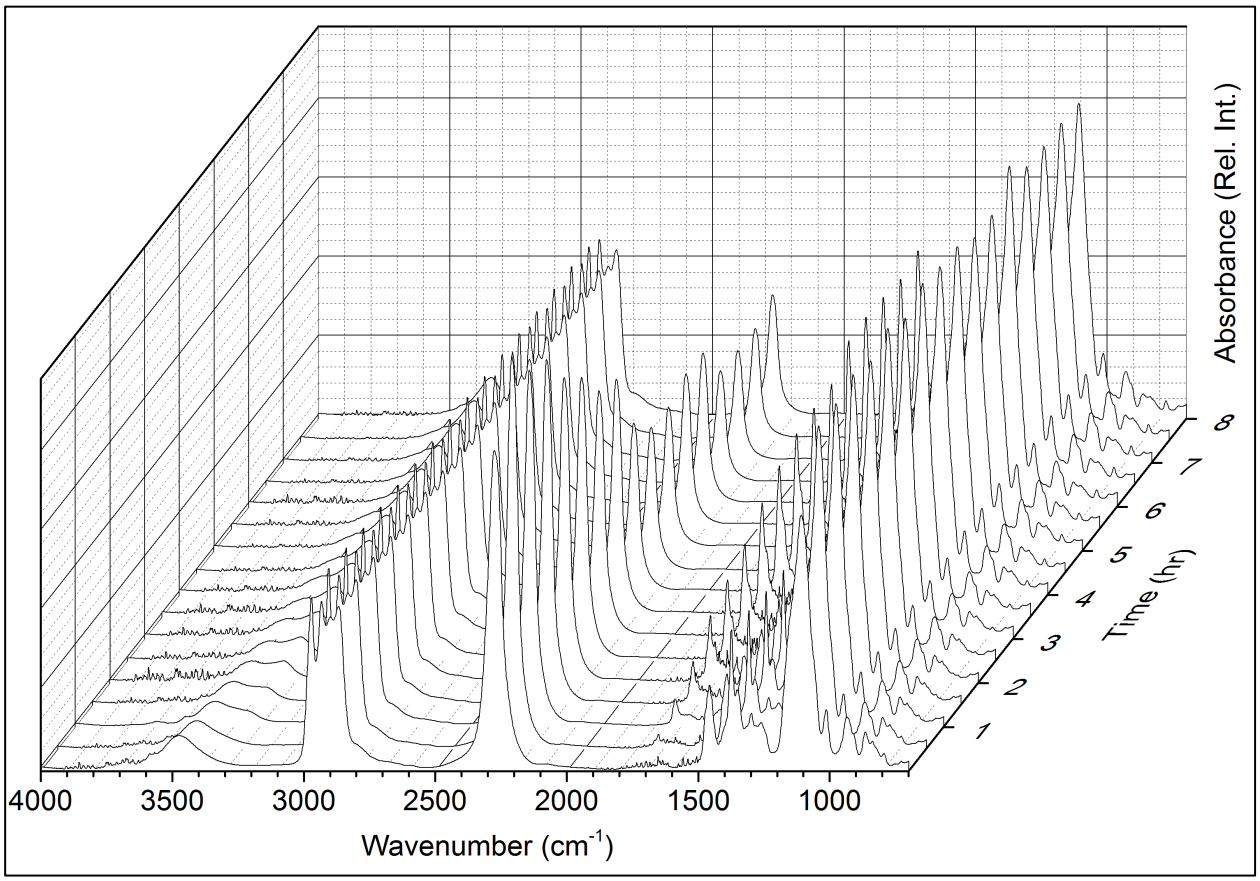

Figure 47: Time Resolved FTIR Spectra of PPG Mn 1000 with HDI Reaction
The figure here shows the spectra, in 30 minute intervals, of the prepolymer reaction between HDI and PPG (M_n 1000 Da) in a molar ratio of 2.01:1.

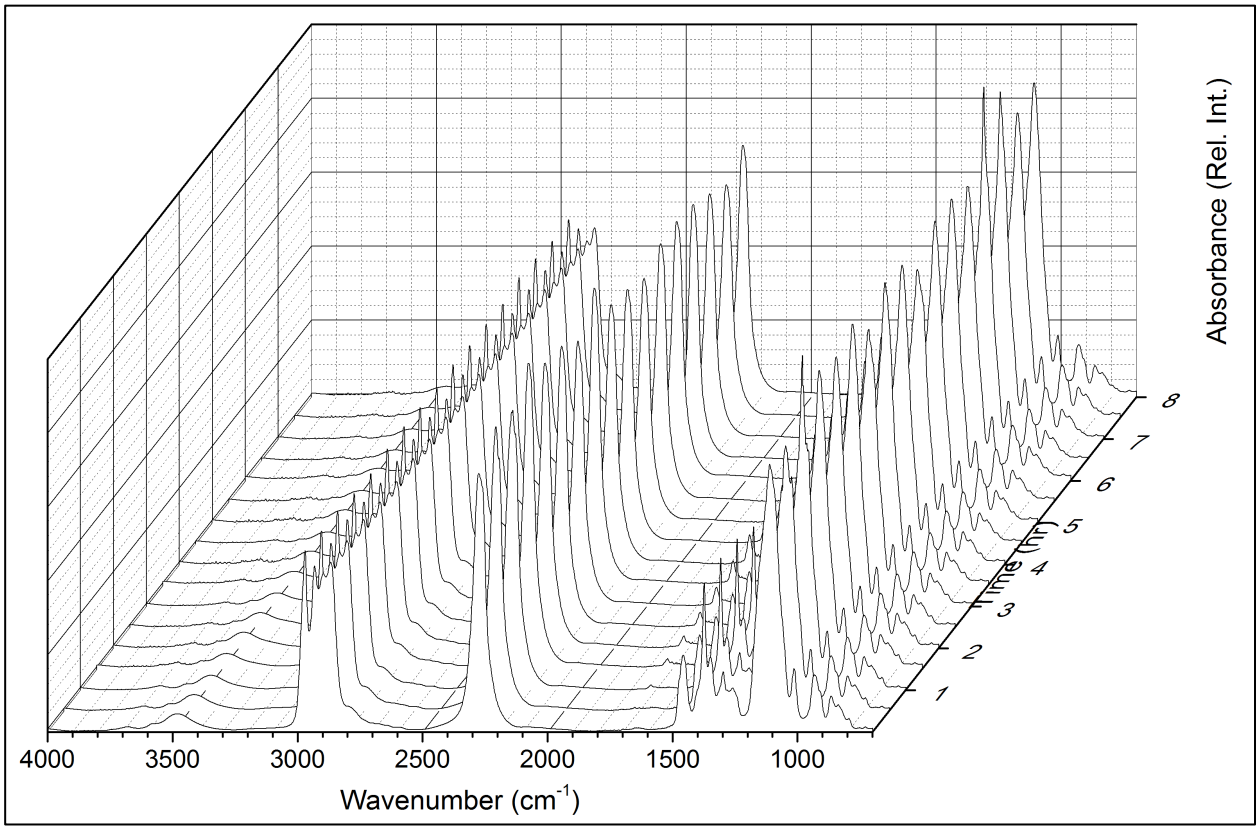

Figure 48: Time Resolved FTIR Spectra of PPG Mn 2000 with HDI Reaction
The figure here shows the spectra, in 30 minute intervals, of the prepolymer reaction between HDI and PPG (M_n 2000 Da) in a molar ratio of 2.01:1.

The areas of the absorption bands at 1530, 1710, and 2272 cm^{-1}, corresponding to N-H bending of the urethane group, the free carbonyl from the urethane group, and the isocyanate peak are presented in Figure 49 through Figure 52 for each PPG soft segment length: 425, 725, 1000, and 2000. Each plot shows as the isocyanate peak decreases and the urethane associated bands at 1530 and 1730 cm^{-1} increase with time as expected.

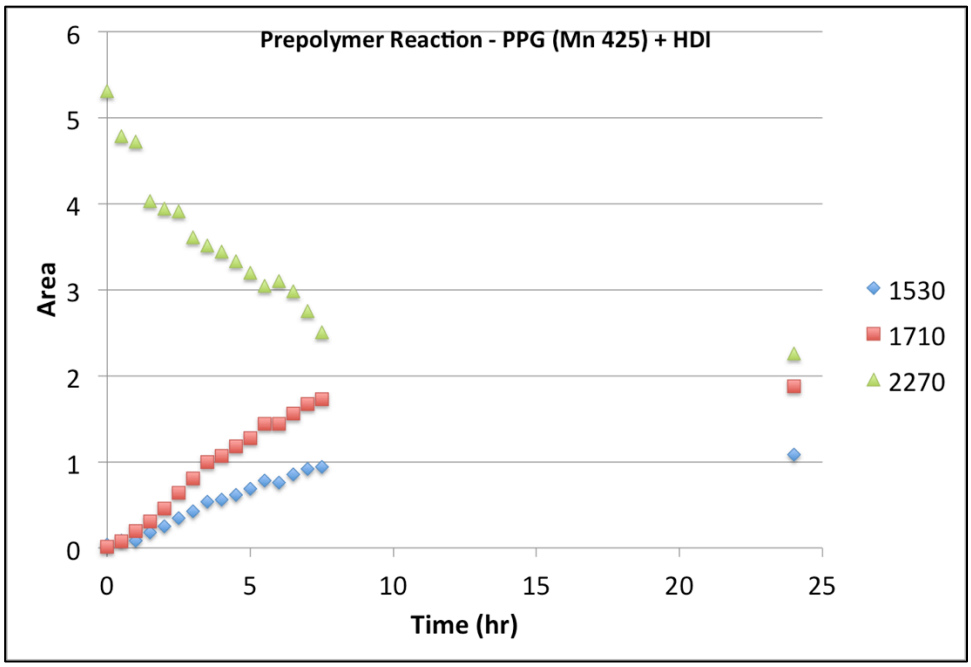

Figure 49: FTIR Peak Areas Versus Time (PPG Mn 425 + HDI)
The area of each peak (1530, 1710, and 2270 peak) is plotted versus time.

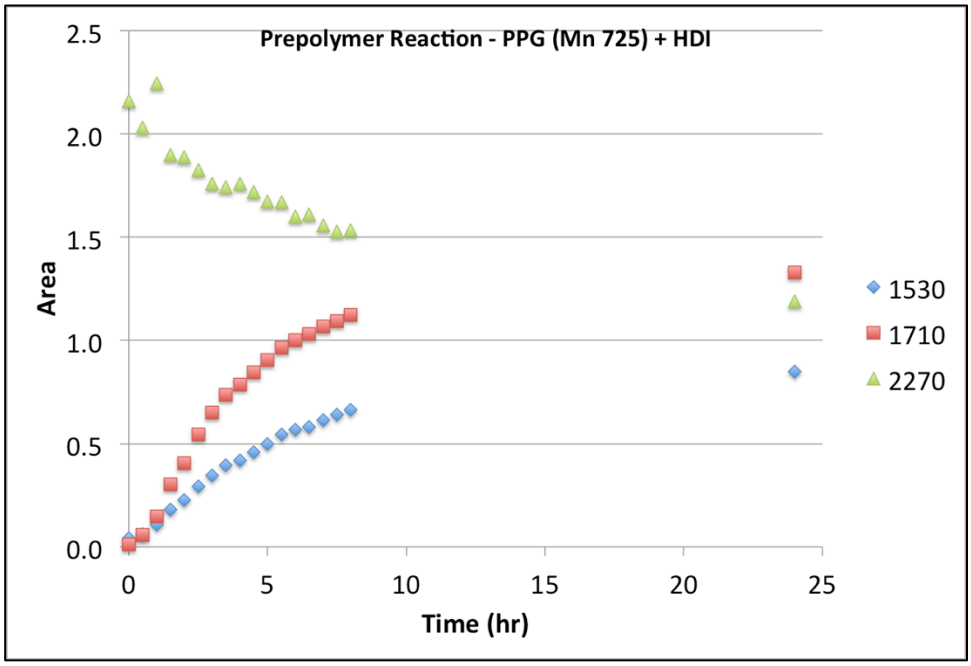

Figure 50: FTIR Peak Areas Versus Time (PPG Mn 725 + HDI)
The area of each peak (1530, 1710, and 2270 peak) is plotted versus time.

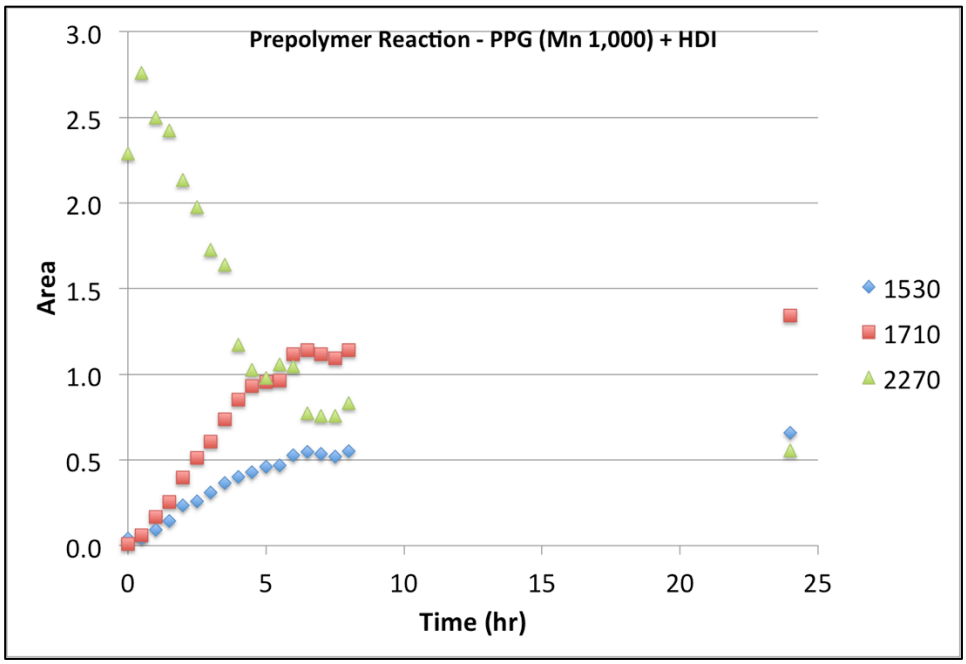

Figure 51: FTIR Peak Areas Versus Time (PPG Mn 1,000 + HDI)
The area of each peak (1530, 1710, and 2270 peak) is plotted versus time.

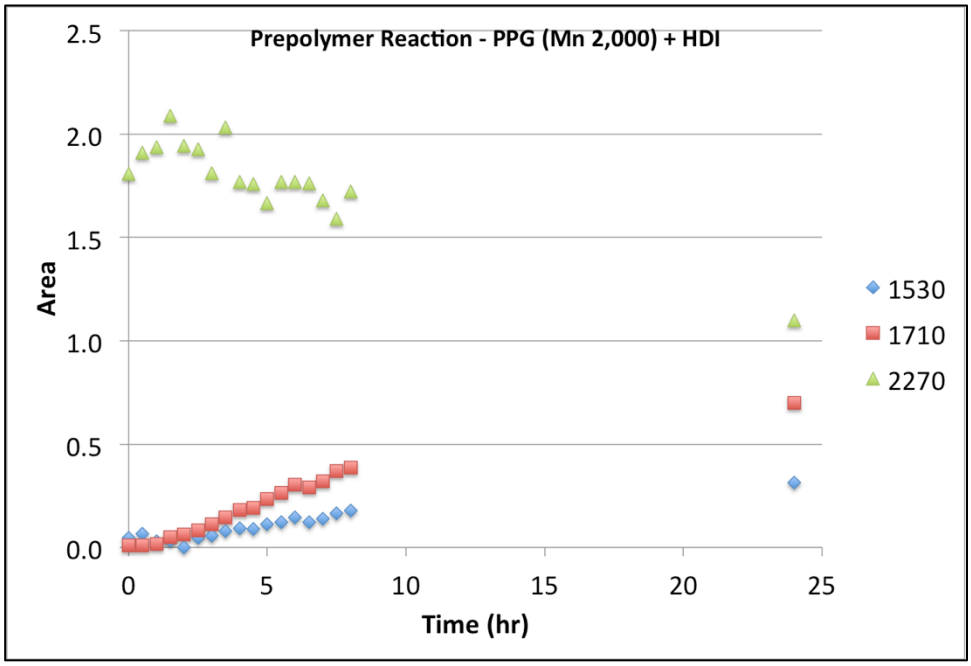

Figure 52: FTIR Peak Areas Versus Time (PPG Mn 2,000 + HDI)
The area of each peak (1530, 1710, and 2270 peak) is plotted versus time.

.

4.3.2. PU-BC Composites Characterization

4.3.2.1. Energy Dispersive X-ray Spectroscopy (EDX)

The presence of the tin octoate in the PU was followed using EDX. The EDX spectra are presented in Figure 53 from a PU sample after synthesis and precipitation in water (Left) and from a PU sample after a hexane purification wash (Right). Table 8 shows the composition by weight percent of tin in the polyurethanes. The tin component is from the stannous octoate catalyst used to synthesize the polyurethanes.

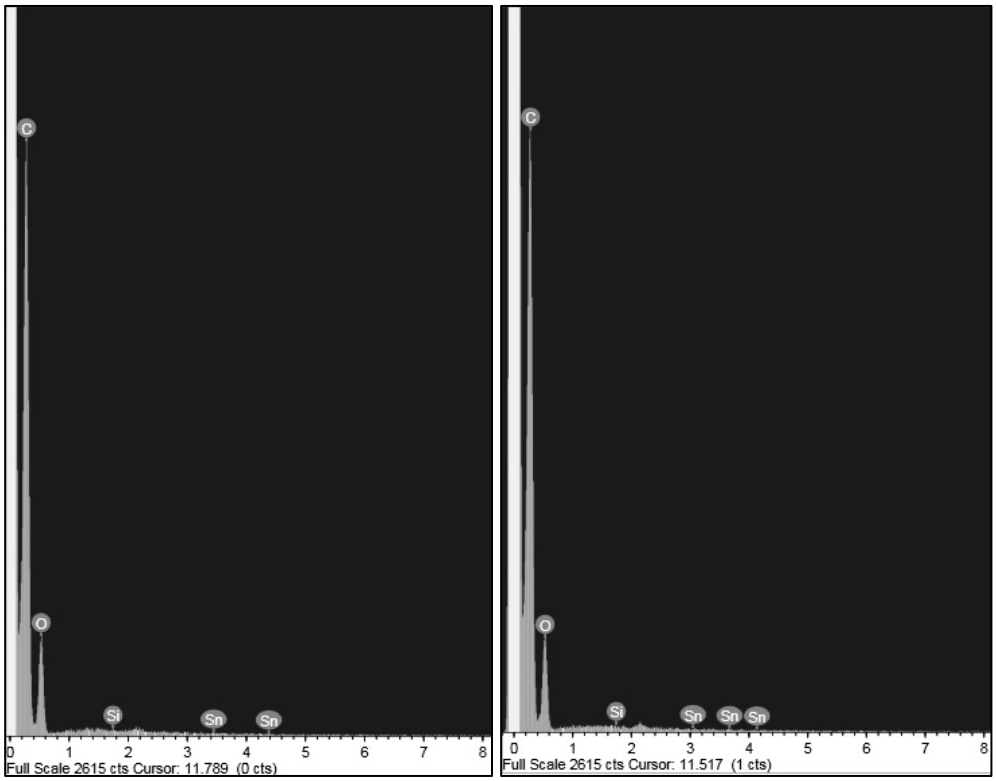

Figure 53: Catalyst Composition by EDX

The compositions of a polyurethane after precipitating in water after synthesis as examined (Left) and polyurethane after a wash in hexane to remove the tin catalyst was examined (Right). No significant differences are found by the spectra, but the peak intensities were used to determine tin concentration (Table 8).

Table 8: Weight Percent Catalyst Composition
Composition of polyurethanes after precipitation in water and after a hexane wash was examined by EDX to evaluate the quantity of tin catalyst in the polyurethane.

Tin (Sn)	Weight Percent
As Synthesized	0.10
Post Hexane Wash	0.03

4.3.2.2. Scanning Electron Microscopy (SEM)

Initial results of PU-BC composite formation are shown in Figure 54. Figure 54A shows the original native BC scaffold. Figure 54B shows the scaffold surface after dip coating with PU containing a PPG 2000 soft segment. Figure 54C and D are produced from liquid nitrogen fracture surfaces. The low magnification provides a view of the overall thickness, while the high magnification shows the fracture surface. This set of composites was prepared using lyophilized BC, which produced a thick sample, shown in Figure 54C, of 195 μm. In the higher magnification image (Figure 54D), it appears that the PU regions are relatively flat with dispersed points. The scattered points are BC fibers that elongated just prior to fracture.

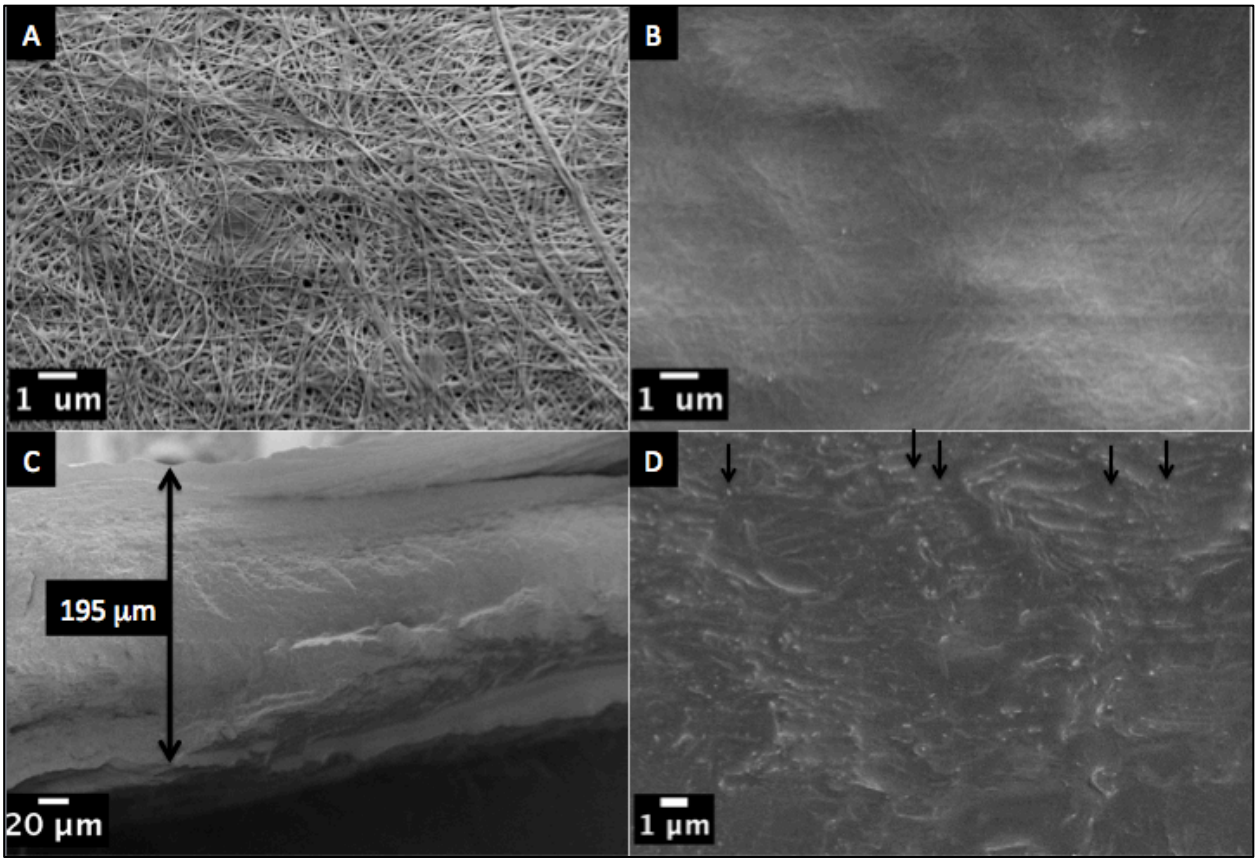

Figure 54: SEM Images of BC Composites
This figure illustrates the native BC fiber surface (A), the surface of PU-BC (B), the fracture surface of PU-BC at low-magnification (C) and the fracture surface of PU-BC at high-magnification (D). The fracture surface in image D has arrows highlighting a few BC fibers that are scattered throughout the image.

Figure 55 shows fracture surfaces of each composite formed by PUs with different soft segments. These composites were formed using vacuum oven dried BC to minimize the thickness and produce thin nonwoven mats of fibers. The images demonstrate the ability to produce a continuous PU phase throughout the BC material using PUs with varying soft segments of PPG 425, 725, 1000, and 2000. Particularly important to note is the minimal thickness on the range of 10 to 20 μm for each composite. Figure 55 shows regions similar to Figure 54D where BC fibers are revealed by the production of the liquid nitrogen fracture surface. Masses of the dried BC mats were acquired before and after dip coating with PU. The masses were taken after an overnight drying period at 80^{o}C and 30 inHg vacuum. The values are reported in Table 9 with no statistical significant difference between experimental groups.

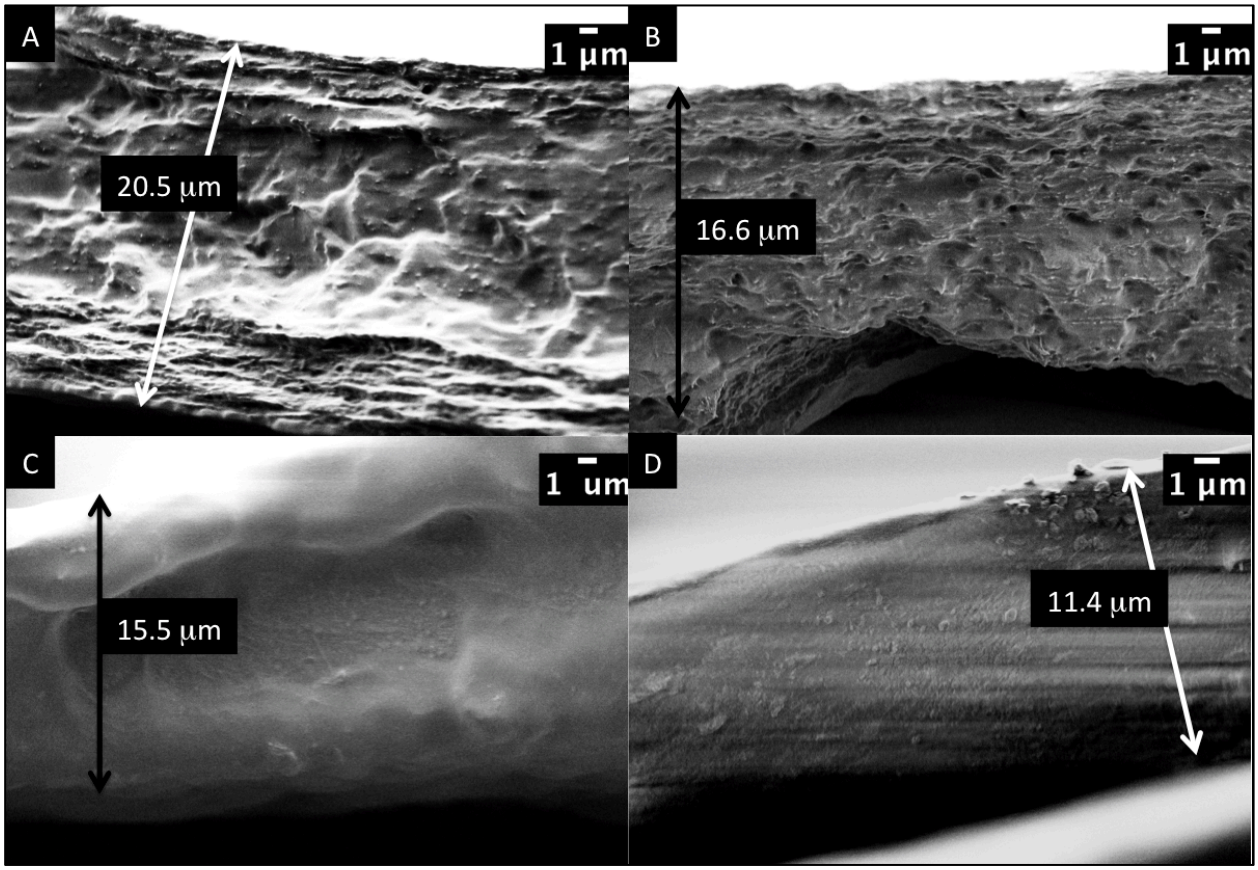

Figure 55: Cross-Section SEM Images of BC Composites
This figure illustrates structure of cross-section viewing composite formed with PU 425 (A), PU 725 (B), PU 1000 (C), and PU 2000 (D).

Table 9: Weight Percent BC in BC/PU Composites
Average weight percent of BC in BC/PU composites are listed with the corresponding 95% confidence intervals. The experimental groups are absent of any statistically significant differences.

Sample	Average wt%	95% CI
BC/PU 425	14.3	9.3
BC/PU 725	16.9	7.2
BC/PU 1000	14.4	10.5
BC/PU 2000	13.5	7.9

4.3.2.3. Mechanical Testing of BC/PU Composites

After testing, the data was converted from load versus elongation into stress versus strain. A representative stress versus strain curve is presented for each

experimental group in Appendix D. The data was analyzed to determine the elastic modulus, the percent elongation at fracture, and the ultimate tensile strength. The elastic modulus is reported in Figure 56 for NBC and BC/PU composites. A considerable increase in the average modulus of BC/PU 725 in comparison to NBC was measured. NBC, BC/PU 425, BC/PU 725, and BC/PU1000 are absent of statistically significant differences, but BC/PU 2000 exhibits a decrease that is statistically significant.

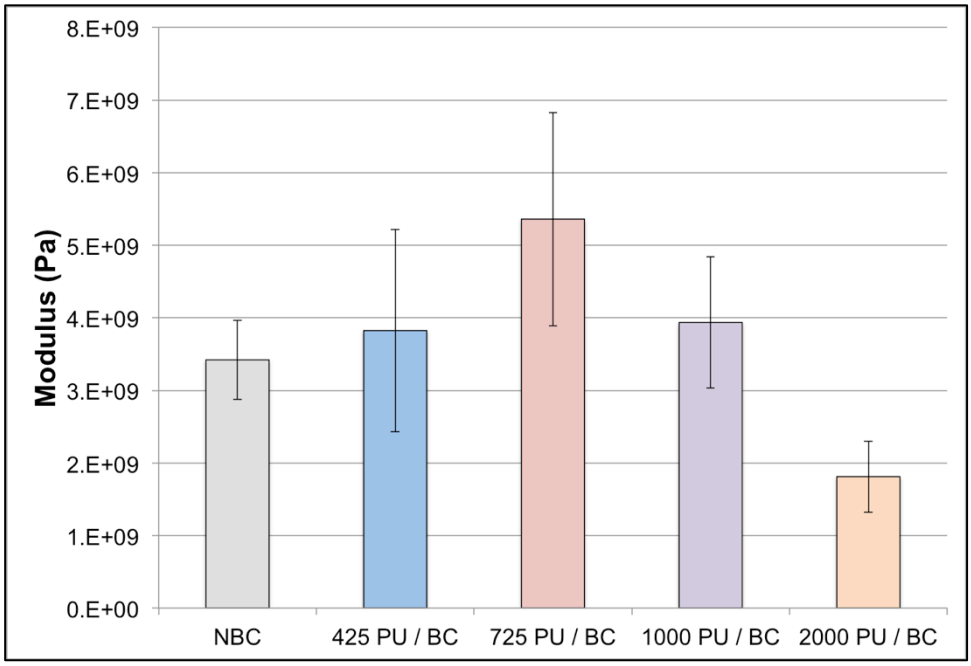

Figure 56: Elastic Modulus of BC and PU/BC Composites
This data shows the elastic modulus average and 95% confidence intervals of native BC (dried) and composites of BC and polyurethanes with varying soft segment lengths of 425, 725, 1,000, and 2,000.

The percent elongation at fracture (Figure 57) shows composites increased in ductility with soft segment lengths of 725, 1,000, and 2,000. The differences between composites of 1000 and 2000 and native BC and the 425 composite are statistically significant.

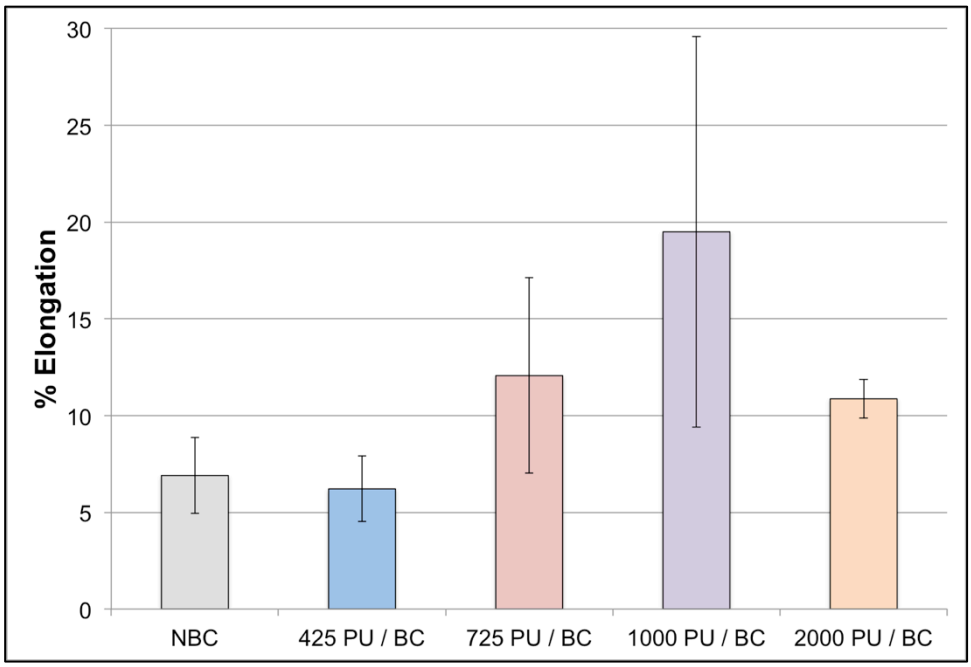

Figure 57: Percent Elongation at Fracture of BC and PU/BC Composites
This plot shows the percent elongation average and 95% confidence intervals of native BC (dried) and composites of BC and polyurethanes with varying soft segment lengths of 425, 725, 1,000, and 2,000.

The ultimate tensile strength (UTS) of NBC and BC/PU composites are summarized in Figure 58. The most significant find is that BC/PU 425 composites decrease in UTS. BC/PU 2000 remains similar to NBC while BC/PU 725 and BC/PU 1000 show a significant increase. BC/PU 1000 exhibits a statistically significant increase from NBC.

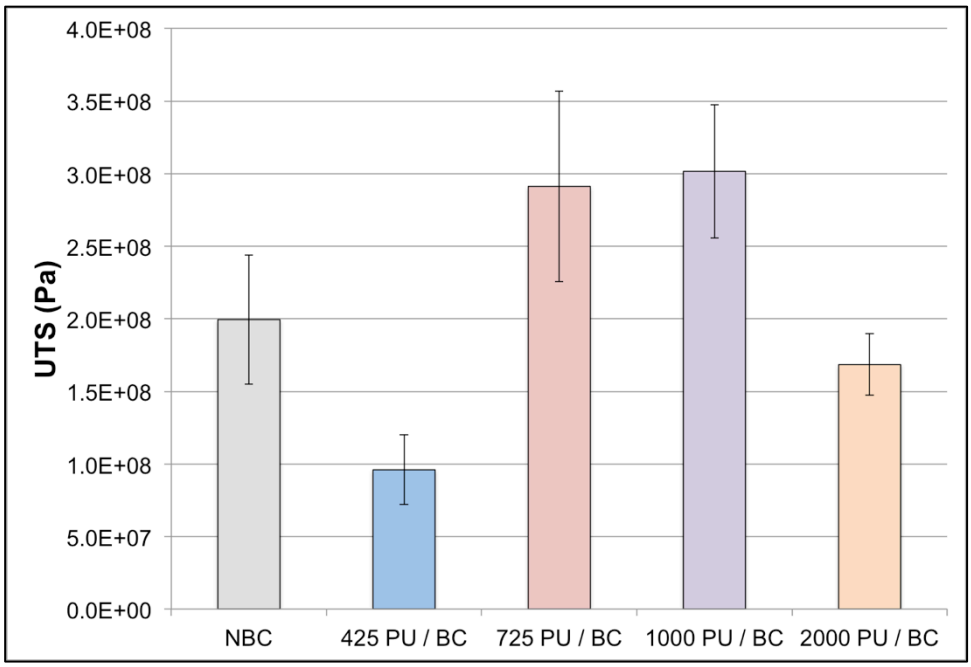

Figure 58: Ultimate Tensile Strength of BC and PU/BC Composites
This shows the ultimate tensile strength (UTS) average and 95% confidence intervals of native BC (dried) and composites of BC and polyurethanes with varying soft segment lengths of 425, 725, 1,000, and 2,000.

4.3.2.4. Contact Angle

The images in Figure 59 show differences in wettability by the changes in angle between the water drop and the material. A dried native bacterial cellulose sample was not analyzed since it readily adsorbed the water and an angle could not be determined. The BC/PU composites exhibited significantly different wettability from the Teflon® control. Comparison of the BC/PU composites shows significantly different wettability properties between BC/PU 1000 and BC/PU 2000. BC/PU 425 and BC/PU 725 are statistically similar to the other composites.

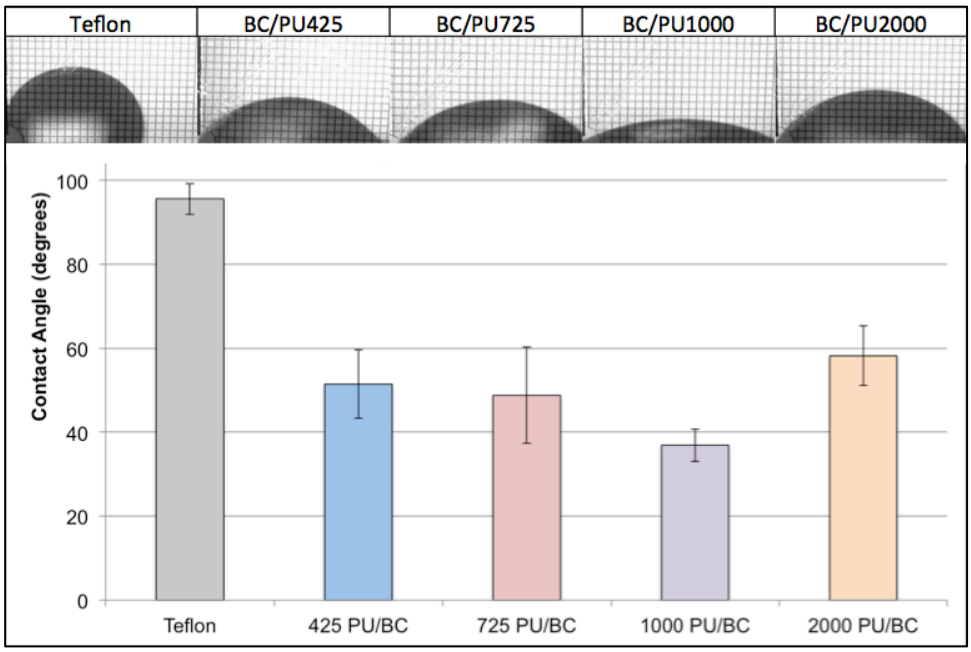

Figure 59: Contact Angle of PU/BC Composites
This figure shows the contact angle of BC/PU composites with varying soft segment lengths of 425, 725, 1,000, and 2,000 in the PU. A Teflon® sample was ran as a control.

4.3.2.5. Cell Culture

Cells were cultured for 72 hours on BC/PU scaffolds. Each scaffold demonstrated support of cell growth. The results are presented in Figure 60. The scaffolds were cultured in chambers with a glass bottom surface. The images show that cells were able to lay down on the surfaces of the scaffolds and extend multi-directionally. The best spreading was observed on BC/PU 725 scaffolds.

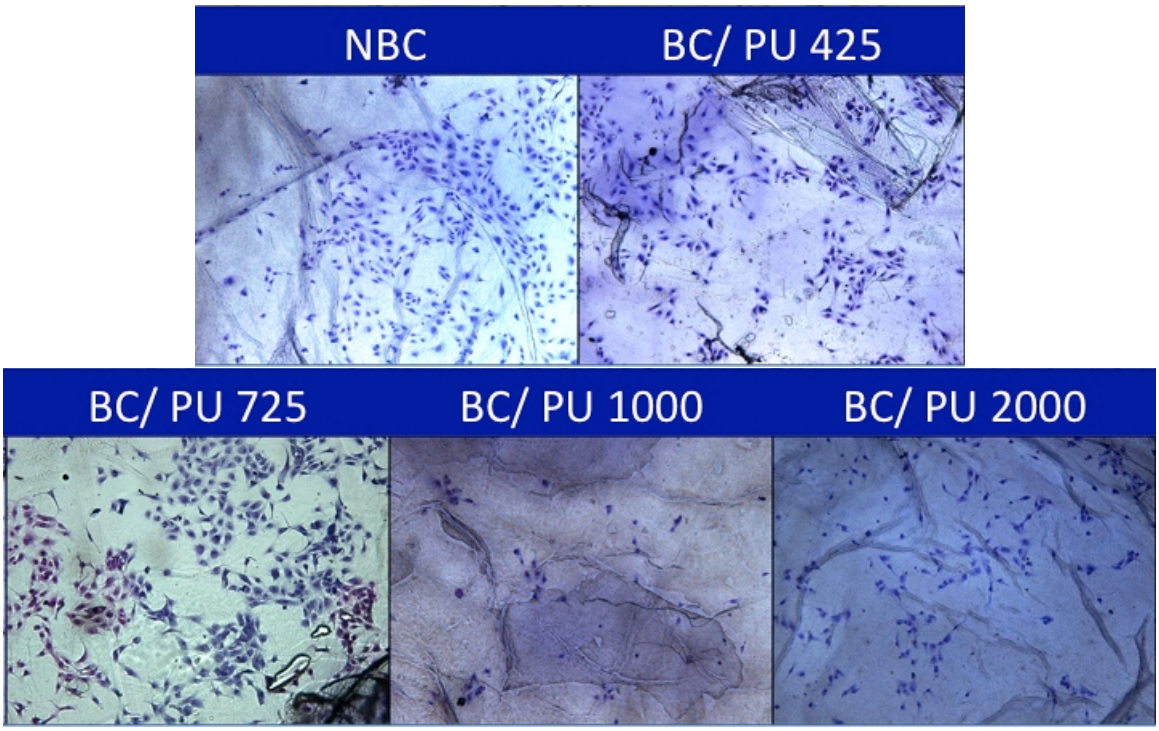

Figure 60: Light Microscopy Images of BC and PU/BC Composites
This figure shows composites of BC and polyurethanes with varying soft segment lengths of 425, 725, 1,000, and 2,000 with stained endothelial cells.

The area not covered by the scaffolds during culture provided an area to analyze the toxicity of the BC/PU scaffolds. During the 72 hour culture period, any leachables from the PU from unreacted or toxic components would be shown by killing cells at a higher rate. Live/dead images are presented in Figure 61. Each composite shows good compatibility with few dead cells and many live cells, illustrating good compatibility of the scaffolds with these cells. The only exception is the BC/PU 2000 composite in this series of images, which showed many dead cells and few live cells. Figure 62 shows the viability of cells as a percentage from cell counts of live and dead cells from three experimental trials. The averaged results show a less significant drop in viability with the BC/PU 2000 from the other composites, but it still shows a reduced cell viability.

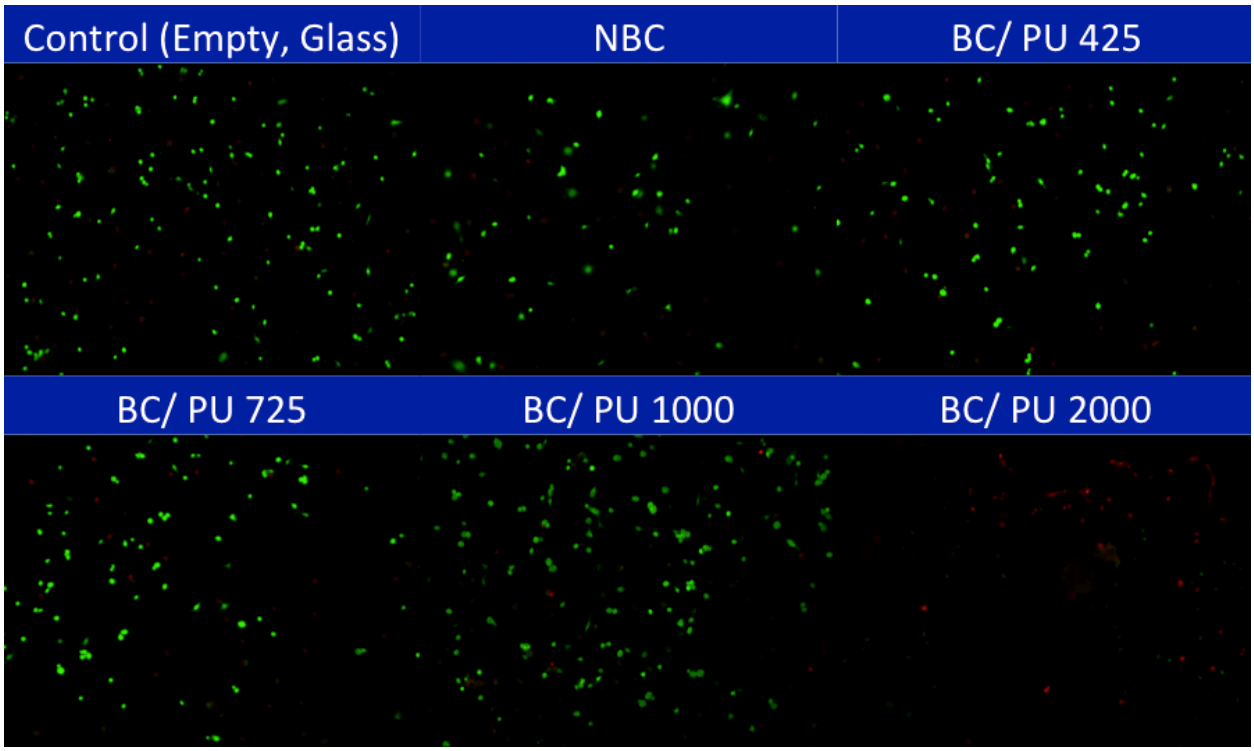

Figure 61: Fluorescent Microscopy Images of Cells Cultured with Composites
This figure shows live (green)/dead (red) cells from cells cultured with the BC/PU composites in the culture chambers.

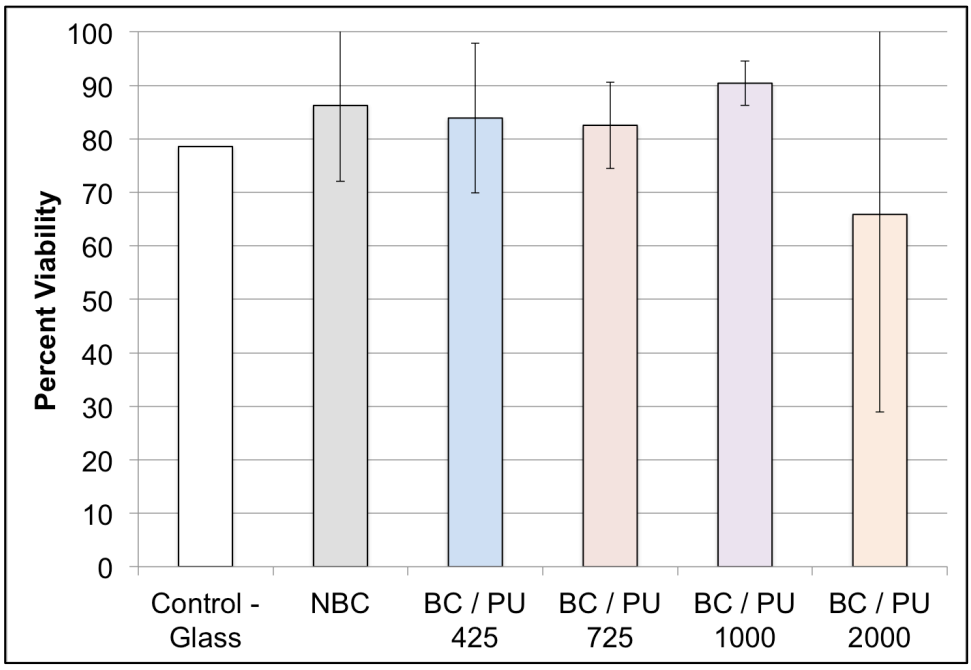

Figure 62: Cell Viability Cells Cultured with Composites
This figure is produced from the live/dead imaging of cells cultured in the same chamber as the composite scaffold. Live/dead images were converted to a viability percentage and presented here with 95% confidence intervals. The control value is the result of a measurement from a single trial while all others are the result of three experimental trials.

4.3.2.6. Protein Absorption

The protein absorption evaluation results are presented in Figure 63. A Teflon® film was used as a control by following the same procedure used for the BC/PU composites. A low amount of BSA was adsorbed onto the Teflon® surface as expected since it is relatively hydrophobic, as shown later by contact angle measurement. In general, the composites have similar albumin adsorption on the surface. The amount of BSA adsorbed on each composite surface is statistically greater than the amount adsorbed on Teflon®.

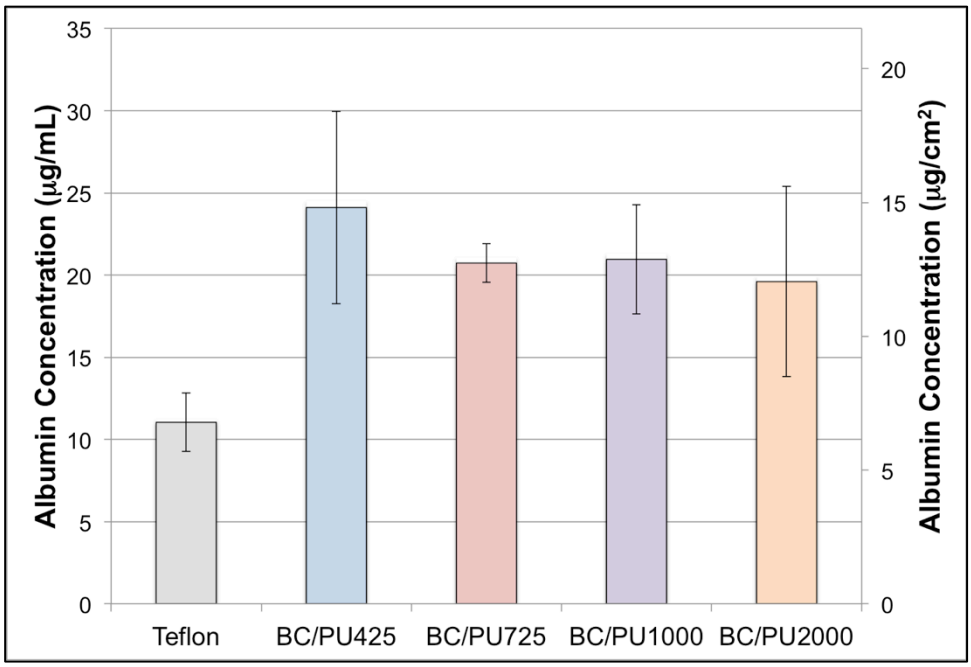

Figure 63: Albumin Deposition on BC and PU/BC Composites
This figure shows average and 95% confidence intervals of native BC (dried) and composites of BC and polyurethanes with varying soft segment lengths of 425, 725, 1,000, and 2,000. The reported quantities are values for specifically adsorbed protein.

4.4. Discussion

4.4.1. Prepolymer Reaction Characterization by Infrared Spectroscopy

Components of the final polyurethane were selected based on previous performance reports in blood contacting studies.[44,135] One study demonstrated the effectiveness of PPG based poly(ether urethane) materials over alternatives including PEG and PTMG in blood contacting uses.[44] Another study showed effective adsorption of blood proteins that inhibit platelet adhesion and subsequent clot formation using poly(ether urethane urea) materials.[135] HDI was used as the hard segment since the aim of the PU is to improve the ductility of BC. The linear, flexible structure of HDI aids in producing an elastomer versus other more rigid isocyanates. The structure of the prepolymer is shown in Figure 39.

A catalyst free system was used in the prepolymer formation since the end use is aimed at medical applications. Characterization of the reaction is necessary in order to ensure the proper reaction took place and to ensure the reaction can be completed in a reasonable time frame. FTIR was used (Figure 44) to track the changes in absorption

bands before and after the reaction. The intensity of the absorption band at 3450 cm^{-1} from the PPG terminal OH is reduced as the intensity of the absorption band at 3350 cm^{-1} from the NH stretching associated with the urethane group increases, indicating the reaction is taking place. Additionally, the presence of the absorption bands at 1710 and 1530 cm^{-1} indicates the formation of the urethane group.

The reaction was performed and measured every 30 minutes by FTIR spectroscopy. The method allowed for monitoring of the isocyanate peak. Similar studies have been previously reported.[136,137] Reaction constants between hydroxyls and isocyanates have been reported for reactions between polyols and diisocyanates. However, these reactions were performed with equal molar ratios, where one hydroxyl on each dihydroxyl molecule would react with one isocyanate on each diisocyanate molecule. That scenario is very different from the reaction performed in this work where each hydroxyl on the polyol is reacted with an isocyanate upon completion. Under ideal conditions, all available hydroxyls are reacted and 50% of the isocyanate functionalities are reacted. This leaves the remaining 50% of unreacted isocyanate groups for later reaction with a chain extender, such as diamines or diols, to convert the prepolymer to the final PU with significant mechanical properties.

Some reports exist analyzing the conversion of urethane polymerizations, and a few analyze prepolymer formation. At the time of the work, no evaluation was found investigating PPG and HDI. The desire to produce the material without a catalyst for use as a biomedical urethane created a need to verify if the reaction could be performed in a reasonable time. The reaction was performed in the melt, absent of solvent, between two NaCl windows. The sandwiched melt was heated in an inert environment and placed in a FTIR spectrometer every half hour to collect spectra. The spectra exhibited smooth decreases in starting material absorption bands and smooth increases in final product absorption bands, shown in Figure 45 through Figure 48. The peak areas show the same trends in Figure 49 through Figure 52.

In order to empirically compare the data, the Carothers' equation was used. This equation relates the conversion (p) of a reaction to a number average degree of polymerization ($\overline{X}_n$), shown in equation 14. Using the isocyanate to define the parameters of the analysis, the prepolymer reaction is complete when half of all

isocyanate groups are reacted with the polyether diol, controlled by stoichiometric balance in a 2:1 ratio, respectively. Assuming half the diisocyanate functional groups are reacted, as designed, it is associated with a conversion of 0.5 and a degree of polymerization of 2. This allows the degree of polymerization to be plotted versus time using the isocyanate peak at time zero as a conversion of zero and at 24 hours as a conversion of 0.5. The peak areas can then be converted to a degree of polymerization and plotted.

$$\overline{X}_n = \frac{1}{1-p} \qquad \text{Eq. 14}$$

The result of this analysis is presented in Figure 64. The reactions proceed in a linear order for the duration of the eight hour collection period. The PPG 1000 shows slower conversion in the reaction while the other three PPG of different chain lengths (425, 725, and 1000) follow nearly identical behavior. Traditional theory suggests as PPG chains increase in length ($\overline{X}_n$), a corresponding increase in the mean square end-to-end distance should be observed. Additionally, the concentration of polymer end-groups decreases as chain lengths increase. The concentration of end-groups effects the frequency of end-group collisions, resulting in slower conversion. Thus, it is expected that the reaction conversion slows down with increasing chain lengths. Also, the reaction was performed in the melt, absent of solvent. Another possible explanation could be a microphase separation between immiscible components. The PPG chains possess increasing hydrophobicity with increasing chain lengths. Therefore, it would be expected that if HDI and PPG 1000 were immiscible, HDI and PPG 2000 would also be immiscible. The data suggests PPG 2000 and HDI are miscible from conversion similar to reactions using PPG 425 and PPG 725. The experiment was performed multiple times with PPG 1000 and PPG 2000 to confirm the unexpected result. This behavior remains unclear.

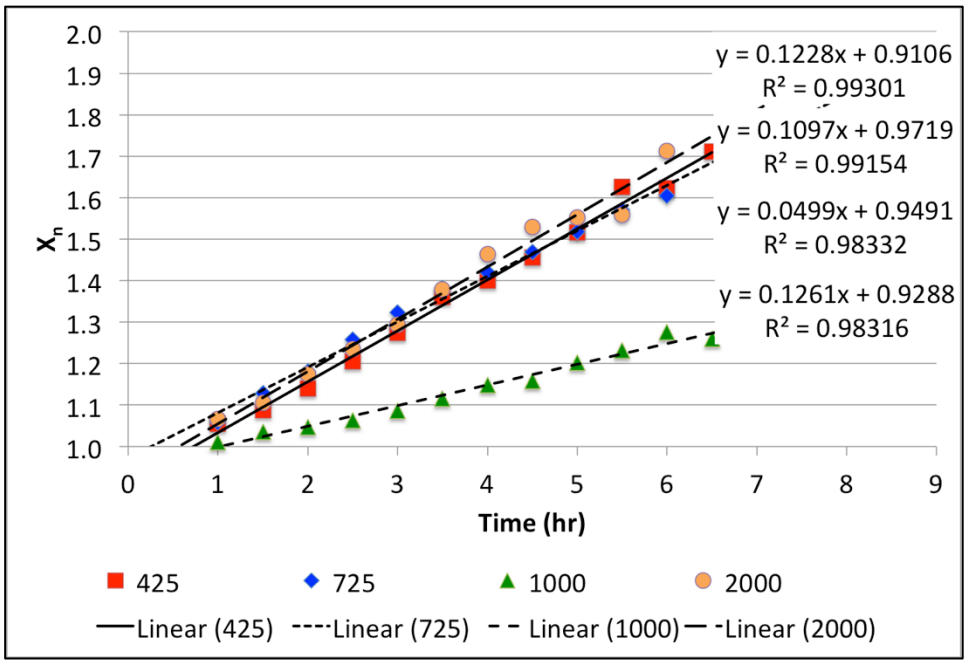

Figure 64: Conversion of Isocyanate to Urethane (PPG + HDI)
The degree of polymerization is shown here. The plot was produced by using peak areas from FTIR and the Carothers' equation.

4.4.2. Synthesis of Polyurethane for Composite Formation

The synthesis for PU can follow two possible routes. Each route produces a different chain structure resulting in different properties. These different chain architectures are described in Figure 65. A statistical polymer is produced when all monomers are combined simultaneously and a block copolymer is produced through a two-step process with a prepolymer intermediate. Since the two-step process with a prepolymer intermediate produces a repeated structure, it was selected to use in this work. PU for use with BC was synthesized using PPG (soft segment), HDI (hard segment), and 1,4 butane diol (chain extender), shown in Figure 40. The polyether soft segment and diisocyanate hard segments were allowed time to react prior to the addition of the chain extending diol to take the material to a higher molecular weight with significant mechanical properties.

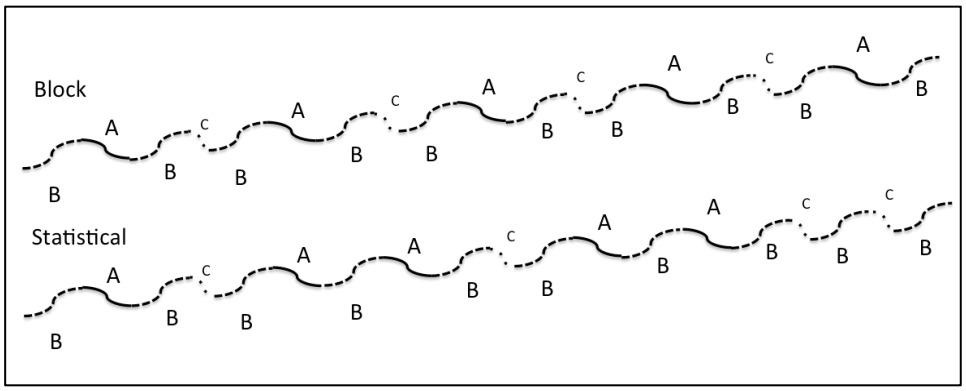

Figure 65: PU Synthesis Control Block vs Statistical Copolymer
Illustrated here are the differences between a statistical copolymer and block copolymer chain structure. Analogous to the work here, the segments represent the polyether diol (A), the diisocyanate (B), and the chain extender diol (C).

A useful measurement would have been the determination of the molecular weight for each PU. Gel permeation chromatography uses a polystyrene standard for calibration. This leads to the measurement being a relative comparison to the standards. The other possible method would determine a viscosity molecular weight. However, this method requires a set of *K* and *a* values for the specific polymer to apply the Mark-Houwink equation. The *K* and *a* values for this PU is not known. For these reasons, the molecular weight of the PUs was not characterized.

4.4.3. Catalyst Concentration in the Polyurethane

A catalyst was used for PU reaction for considerations of time in producing multiple polyurethanes for characterization. Stannous octoate (tin (II) 2-ethylhexanoate) (Figure 66) was selected since it is a common catalyst in urethane and poly(lactic acid) reactions and is approved by the FDA as a food stabilizer. However, the toxicity of this catalyst, while incorporated in the material, is debatable. Some studies show that the presence at levels of 2.0 wt% is toxic[138] while others show similar levels where the compound does not have any adverse reactions with cells.[139] Table 10 shows low weight percentages of the catalyst were used in each reaction. Still, in order to avoid debate, an additional step is used to remove the catalyst by washing with hexane.

A hexane wash is used with the PU and DMF to ensure that tin catalyst is removed before the PU is precipitated in water. Hexane and DMF are immiscible, allowing the catalyst to be transferred from DMF to hexane. The immiscible nature of

the two solvents is supported by their differing solubility parameter presented in Table 1. The transfer of stannous octoate from DMF to hexane is shown to be thermodynamically favorable by the similar solubility parameters of hexane and stannous octoate in Table 1. The hexane and DMF phases can easily be separated since they are immiscible. The PU can the then be precipitated out of solution with DMF in water.

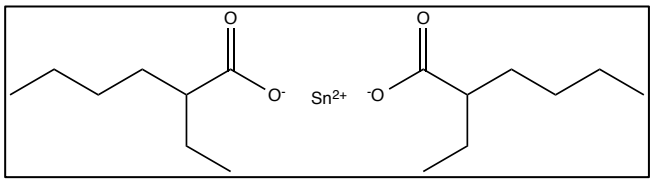

Figure 66: Stannous Octoate Chemical Structure
This figure shows the chemical structure of the catalyst used in the polyurethane reaction.

Table 10: Weight Percentage Stannous Octoate at 0.4mol%
The values for weight percent stannous octoate were determined by conversion of 0.4mol% to a weight percentage. The values represent a maximum concentration of the catalyst that can be present in the PU.

Polymer	425 PU	725 PU	1000 PU	2000 PU
Wt% Stannous Octoate	0.76	0.56	0.46	0.27

While the removal of catalysts from some medical polymers follow a procedure similar to the one performed here with a hexane wash, there are other alternatives, each with their own drawbacks. One option is a metal scavenging system, and the other is using a biomedical compatible catalyst. However, each of these options are more costly than the method used here to demonstrate the concept for producing a high-strength composite for vascular and venous applications.

4.4.4. BC/PU Composite Formation

DMF is used as a solvent for the PU reaction and to make a solution of PU for composite formation with BC. It is important to note that DMF will not affect the fibers or structure of BC. This was explained in greater detail in section 2.4.4 using a similar

discussion with cellulose and xylene. The difference in solubility parameters of DMF and BC are too great for dissolution or alteration of the BC fibers to take place. Further, the hydrogen bonding of cellulose will still prevent solvation by polar solvents with similar solubility parameters.[14,89]

Through control of the processing conditions, a biomimetic composite was formed. The overall composite dimensions, shown in Figure 55, mimicked that of the natural venous valve leaflets thicknesses with dimensions of 10 to 20 μm.[33] BC serves as a collagen mimicking component since the two materials have similar dimensional properties.[140] The fracture surface images reveal nano-sized features across the fracture surface and are the BC fibers. The fibers elongated slightly before fracture, thus producing the short rods observed in the images. This process is reasonable since the PU likely has a higher glass transition temperature (T_g) than the BC, which has a T_g of -16°C.[141] The glass transition temperature is a transition between rubber behavior (above the T_g) and rigid, brittle behavior (below the T_g). When the PU is behaving as a brittle material and BC is behaving as a more rubbery material, in comparison, the cellulose is able to deform before fracture while the PU produces a clean, smooth fracture surface. The images presented in Figure 55 show a correlation with thickness and the polyurethane soft segment length. However, this was not a measurement that was evaluated for statistical significance.

Table 9 lists average weight percent of BC in each BC/PU composite. The averages for each experimental group are statistically similar. The composites were produced from BC harvested from the same culture and processed with PU/DMF solutions identically. The average composite mass measured was 11 mg due to the very thin sample thickness of the 1.9 cm^2 samples. The small samples coupled with differences in the mass of adsorbed polyurethane between BC fibers produced samples with variance in overall weight percent composition. Still, all composites were statistically similar.

4.4.5. Mechanical Testing of BC/PU Composites

The goal of this work was to produce a composite with high strength and good blood compatibility. After formation of the composite, the mechanical properties are to be improved over NBC. The results in Figure 56 through Figure 58 show a strengthened

composite with optimal properties using the 1000 PPG based PU. The BC/PU 425 composite retains similar modulus and elongation to NBC. However there is a significant reduction in the strength of the composite versus NBC. The PU/BC 725 is the stiffest material (Figure 56), BC/PU 725 and BC/PU 1000 exhibit similar increased ductility (Figure 57), and the BC/PU 1000 shows the greatest strength (Figure 58). The BC/PU 2000 composite performed as a soft, weak material. Important improvements over NBC to note are a 57% increase in the modulus with BC/PU725, a 51% increase in the strength with BC/PU 1000, and an increase of 182% in the ductility using BC/PU 1000.

The trends observed in mechanical testing of BC/PU composites closely follow the trends measured in a similar PU using PPG as a soft segment.[44] The strongest neat PUs were produced using PPG 725 and 1000. The most rigid neat PUs were produced from PPG 425 and 725. The most ductile neat PU was produced using PPG 1000. The trends of neat PU reflected the trends from BC/PU composites, showing that changes in neat PU properties can predict changes in BC/PU composite properties.

Work by Takahara *et al.* explained observed trends in blood compatibility by microphase separation in PU materials.[44] The same discussion can be applied to this mechanical properties evaluation. The HDI hard segment and the PPG soft segment separate, driven by thermodynamic equilibrium, into two distinct microdomains. The hard segment can produce hydrogen bonds between the hard segment components while the soft segment can, depending on chemical structure and molecular weight, crystallize and contribute additional strength. The microdomains are structured as a continuous phase with a discontinuous phase or as two continuous phases. When the hard segment is in high concentration, it is the continuous phase.[44] The performance of BC/PU 425 suggests that the higher concentration of HDI is detrimental to the composite's performance. Once the HDI concentration is lowered due to the longer soft segment lengths, the composites show improved mechanical properties. This suggests the discontinuous phase is HDI and is ineffective as high concentration filler in PPG 425.

The results here do not follow traditional composite theory, from equations 1 and 2, where the composite exhibits properties as a weighted average based on the volume

fraction of fibers in the polymer matrix. One explanation is where fiber-reinforced composites perform as series of load bearing phases.[142] This leads to strength that exceeds the strength of the individual components that form the composite. Unlike the traditional theory, the composites formed here exceeded NBC in ductility, modulus, and strength. The results show that the PU and BC work together to accommodate the load, producing increased UTS in PU/BC 725 and PU/BC 1000 and an increased modulus in PU/BC 725. The increased elongation can be attributed to the ductile PU materials preventing fiber-fiber interactions that contribute to the brittle behavior of NBC.

4.4.6. In Vitro Testing of BC/PU Composites with HAEC's

This work shows that cells on the BC/PU scaffolds are viable after a 72 hour period (Figure 60). No effects of polyether molecular weight on cell viability were observed (Figure 61 and Figure 62) with the exception of PU with PPG 2000. This finding follows a similar trend as reported by Lyman *et al*.[135] The report by Lyman *et al* demonstrated that fibroblast cells were viable on poly(ether urethanes) after 48 hours. Between 48 and 96 hours, the scaffolds showed a dependence on the polyether molecular weight. PPG molecular weights of 425 and 725 continued to support cell growth at 96 hours, but higher molecular weight PPG poly(ether urethanes) showed cell growth ceased. The 72 hour time period used in the evaluation of BC/PU composites revealed a similar result with a decrease in cell viability on BC/PU 2000. More importantly, the assessment used here evaluated a more analogous cell line for the targeted application by culturing HAECs.

4.4.7. Protein Adsorption by BC/PU Composites

The findings in this evaluation show the materials can effectively adsorb BSA (Figure 63). This property is advantageous as the adsorption of albumin over other blood clot initiating proteins, such as fibrinogen and fibronectin, is desirable.[135,143] The values in this study are lower than some reports[103] and higher than others.[98] The conact angle decreases with longer soft segment lengths. The shorter soft segments with greater concentrations of hydrophilic urethane linkages adsorbs protein and decreases with greater soft segment length. However, the trend is absent of statistical significance. The processing method used here was utilized for all composites since it has been shown that the material these PUs are formed against can change the surface

properties.[133] Each composite was solution dip coated and dried in vacuum with heat while placed against a Teflon® film. This produced samples with a more hydrophobic surface, promoted by the drying step against a hydrophobic material and keeping hydrophilic groups in the sample bulk. In comparison, a more hydrophilic surface could be produced by forming against a hydrophilic substrate, such as glass.

The optimal mechanical performance of BC/PU 1000 is desirable since other studies using analogous PUs displayed good non-thrombogenic properties and cell behavior using PUs with PPG 1000.[44,56,144] One thrombogenicity study demonstrated PU with PPG 1000 performed best by adsorbing minimal platelets on the surface after incubation in platelet rich plasma.[44] It has also been demonstrated that adsorption of albumin occurred on PUs with PPG 1000 and exhibited minimal adsorption of coagulation initiating proteins, such as globulin or fibrinogen.[135] It was not noted in the study if the test was conducted for a long enough time period to evaluate the Vroman effect. This effect describes the dependency of protein adsorption on protein mobility. Albumin is a more mobile protein and, therefore, adsorbs before other proteins. At longer time periods, larger proteins, such as globulin and fibrinogen, can displace albumin depending on the affinity of each protein for the substrate. From these previous reports, it can be predicted that the PUs in this study will exhibit similar non-thrombogenic behavior and preferential adsorption of albumin since the chemical structure of the PU used here also utilizes a PPG soft segment.[44,135]

4.5. Conclusions

This work has shown the ability to form BC composites similar to previous studies. The difference in this work is the production of enhanced ductility by controlling the chemical structure to form an appropriate elastomer. Still, properties were enhanced up to 57% for the modulus, 51% for the strength, and 182% for ductility. The use of the polyurethane with BC fibers did not change cell and protein behavior from what was expected based upon previous literature with good cell viability after three days. While previous researchers using PU with PPG 1000 have shown promising resistance to platelet adhesion and adsorption of albumin, further evaluation of these BC/PU composites is necessary to evaluate the blood contacting properties of the composites.

Chapter 5
Future Work

5.1. BC/CdHA Interconnected Macroporous Scaffolds

The future work with BC/CdHA should examine a composite that exhibits: 1) resorbable components, 2) bone stimulating components, and 3) interconnected macroporosity, The work here demonstrated that OBC is resorbable under physiological conditions, CdHA can be deposited on NBC and OBC, and macroporous BC-CdHA can be produced. However, the macroporous structures shown here can be further improved by engineering scaffolds with interconnected macroporosity.

The porogen-leaching method described and demonstrated in this work utilizes microspheres that are allowed to self assemble in culture media and then grow cellulose around the microspheres. This method allows for point contacts between each sphere, but does not produce interconnectivity between each major void in the final cellulose structure, shown by Figure 24. Prior to culturing bacteria in the presence of the microspheres, an annealing step can be performed to produce a final structure with interconnected macroporosity. The annealing treatment allows for increased molecular motions resulting in a softened material. The softened microspheres allow the contact surface area to be increased and will lead to an interconnected macroporous scaffold. The general procedure for this would be: 1) allow the microspheres to self assemble in a container, 2) anneal the microspheres for greater contact area, 3) grow bacterial cellulose around the spheres, 4) leach out the porogen from the cellulose scaffold. Future animal model evaluations should utilize interconnected macroporous structures with resorbable bone stimulating components.

5.2. BC/PU Scaffolds

The PU chemical structure can be modified to include more rigid, hard segments due to ring structures between the diisocyanate groups (i.e. methylene diphenyl diisocyanate). The change in the hard segment can modify the mechanical properties of the PU and the composite once combined with BC. Another variable that can be evaluated is the effect of chemical crosslinks on the properties of PUs. The chemical

crosslinks can be produced by the incorporation of multifunctional monomers with three or more reactive end groups per molecule. Chemical crosslinking can enhance properties, but above a certain degree of crosslinking, the PU will no longer go into solution.

BC/PU composites with enhanced mechanical properties were produced and evaluated by tensile testing. The test method demonstrated the improved properties, but the method does not directly correlate with the targeted application of the native venous valve leaflet. Additional testing using a burst pressure test would provide further insight into the BC/PU composite properties. The burst pressure test is more analogous to the loading conditions the composite must withstand in the vein.

Traditional composite theory, as discussed previously, shows a dependency on performance based upon the composite components and the interaction between the composite components. The surface chemistry of the BC fibers can be modified to include more hydrophobic groups to improve interaction between the hydrophilic cellulose fibers and the more hydrophobic PU. This can be performed by nucleophilic substitution in basic solution with reaction between hydroxyls of the cellulose and alkyl chloride molecules. An alkyl ester is produced by the alkyl groups grafted to the surface of cellulose with a salt byproduct.

The BC/PU composite formed here can be produced by a different method, described in Figure 67 where the prepolymer is placed with cellulose and allowed to react. Modifying the cellulose surface chemistry can alter the bonding chemistry between cellulose and the polyether prepolymer. A urea bond between the polyether prepolymer and BC is more desirable as the reaction between amines and isocyanates is much quicker than for hydroxyls and isocyanates. Additionally, urea linkages have slower hydrolysis rates than urethane linkages, which is advantageous for long-term performance in aqueous environments. Amine functional groups can be added to the surface of cellulose fibers following an identical procedure described for the addition of alkyl groups to the cellulose hydroxyls. The cellulose fibers can be placed in a basic environment and reacted with 2-chloroethylamine. The reaction leaves an amine end group on the cellulose surface. The chemically linked prepolymer and fibers could exhibit different properties from the BC/PU composites reported here.

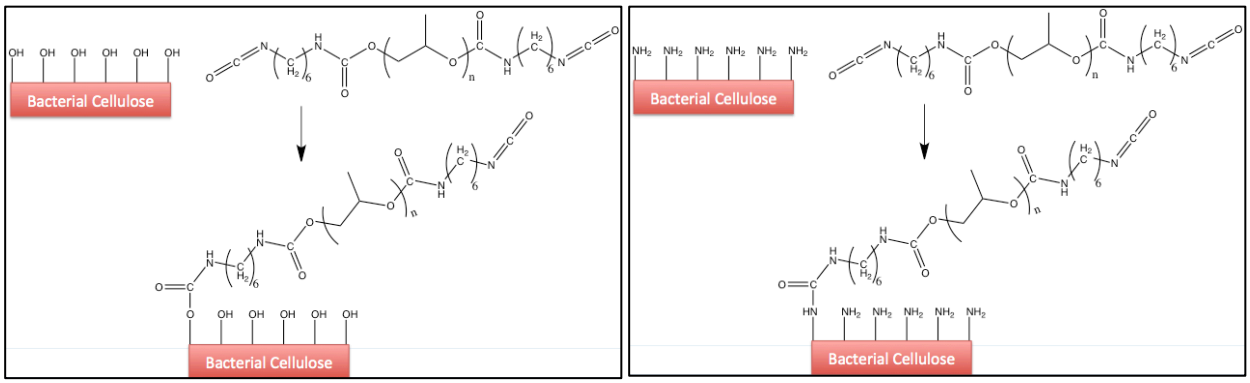

Figure 67: Reaction between the HDI-PPG-HDI prepolymer and Native BC
The bonding chemistry between the polyurethane prepolymer and the cellulose fiber can be formed (Left). Additionally, the speed of the reaction and be increased by amination (shown below) of the BC surface (Right). This also produces a more hydrolytically stable urea bond.

References

1. Fontana, JD, Desouza, AM, Fontana, CK, Torriani, IL, Moreschi, JC, Gallotti, BJ, Desouza, SJ, Narcisco, GP, Bichara, JA, and Farah, LFX, Acetobacter cellulose pellicle as a temporary skin substitue. Appl. Biochem. Biotechnol., 1990. 24-5: p253.
2. Czaja, W, Krystynowicz, A, Bielecki, S, and Brown, RM, Microbial cellulose - the natural power to heal wounds. Biomaterials, 2006. 27 (2): p145.
3. Klemm, D, Schumann, D, Udhardt, U, and Marsch, S, Bacterial synthesized cellulose - artificial blood vessels for microsurgery. Prog. Polym. Sci., 2001. 26 (9): p1561.
4. Backdahl, H, Risberg, B, and Gatenholm, P, Observations on bacterial cellulose tube formation for application as vascular graft. Materials Science & Engineering C-Materials for Biological Applications, 2011. 31 (1): p14.
5. Klemm, DO, Udhardt, URE, Schumann, DA, and Marsch, SE, Moulded biomaterial basyc (bacterial synthesized cellulose) - a promising artificial blood vessel for microsurgical use. Abstracts of Papers of the American Chemical Society, 2004. 227: p156.
6. Zaborowska, M, Bodin, A, Backdahl, H, Popp, J, Goldstein, A, and Gatenholm, P, Microporous bacterial cellulose as a potential scaffold for bone regeneration. Acta Biomater., 2010. 6 (7): p2540.
7. Hutchens, SA, Benson, RS, Evans, BR, Rawn, CJ, and O'Neill, H, A resorbable calcium-deficient hydroxyapatite hydrogel composite for osseous regeneration. Cellulose, 2009. 16 (5): p887.
8. Svensson, A, Nicklasson, E, Harrah, T, Panilaitis, B, Kaplan, DL, Brittberg, M, and Gatenholm, P, Bacterial cellulose as a potential scaffold for tissue engineering of cartilage. Biomaterials, 2005. 26 (4): p419.
9. Andersson, J, Stenhamre, H, Backdahl, H, and Gatenholm, P, Behavior of human chondrocytes in engineered porous bacterial cellulose scaffolds. J Biomed Mater Res A, 2010. 94A (4): p1124.
10. Jonas, R and Farah, LF, Production and application of microbial cellulose. Polym. Degrad. Stab., 1998. 59 (1-3): p101.
11. Brown, RM, Willison, JHM, and Richardson, CL, Cellulose biosynthesis in acetobacter-xylinum - visualization of site of synthesis and direct measurement of invivo process. Proceedings of the National Academy of Sciences of the United States of America, 1976. 73 (12): p4565.
12. Klemm, D, Schumann, D, Kramer, F, Hessler, N, Hornung, M, Schmauder, HP, and Marsch, S, Nanocelluloses as innovative polymers in research and application. Polysaccharides Ii, 2006. 205: p49.
13. Roy, D, Semsarilar, M, Guthrie, JT, and Perrier, S, Cellulose modification by polymer grafting: A review. Chem. Soc. Rev., 2009. 38 (7): p2046.
14. Helenius, G, Backdahl, H, Bodin, A, Nannmark, U, Gatenholm, P, and Risberg, B, In vivo biocompatibility of bacterial cellulose. J Biomed Mater Res A, 2006. 76A (2): p431.
15. Nevell, T, Methods in carbohydrate chemistry1962, New York: Academic Press.
16. Saito, T, Shibata, I, Isogai, A, Suguri, N, and Sumikawa, N, Distribution of carboxylate groups introduced into cotton linters by the tempo-mediated oxidation. Carbohydr. Polym., 2005. 61 (4): p414.

17. Tahiri, C and Vignon, MR, Tempo-oxidation of cellulose: Synthesis and characterisation of polyglucuronans. Cellulose, 2000. 7 (2): p177.
18. Painter, TJ, Control of depolymerization during the preparation of reduced dialdehyde cellulose. Carbohydr. Res., 1988. 179: p259.
19. Singh, M, Ray, AR, Vasudevan, P, Verma, K, and Guha, SK, Potential biosoluble carriers - biocompatibility and biodegradability of oxidized cellulose. Biomaterials Medical Devices and Artificial Organs, 1979. 7 (4): p495.
20. Singh, M, Ray, AR, and Vasudevan, P, Biodegradation studies on periodate oxidized cellulose. Biomaterials, 1982. 3 (1): p16.
21. RoyChowdhury, P and Kumar, V, Fabrication and evaluation of porous 2,3-dialdehydecellulose membrane as a potential biodegradable tissue-engineering scaffold. J Biomed Mater Res A, 2006. 76A (2): p300.
22. Kim, UJ, Kuga, S, Wada, M, Okano, T, and Kondo, T, Periodate oxidation of crystalline cellulose. Biomacromolecules, 2000. 1 (3): p488.
23. Frederick, EW, Smith, LH, Rabkin, MT, and Richie, RH, Studies on primary hyperoxaluria .1. In vivo demonstration of a defect in glyoxylate metabolism. New Engl. J. Med., 1963. 269 (16): p821.
24. Hutchens, SA, Characterization of a calcium-deficient hydroxyapatite bacterial cellulose composite, in Biomed. Eng.2007, University of Tennessee: Knoxville.
25. Martini, F, Timmons, MJ, and Tallitsch, RB, Human anatomy. 6th ed2009, San Francisco: Pearson Benjamin Cummings. xxxiii, 869 p.
26. Daculsi, G, Legeros, RZ, and Mitre, D, Crystal dissolution of biological and ceramic apatites. Calcif. Tissue Int., 1989. 45 (2): p95.
27. LeGeros, RZ and LeGeros, JP, Calcium phosphate bioceramics: Past, present and future. Bioceramics 15, 2003. 240-2: p3.
28. Bourgeois, B, Laboux, O, Obadia, L, Gauthier, O, Betti, E, Aguado, E, Daculsi, G, and Bouler, JM, Calcium-deficient apatite: A first in vivo study concerning bone ingrowth. J Biomed Mater Res A, 2003. 65A (3): p402.
29. Vallet-Regi, M, Rodriguez-Lorenzo, LM, and Salinas, AJ, Synthesis and characterisation of calcium deficient apatite. Solid State Ionics, 1997. 101: p1279.
30. Suchanek, W and Yoshimura, M, Processing and properties of hydroxyapatite-based biomaterials for use as hard tissue replacement implants. J. Mater. Res., 1998. 13 (1): p94.
31. Hutchens, SA, Benson, RS, Evans, BR, O'Neill, HM, and Rawn, CJ, Biomimetic synthesis of calcium-deficient hydroxyapatite in a natural hydrogel. Biomaterials, 2006. 27 (26): p4661.
32. Park, JB, Biomaterials science and engineering1984, New York: Plenum Press. xv, 459 p.
33. Sumner, D and Zierler, R, Vascular physiology, in Vascular surgery, Rutherfer, R, Editor 2005, Elsevier.
34. Chronic deep vein incompetence, in Diseases of the veins, Browse, N, et al., Editors. 1999, Arnold Publishers: London.
35. Sumner, Vascular physiology, in Vascular surgery, Rutherfer, Editor 2005, Elsevier.
36. Lurie, F, The functioning of venous valves in normal and pathological conditions. Medicographia, 2008. 30: p95.

37. Lurie, F, Kistner, RL, Eklof, B, and Kessler, D, Mechanism of venous valve closure and role of the valve in circulation: A new concept. J Vasc Surg, 2003. 38 (5): p955.
38. Odian, GG, Principles of polymerization. 4th ed2004, Hoboken, N.J.: Wiley-Interscience. xxiv, 812 p.
39. Braun, D, Cherdron, H., Kern, W., Techniques of polymer syntheses and characterization1972: New York, Wiley-Interscience.
40. Lyman, DJ, Polyurethanes .1. The solution polymerization of diisocyanates with ethylene glycol. Journal of Polymer Science, 1960. 45 (145): p49.
41. Stevens, MP, Polymer chemistry : An introduction. 3rd ed1999, New York: Oxford University Press. xix, 551 p.
42. Blackwell, J and Gardner, KH, Structure of the hard segments in polyurethane elastomers. Polymer, 1979. 20 (1): p13.
43. Takahara, A, Tashita, J, Kajiyama, T, and Takayanagi, M, Effect of aggregation state of hard segment in segmented poly(urethaneureas) on their fatigue behavior after interaction with blood components. Journal of Biomedical Materials Research, 1985. 19 (1): p13.
44. Takahara, A, Tashita, J, Kajiyama, T, Takayanagi, M, and Macknight, WJ, Microphase separated structure, surface-composition and blood compatibility of segmented poly(urethaneureas) with various soft segment components. Polymer, 1985. 26 (7): p987.
45. Chu, B, Gao, T, Li, YJ, Wang, J, Desper, CR, and Byrne, CA, Microphase separation kinetics in segmented polyurethanes - effects of soft segment length and structure. Macromolecules, 1992. 25 (21): p5724.
46. Gorna, K, Polowinski, S, and Gogolewski, S, Synthesis and characterization of biodegradable poly(epsilon-caprolactone urethane)s. I. Effect of the polyol molecular weight, catalyst, and chain extender on the molecular and physical characteristics. Journal of Polymer Science Part a-Polymer Chemistry, 2002. 40 (1): p156.
47. Blackwell, J, Nagarajan, MR, and Hoitink, TB, Structure of polyurethane elastomers - effect of chain extender length on the structure of mdi diol hard segments. Polymer, 1982. 23 (7): p950.
48. Zhang, CH, Zhang, N, and Wen, XJ, Improving the elasticity and cytophilicity of biodegradable polyurethane by changing chain extender. Journal of Biomedical Materials Research Part B-Applied Biomaterials, 2006. 79B (2): p335.
49. Tatai, L, Moore, TG, Adhikari, R, Malherbe, F, Jayasekara, R, Griffiths, I, and Gunatillake, PA, Thermoplastic biodegradable polyurethanes: The effect of chain extender structure on properties and in-vitro degradation. Biomaterials, 2007. 28 (36): p5407.
50. Wilkes, GL, Dziemianowicz, TS, Ophir, ZH, Artz, E, and Wildnauer, R, Thermally induced time-dependence of mechanical-properties in biomedical grade polyurethanes. Journal of Biomedical Materials Research, 1979. 13 (2): p189.
51. Kojio, K, Furukawa, M, Nonaka, Y, and Nakamura, S, Control of mechanical properties of thermoplastic polyurethane elastomers by restriction of crystallization of soft segment. Materials, 2010. 3 (12): p5097.

52. Petrovic, ZS, Ilavsky, M, Dusek, K, Vidakovic, M, Javni, I, and Banjanin, B, The effect of cross-linking on properties of polyurethane elastomers. J. Appl. Polym. Sci., 1991. 42 (2): p391.
53. Butnaru, M, Bredetean, O, Macocinschi, D, Dimitriu, CD, Knieling, L, and Harabagiu, V, Biocompatibility and biological performance of the improved polyurethane membranes for medical applications, in Polyurethane, Zafar, DF, Editor 2012, InTech.
54. Reed, A, Potter, J, and Szycher, M, A solution grade biostable polyurethane elastomer: Chronoflex ar. J. Biomater. Appl., 1994. 8 (3): p210.
55. Lyman, DJM, L. C.; Albo, D. Jr.; Richards, K. F.; Lamb, J., The effect of chemical structure and surface properties of synthetic polymers on the coagulation of blood. Iii. In vivo adsorption of proteins on polymer surfaces. American Society for Artificial Internal Organs, 1974. 20 (1): p474.
56. Lyman, DJ, Metcalf, LC, Albo, D, Richards, KF, and Lamb, J, Effect of chemical-structure and surface properties of synthetic-polymers on coagulation of blood .3. Invivo adsorption of proteins on polymer surfaces. Transactions American Society for Artificial Internal Organs, 1974. B 20: p474.
57. Shibatani, K, Lyman, DJ, Shieh, DF, and Knutson, K, Polyurethanes .4. Effect of poly(propylene glycol) tacticity on properties of block copolyether-urethanes. Journal of Polymer Science Part a-Polymer Chemistry, 1977. 15 (7): p1655.
58. Callister, WD, Materials science and engineering : An introduction. 7th ed2007, New York: John Wiley & Sons. xxv, 721, A41, G14, S5, I22 p.
59. Fried, JR, Polymer science and technology. 2nd ed2003, Upper Saddle River, NJ: Prentice Hall Professional Technical Reference. xvii, 582 p.
60. Van Krevelen, DW, Hoftyzer, P.J., Properties of polymers: Correlations with chemical structure1997, New York: Elsevier Pub. Co. 427.
61. Horvath, AL, Solubility of structurally complicated materials: I. Wood. J. Phys. Chem. Ref. Data, 2006. 35 (1): p77.
62. Hansen, CM and Bjorkman, A, The ultrastructure of wood from a solubility parameter point of view. Holzforschung, 1998. 52 (4): p335.
63. Hansen, CM, Hansen solubility parameters [electronic resource] : A user's handbook2000, Boca Raton, Fla.: Boca Raton, Fla. : CRC Press.
64. Gatenholm, P and Klemm, D, Bacterial nanocellulose as a renewable material for biomedical applications. MRS Bull., 2010. 35 (3): p208.
65. Rowland, SP and Cousins, ER, Periodate oxidative decrystallization of cotton cellulose. Journal of Polymer Science Part a-1-Polymer Chemistry, 1966. 4 (4PA1): p793.
66. Hou, QX, Liu, W, Liu, ZH, and Bai, LL, Characteristics of wood cellulose fibers treated with periodate and bisulfite. Industrial & Engineering Chemistry Research, 2007. 46 (23): p7830.
67. Lyons, KM, Pelton, RW, and Hogan, BLM, Organogenesis and pattern-formation in the mouse - rna distribution patterns suggest a role for bone morphogenetic protein-2a (bmp-2a). Development, 1990. 109 (4): p833.
68. Centrella, M, Horowitz, MC, Wozney, JM, and McCarthy, TL, Transforming growth-factor-beta gene family members and bone. Endocr. Rev., 1994. 15 (1): p27.

69. Simmons, CA, Alsberg, E, Hsiong, S, Kim, WJ, and Mooney, DJ, Dual growth factor delivery and controlled scaffold degradation enhance in vivo bone formation by transplanted bone marrow stromal cells. Bone, 2004. 35 (2): p562.
70. Deckers, MML, van Bezooijen, RL, van der Horst, G, Hoogendam, J, van der Bent, C, Papapoulos, SE, and Lowik, C, Bone morphogenetic proteins stimulate angiogenesis through osteoblast-derived vascular endothelial growth factor a. Endocrinology, 2002. 143 (4): p1545.
71. Huang, YC, Kaigler, D, Rice, KG, Krebsbach, PH, and Mooney, DJ, Combined angiogenic and osteogenic factor delivery enhances bone marrow stromal cell-driven bone regeneration. J. Bone Miner. Res., 2005. 20 (5): p848.
72. Kanczler, JM, Ginty, PJ, White, L, Clarke, NMP, Howdle, SM, Shakesheff, KM, and Oreffo, ROC, The effect of the delivery of vascular endothelial growth factor and bone morphogenic protein-2 to osteoprogenitor cell populations on bone formation. Biomaterials, 2010. 31 (6): p1242.
73. Saska, S, Scarel-Caminaga, RM, Teixeira, LN, Franchi, LP, dos Santos, RA, Gaspar, A, de Oliveira, PT, Rosa, A, Takahashi, C, Messaddeq, Y, Ribeiro, SJL, and Marchetto, R, Characterization and in vitro evaluation of bacterial cellulose membranes functionalized with osteogenic growth peptide for bone tissue engineering. Journal of Materials Science-Materials in Medicine, 2012. 23 (9): p2253.
74. Muller, A, Ni, ZX, Hessler, N, Wesarg, F, Muller, FA, Kralisch, D, and Fischer, D, The biopolymer bacterial nanocellulose as drug delivery system: Investigation of drug loading and release using the model protein albumin. J. Pharm. Sci., 2013. 102 (2): p579.
75. Wan, YZ, Gao, C, Han, M, Liang, H, Ren, KJ, Wang, YL, and Luo, HL, Preparation and characterization of bacterial cellulose/heparin hybrid nanofiber for potential vascular tissue engineering scaffolds. Polym. Adv. Technol., 2011. 22 (12): p2643.
76. Reddi, AH, Role of morphogenetic proteins in skeletal tissue engineering and regeneration. Nat. Biotechnol., 1998. 16 (3): p247.
77. Backdahl, H, Helenius, G, Bodin, A, Nannmark, U, Johansson, BR, Risberg, B, and Gatenholm, P, Mechanical properties of bacterial cellulose and interactions with smooth muscle cells. Biomaterials, 2006. 27 (9): p2141.
78. Backdahl, H, Esguerra, M, Delbro, D, Risberg, B, and Gatenholm, P, Engineering microporosity in bacterial cellulose scaffolds. Journal of Tissue Engineering and Regenerative Medicine, 2008. 2 (6): p320.
79. Schramm, M and Hestrin, S, Factors affecting production of cellulose at the air liquid interface of a culture of acetobacter-xylinum. J. Gen. Microbiol., 1954. 11 (1): p123.
80. Yadav, V, Paniliatis, BJ, Shi, H, Lee, K, Cebe, P, and Kaplan, DL, Novel in vivo-degradable cellulose-chitin copolymer from metabolically engineered gluconacetobacter xylinus. Appl. Environ. Microbiol., 2010. 76 (18): p6257.
81. Feng, YH, Li, JC, Lin, Q, Pang, SJ, Zhang, MY, Wang, XB, Wu, ZX, and Sun, ZL, Determination methods of dialdehyde celluloses from bacterial cellulose, 2008. p507-510.

82. Grafahrend, D, Heffels, KH, Beer, MV, Gasteier, P, Moller, M, Boehm, G, Dalton, PD, and Groll, J, Degradable polyester scaffolds with controlled surface chemistry combining minimal protein adsorption with specific bioactivation. Nature Materials, 2011. 10 (1): p67.
83. Kim, J, Kim, SW, Park, S, Lim, KT, Seonwoo, H, Kim, Y, Hong, BH, Choung, Y, Chung, JH, Bacterial cellulose nanofibrillar patch as a wound healing platform of tympanic membrane perforation. Advanced Healthcare Materials, 2013.
84. Tihlarik, K and Pasteka, M, Cellulose dialdehyde - comparison of the methods of determination. Cellul. Chem. Technol., 1993. 27 (3): p267.
85. Zhao, H and Heindel, ND, Determination of degree of substitution of formyl groups in polyaldehyde dextran by the hydroxylamine hydrochloride method. Pharm. Res., 1991. 8 (3): p400.
86. Li, J, Wan, YZ, Li, LF, Liang, H, and Wang, JH, Preparation and characterization of 2,3-dialdehyde bacterial cellulose for potential biodegradable tissue engineering scaffolds. Materials Science & Engineering C-Biomimetic and Supramolecular Systems, 2009. 29 (5): p1635.
87. Kristiansen, KA, Potthast, A, and Christensen, BE, Periodate oxidation of polysaccharides for modification of chemical and physical properties. Carbohydr. Res., 2010. 345 (10): p1264.
88. Wang, D, Christensen, K, Chawla, K, Xiao, GZ, Krebsbach, PH, and Franceschi, RT, Isolation and characterization of mc3t3-e1 preosteoblast subclones with distinct in vitro and in vivo differentiation mineralization potential. J. Bone Miner. Res., 1999. 14 (6): p893.
89. Gilbert, R and Kadla, J, Cellulose modification. Polymer modification: Principles, techniques, and applications, ed. Meister, JJ2000, New York: New York : Marcel Dekker.
90. McCormick, CL, Callais, PA, and Hutchinson, BH, Solution studies of cellulose in lithium-chloride and n,n-dimethylacetamide. Macromolecules, 1985. 18 (12): p2394.
91. da Silva, J, Lautenschlager, F, Sivaniah, E, and Guck, JR, The cavity-to-cavity migration of leukaemic cells through 3d honey-combed hydrogels with adjustable internal dimension and stiffness. Biomaterials, 2010. 31 (8): p2201.
92. Peyton, SR, Kalcioglu, ZI, Cohen, JC, Runkle, AP, Van Vliet, KJ, Lauffenburger, DA, and Griffith, LG, Marrow-derived stem cell motility in 3d synthetic scaffold is governed by geometry along with adhesivity and stiffness. Biotechnol. Bioeng., 2011. 108 (5): p1181.
93. Schlufter, K, Schmauder, HP, Dorn, S, and Heinze, T, Efficient homogeneous chemical modification of bacterial cellulose in the ionic liquid 1-n-butyl-3-methylimidazolium chloride. Macromol. Rapid Commun., 2006. 27 (19): p1670.
94. Williams, PT and Besler, S, The influence of temperature and heating rate on the pyrolysis of biomass. Renewable Energy, 1996. 7 (3): p233.
95. Roman, M and Winter, WT, Effect of sulfate groups from sulfuric acid hydrolysis on the thermal degradation behavior of bacterial cellulose. Biomacromolecules, 2004. 5 (5): p1671.

96. Zhang, YHP and Lynd, LR, Toward an aggregated understanding of enzymatic hydrolysis of cellulose: Noncomplexed cellulase systems. Biotechnol. Bioeng., 2004. 88 (7): p797.
97. Anthony, JC and Clarke, AJ, Biodegradation of cellulose : Enzymology and biotechnology1997, Lancaster, Pa.: Lancaster, Pa. : Technomic Pub. Co.
98. Howell, JA and Stuck, JD, Kinetics of solka floc cellulose hydrolysis by trichoderma-viride cellulase. Biotechnol. Bioeng., 1975. 17 (6): p873.
99. Hammonds, RL, Harrison, MS, Cravanas, TC, Gazzola, WH, Stephens, CP, and Benson, RS, Biomimetic hydroxyapatite powder from a bacterial cellulose scaffold. Cellulose, 2012. 19: p1923.
100. Mostafa, NY, Characterization, thermal stability and sintering of hydroxyapatite powders prepared by different routes. Mater. Chem. Phys., 2005. 94 (2-3): p333.
101. Mortier, A, Lemaitre, J, and Rouxhet, PG, Temperature-programmed characterization of synthetic calcium-deficient phosphate apatites. Thermochim. Acta, 1989. 143: p265.
102. Posner, AS, Crystal chemistry of bone mineral. Physiol. Rev., 1969. 49 (4): p760.
103. Sullivan, AL and Ball, R, Thermal decomposition and combustion chemistry of cellulosic biomass. Atmos. Environ., 2012. 47: p133.
104. Bohn, A, Fink, HP, Ganster, J, and Pinnow, M, X-ray texture investigations of bacterial cellulose. Macromol. Chem. Phys., 2000. 201 (15): p1913.
105. Czaja, W, Romanovicz, D, and Brown, RM, Structural investigations of microbial cellulose produced in stationary and agitated culture. Cellulose, 2004. 11 (3-4): p403.
106. Meissner, M, Moneta, G, Burnand, K, Gloviczki, P, Lohr, J, Lurie, F, Mattos, M, McLafferty, R, Mozes, G, Rutherford, R, Padberg, F, and Sumner, D, The hemodynamics and diagnosis of venous disease. Journal of Vascular Surgery, 2007. 46: p4S.
107. Criado, E and Johnson, G, Venous disease. Current Problems in Surgery, 1991. 28 (5): p339.
108. Eklof, B, Perrin, M, Delis, KT, Rutherford, RB, and Gloviczki, P, Updated terminology of chronic venous disorders: The vein-term transatlantic interdisciplinary consensus document. J Vasc Surg, 2009. 49 (2): p498.
109. Meissner, MH, Eklof, B, Gloviczki, P, Lohr, JM, Lurie, F, Kistner, R, Moneta, G, and Wakefield, TW, Mapping the future: Organizational, clinical, and research priorities in venous disease. J Vasc Surg, 2007. 46: p84S.
110. Corcos, L, Peruzzi, G, Procacci, T, Spina, T, Cavina, C, and DeAnna, D, A new autologous venous valve by intimal flap. One case report. Minerva Cardioangiol., 2003. 51 (4): p395.
111. Taheri, S and Schultz, R, Experimental prosthetic vein valve: Long term results. Angiology, 1995. 46: p299.
112. Pavcnik, D, Update on venous valve replacement: Long term clinical results. Vascular, 2006. 14: p106.
113. Pavcnik, D, Kaufman, J, Uchida, B, Case, B, Corea, O, Hamada, A, Keller, F, and FS, R, Significance of spatial orientation of percutaneously placed bioprosthetic valve in an ovine model. JVIR, 2005. 16: p1511.

114. DeBorst, G, Teijink, J, Patterson, M, Quijano, T, and Moll, F, A percutaneous approach to deep venous valve insufficiency with a new self-expanding venous frame valve. J Endovasc Ther, 2003. 10: p341.
115. Sathe, R, Design and development of a novel implantable prosthetic vein valve, in Mechanical Engineering2006, Georgia Institute of Technology Atlanta, GA.
116. Rittgers, S, Oberdier, M, and Pottala, S, Physiologically-based testing system for the mechanical characterization of prosthetic vein valves. . Biomedical Engineering, 2007. 6: p29.
117. Tashiro, K and Kobayashi, M, Theoretical evaluation of 3-dimensional elastic-constants of native and regenerated celluloses - role of hydrogen-bonds. Polymer, 1991. 32 (8): p1516.
118. Turbak, AFS, F.W.; Sandberg, K.R. Microfibrillated cellulose, a new cellulose product: Properties, uses, and commercial potential. in J. Appl. Polym. Sci.: Appl. Polym. Symp. 1983. Syracuse, NY.
119. Herrick, FWC, R.L.; Hamilton, J.K.; Sandberg, K.R. Microfibrillated cellulose: Morphology and accessibility. in J. Appl. Polym. Sci.: Appl. Polym. Symp. 1983. Syracuse, NY.
120. Eichhorn, SJ, Dufresne, A, Aranguren, M, Marcovich, NE, Capadona, JR, Rowan, SJ, Weder, C, Thielemans, W, Roman, M, Renneckar, S, Gindl, W, Veigel, S, Keckes, J, Yano, H, Abe, K, Nogi, M, Nakagaito, AN, Mangalam, A, Simonsen, J, Benight, AS, Bismarck, A, Berglund, LA, and Peijs, T, Review: Current international research into cellulose nanofibres and nanocomposites. Journal of Materials Science, 2010. 45 (1): p1.
121. Siro, I and Plackett, D, Microfibrillated cellulose and new nanocomposite materials: A review. Cellulose, 2010. 17 (3): p459.
122. Hsieh, YC, Yano, H, Nogi, M, and Eichhorn, SJ, An estimation of the young's modulus of bacterial cellulose filaments. Cellulose, 2008. 15 (4): p507.
123. Nishi, Y, Uryu, M, Yamanaka, S, Watanabe, K, Kitamura, N, Iguchi, M, and Mitsuhashi, S, The structure and mechanical-properties of sheets prepared from bacterial cellulose .2. Improvement of the mechanical-properties of sheets and their applicability to diaphragms of electroacoustic transducers. Journal of Materials Science, 1990. 25 (6): p2997.
124. Seydibeyoglu, MO and Oksman, K, Novel nanocomposites based on polyurethane and micro fibrillated cellulose. Composites Sci. Technol., 2008. 68 (3-4): p908.
125. Pei, AH, Malho, JM, Ruokolainen, J, Zhou, Q, and Berglund, LA, Strong nanocomposite reinforcement effects in polyurethane elastomer with low volume fraction of cellulose nanocrystals. Macromolecules, 2011. 44 (11): p4422.
126. Juntaro, J, Pommet, M, Mantalaris, A, Shaffer, M, and Bismarck, A, Nanocellulose enhanced interfaces in truly green unidirectional fibre reinforced composites. Compos. Interfaces, 2007. 14 (7-9): p753.
127. Yano, H, Sugiyama, J, Nakagaito, AN, Nogi, M, Matsuura, T, Hikita, M, and Handa, K, Optically transparent composites reinforced with networks of bacterial nanofibers. Adv. Mater., 2005. 17 (2): p153.
128. Ganß, K, Nechwatal, A, Frankenfeld, K, and Schlufter, K, Difficulties in the use of ground bacterial cellulose (bc) as reinforcement of polylactid acid (pla) using

melt-mixing and extrusion technologies. Open Journal of Composite Materials, 2012. 2 (3): p97.
129. Nakagaito, AN, Iwamoto, S, and Yano, H, Bacterial cellulose: The ultimate nano-scalar cellulose morphology for the production of high-strength composites. Applied Physics a-Materials Science & Processing, 2005. 80 (1): p93.
130. Gindl, W and Keckes, J, Tensile properties of cellulose acetate butyrate composites reinforced with bacterial cellulose. Composites Sci. Technol., 2004. 64 (15): p2407.
131. Woo, KM, Chen, VJ, and Ma, PX, Nano-fibrous scaffolding architecture selectively enhances protein adsorption contributing to cell attachment. J Biomed Mater Res A, 2003. 67A (2): p531.
132. Bummer, PM and Knutson, K, Infrared spectroscopic examination of the surfaces of hydrated copoly(ether-urethane-ureas). Macromolecules, 1990. 23 (20): p4357.
133. Knutson, K and Lyman, DJ, Morphology of block copolyurethanes. Ii. Ftir and esca techniques for studying surface morphology, in Biomedical and dental applications of polymers, Gebelein, CG and Koblitz, FF, Editors. 1980, Plenum Press: New York p173–188.
134. Knutson, K and Lyman, DJ, The effect of polyether segment molecular-weight on the bulk and surface morphologies of copolyether-urethane ureas. Adv. Chem. Ser., 1982 (199): p109.
135. Lyman, DJ, Knutson, K, McNeill, B, and Shibatani, K, Effects of chemical-structure and surface properties of synthetic-polymers on coagulation of blood .4. Relation between polymer morphology and protein adsorption. Transactions American Society for Artificial Internal Organs, 1975. 21: p49.
136. HG Wissman, LR, KC Frisch, Kinetics of polyether polyols–diisocyanate reactions. J. Appl. Polym. Sci., 1964. 8 (6): p2971.
137. Page, JM, Prieto, EM, Dumas, JE, Zienkiewicz, KJ, Wenke, JC, Brown-Baer, P, and Guelcher, SA, Biocompatibility and chemical reaction kinetics of injectable, settable polyurethane/allograft bone biocomposites. Acta Biomater., 2012. 8 (12): p4405.
138. Tanzi, MC, Verderio, P, Lampugnani, MG, Resnati, M, Dejana, E, and Sturani, E, Cytotoxicity of some catalysts commonly used in the synthesis of copolymers for biomedical use. Journal of Materials Science-Materials in Medicine, 1994. 5 (6-7): p393.
139. Guan, JJ, Fujimoto, KL, Sacks, MS, and Wagner, WR, Preparation and characterization of highly porous, biodegradable polyurethane scaffolds for soft tissue applications. Biomaterials, 2005. 26 (18): p3961.
140. Torres, FGC, S.; Troncoso, O.P. , Biocompatibility of bacterial cellulose based biomaterials. Journal of Functional Biomaterials, 2012. 3 (4): p864.
141. Barud, HS, Ribeiro, CA, Crespi, MS, Martines, MAU, Dexpert-Ghys, J, Marques, RFC, Messaddeq, Y, and Ribeiro, SJL, Thermal characterization of bacterial cellulose-phosphate composite membranes. J. Therm. Anal. Calorim., 2007. 87 (3): p815.
142. McCrum, NG, Buckley, CP, and Bucknall, CB, Principles of polymer engineering. 2nd ed1997, Oxford ; New York: Oxford University Press. xiv, 447 p.

143. Maria Butnaru, OB, Doina Macocinschi, Cristina Daniela Dimitriu, Laura Knieling and Valeria Harabagiu, Biocompatibility and biological performance of the improved polyurethane membranes for medical applications, polyurethane, in Polyurethane, Zafar, DF, Editor 2012, InTech.
144. Lyman, DJ, Brash, JL, Chaikin, SW, Klein, KG, and Carini, M, Effect of chemical structure and surface properties of synthetic polymers on coagulation of blood .2. Protein and platelet interaction with polymer surfaces. Transactions American Society for Artificial Internal Organs, 1968. 14 (APR): p250.
145. Elidrissi, A, Barkany, SE, Amhamdi, H, Maaroufi, A, and Hammouti, B, New approach to predict the solubility of polymers application: Cellulose acetate at various ds, prepared from alfa "stipa -tenassicima" of eastern morocco. Journal of Materials and Environmental Studies, 2012. 3 (2): p270.

Appendix

Appendix A. List of Abbreviations

BC	Bacterial Cellulose
BMP	Bone Morphogenetic Protein
BSA	Bovine Serum Albumin
CdHA	Calcium-deficient Hydroxyapatite
DMAc	*N,N*-dimethyl acetamide
DMF	Dimethylformamide
FGF	Fibroblast Growth Factor
FTIR	Fourier-Transform Infrared Spectroscopy
HA	Hydroxyapatite
HAEC	Human Aortic Endothelial Cells
HDI	Hexamethylene Diisocyanate
MFC	Microfibrillated Cellulose
NBC	Native Bacterial Cellulose
OBC	Oxidized Bacterial Cellulose
PBS	Phosphate Buffered Saline
PPG	Poly(propylene glycol)
PU	Polyurethane
SEM	Scanning Electron Microscopy
TGA	Thermogravimetric Analysis
TGF	Transforming Growth Factor
VEGF	Vascular Endothelial Growth Factor
UTS	Ultimate Tensile Strength

Appendix B. Solubility Parameters by Group Contribution Method

The group contribution method was used to determine the solubility parameters for cellulose and stannous octoate. The dispersion components (F_{di}), polar components (F_{pi}), cohesive energies (E_h), and molar volumes (V) from VanKrevelen and Hoftyzer[60] are listed below in Table 11 and Table 12 along with the number of groups for each material. The final solubility parameters are reported in Table 1. The solubility parameters were calculated and reported for cellulose. A similar number of groups and solubility parameters were reported by Elidrissi *et al*.[145] Small differences in the solubility parameters in this work and those reported by Elidrissi *et al* are attributed to small differences in component group contributions values. No previously reported solubility parameters for stannous octoate were found in the literature.

Table 11: Group Contribution Determination for Cellulose
Values were obtained from VanKrevelen and Hoftyzer[60] and the number of groups was determined by the number of groups in the repeat structure of cellulose.

Group	F_{di} ($J^{1/2}$ $cm^{3/2}$ mol^{-1})	F_{pi} ($J^{1/2}$ $cm^{3/2}$ mol^{-1})	E_h ($J\ mol^{-1}$)	V ($cm^3\ mol^{-1}$)	Number of Groups
$-CH_2-$	270	0	0	16.1	1
>CH-	80	0	0	-1	5
-OH	210	500	2000	10	3
-O-	100	400	3000	3.8	2
Ring	190	0	0	16	1

Table 12: Group Contribution Determination for Stannous Octoate
Values were obtained from VanKrevelen and Hoftyzer[60] and the number of groups was determined by the number of groups in the repeat structure of cellulose.

Group	F_{di} ($J^{1/2}$ $cm^{3/2}$ mol^{-1})	F_{pi} ($J^{1/2}$ $cm^{3/2}$ mol^{-1})	E_h ($J\ mol^{-1}$)	V ($cm^3\ mol^{-1}$)	Number of Groups
$-CH_3$	420	0	0	33.5	4
$-CH_2-$	270	0	0	16.1	8
>CH-	80	0	0	-1	2
-COOH	530	420	10000	28.5	2

Appendix C. Stress versus Strain Plots of NBC and OBC

Representative curves from the stress and strain data of NBC and OBC are presented in Figure 68. Multiple samples were tested for each experimental group, but representative curves from each experimental group are presented in the figure for clarity. Each curve exhibits a relatively linear behavior followed by a short period of yielding where the data has a slightly curved peak and quickly fails after that point. The maximum stress declines in order from a maximum for native BC down to the most highly oxidized BC.

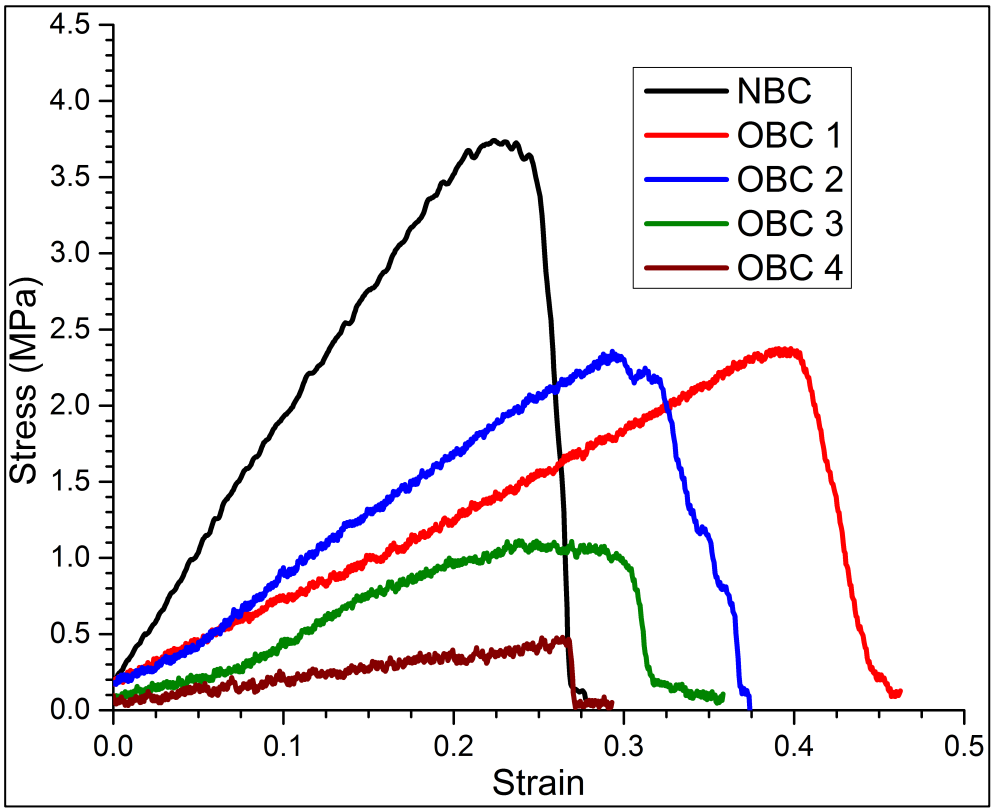

Figure 68: Stress vs Strain Curves of Native and Oxidized Bacterial Cellulose
Selected stress vs strain curves for each experimental group are presented here that are representative of the behavior within each group of material.

Appendix D. Stress versus Strain Plots of BC/PU Composites

A representative stress versus strain curve for each experimental group is presented in Figure 69. The BC/PU composites displayed strong properties. The BC/PU composites exhibited enough ductility to undergo yielding and plastic deformation before fracturing, shown by the nonlinear regions of the stress versus strain curves. This is significant improvement over the brittle behavior of NBC.

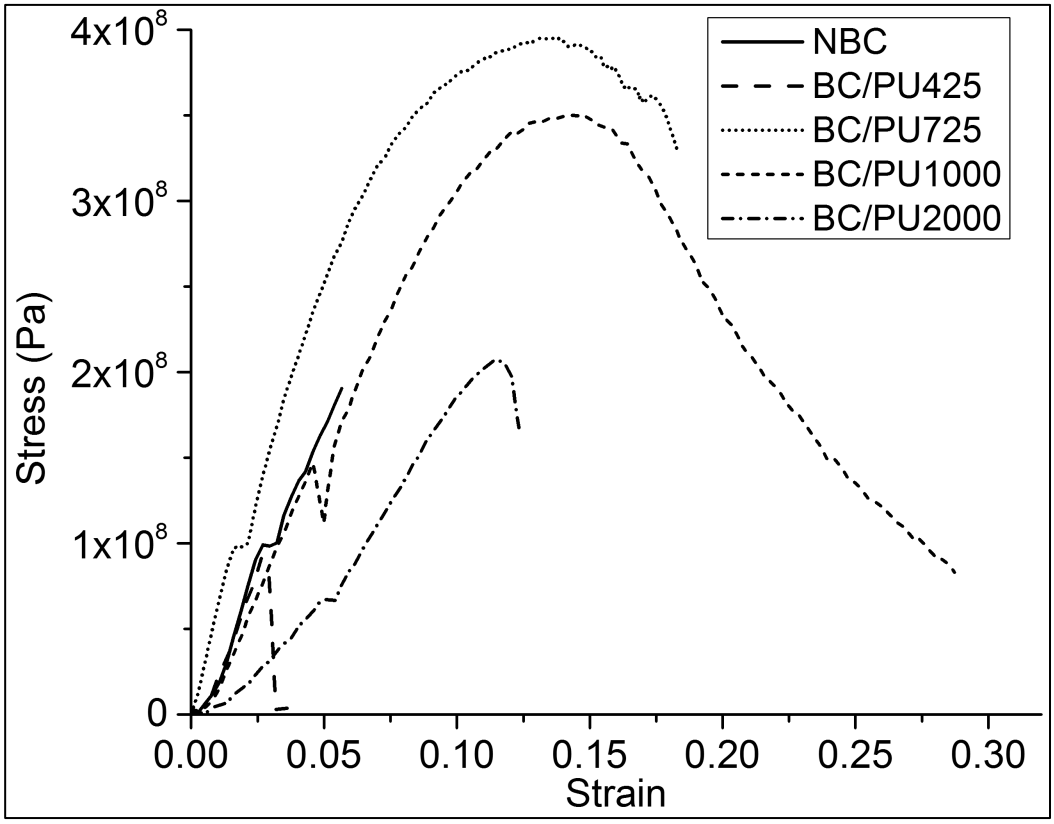

Figure 69: Representative Stress vs Strain Curves of BC and PU/BC Composites
The stress versus strain illustrates the strength and ductility of NBC (dried) and composites of BC and polyurethanes with varying soft segment lengths of 425, 725, 1,000, and 2,000.

Vita

Ryan Hammonds was born in Kingsport, TN. He attended Dobyns-Bennett High School and graduated in 2003. He received a Bachelor of Science in Biomedical Engineering at The University of Tennessee in 2008. Later in 2008, he began graduate school at the University of Tennessee and will receive his Doctor of Philosophy degree in Polymer Engineering in December 2013.